Spring 2021

Development of intelligent stimuli-responsive biomaterials and nanodevices

Shuo Yang
Missouri University of Science and Technology

Department: Chemistry

DEVELOPMENT OF INTELLIGENT STIMULI-RESPONSIVE BIOMATERIALS AND NANODEVICES

by

SHUO YANG

A DISSERTATION

Presented to the Graduate Faculty of the

MISSOURI UNIVERSITY OF SCIENCE AND TECHNOLOGY

In Partial Fulfillment of the Requirements for the Degree

DOCTOR OF PHILOSOPHY

in

CHEMISTRY

2021

Approved by:

Dr. Risheng Wang, Advisor
Dr. Nuran Ercal
Dr. Manashi Nath
Dr. Paul Nam
Dr. Yue-Wern Huang

PUBLICATION DISSERTATION OPTION

This dissertation consists of the following three articles, formatted in the style used by the Missouri University of Science and Technology:

Paper I, "Metal-Ion Responsive Reversible Assembly of DNA Origami Dimer: G-Quadruplex Induced Intermolecular Interaction", found on pages 14–45, has been published in Nanoscale.

Paper II, "Control of The Stepwise Assembly-Disassembly of DNA Origami Nanoclusters by pH Stimuli-Responsive DNA", found on pages 46–79, has been published in Nanoscale.

Paper III, "Bottom-Up Fabrication of Large-Scale Gold Nanorod Arrays by Surface Diffusion-Mediated DNA Origami Assembly", found on pages 80–117, is ready for journal submission.

ABSTRACT

Structural DNA nanotechnology utilizes DNA molecules as building blocks to fabricate ordered artificial nanostructures at the molecular level. Among all DNA-based techniques, DNA origami has been considered as one of the most powerful tools for constructing artificial nanostructures with excellent programmability and addressability. Currently, most DNA origami nanostructures are static and do not have the ability to response to environmental stimulation. The development of environmental-responsive DNA origami nanostructures is a critical step towards the realization of intelligent dynamic DNA origami-based nanodevices. This research focuses on the design and fabrication process of both static and dynamic DNA origami nanostructures and their supported assembly of functional nanomaterials.

This research consists of three journal topics. The first topic describes the metal ion-responsive assembly/disassembly of DNA origami dimers. The association/dissociation of dimer structures is realized by using G-quadruplexes as dynamic bridges because of their facile stimulus-responsive capability induced by metal-ions, such as potassium (K^+) and sodium (Na^+). The second topic introduces the study of stepwise reversible assembly of DNA origami nanoclusters via pH stimulation. The association and dissociation processes are realized by the conformation changes of DNA triplex under different pH conditions. The last topic represents the fabrication of well-aligned two-dimensional AuNR arrays guided by DNA origami on solid surface. The as-fabricated nanostructures have shown promising applications in nanoelectronics, nanoplasmonics and nanophotonics.

ACKNOWLEDGMENTS

Firstly, I would like to thank my advisor, Dr. Risheng Wang, for the opportunity to work with her, and for her conscientious support and encouragement throughout my study in Missouri University of Science and Technology. Her diligence, wealth of knowledge and enthusiasm in research always keep me motivated during five years of Ph.D. study. Without her valuable input and persistent support, it would be impossible for me to complete my work.

I would like to extend my gratitude to the professors on my committee, Dr. Nuran Ercal, Dr. Manashi Nath, Dr. Paul Nam and Dr. Yue-Wern Huang for their encouragement, incredible suggestions, and guidance on my work. I sincerely appreciate their generous help.

I will always be grateful to Dr. Wenyan Liu for his selfless support and sound advices on my research. I really appreciate the help and support from my labmates, Dr. Yun Zeng, Dr. Shuo Han, Krishna Thapa, Yuwei Zhang and Rachel Nixon. I would like to thank Dr. Eric W. Bohannan for his technical support in AFM.

Last but not the least, I would like to express my special gratitude to my family members for their unconditional love throughout my life.

TABLE OF CONTENTS

Page

LIST OF ILLUSTRATIONS

SECTION Page

PAPER II

PAPER III

1. INTRODUCTION

1.1. BACKGROUND

Self-assembly is a spontaneous process in which molecular components form ordered structures as a result of internal interactions among these components.[1,2] These interactions are mainly noncovalent interactions, such as hydrogen bonds, hydrophobic interactions, electrostatic interactions and van der Waals interactions, which play a vital role in various biological processes. For examples, two complementary single-stranded DNA (ssDNA) wind around each other to form a DNA double helix through base paring, two lipid monolayers form a lipid bilayer, and polypeptide chains fold into secondary structures by hydrogen bonds. The understanding of the self-assembly processes guided by these interactions has provided the fundamentals of knowledge for researchers to build well-ordered artificial nanostructures at the molecular level. To date, numbers of well-organized nanostructures have been realized through the controllable fabrication of various molecules including protein,[3] DNA molecules,[4] and lipid.[5] An appealing candidate among these assembling molecules is DNA molecules with unique features. Firstly, the construction of DNA structures with nanoscale precision (Figure 1.1) is achievable, because the B-form DNA is a double helix with a diameter of ~2 nm and a vertical rise of ~0.34 nm per base pair. Secondly, the development of solid support-based DNA synthesis[6] has provided a rapid and cost-effective way to obtain DNA in desired sequences. More importantly, the DNA molecules are assembled through the unique interactions controlled by Watson-Crick base pairing, in which cytosine (C) pairs with guanine (G) through three hydrogen bonds, and adenine (A) pairs with thymine (T)

through two hydrogen bonds. Such unique interactions lead to the highly flexible programmability of DNA molecules. Utilizing DNA molecules as the basic building blocks for the fabrication of artificial nanostructures represents the core concept of structural DNA nanotechnology.

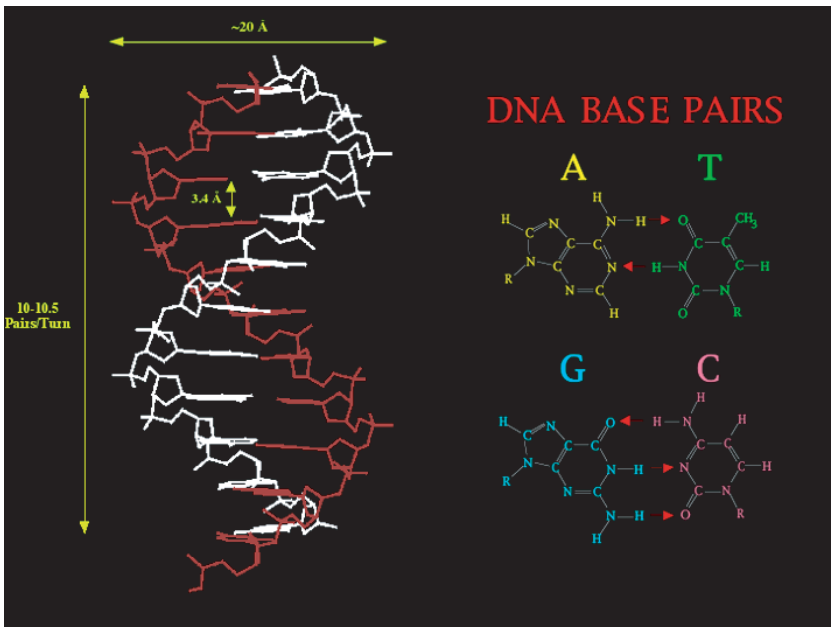

Figure 1.1. B-form DNA. The molecular structure and dimensions of key features of DNA is shown on the left. The base pairs are shown on the right, where red arrows represent hydrogen bonded interactions.[7]

The very beginning work of structural DNA nanotechnology can be traced back to 1982, when Dr. Seeman proposed using DNA strands as a building material to artificially construct protein crystals.[4,8] Rather than linear duplexes, DNA strands were designed to form branched DNA molecules. These branched molecules were expected to assemble into periodic lattices, which served as scaffolds to aid the crystallization of proteins via DNA-protein interaction. The first artificial branched molecule proposed in this work,

called immobile junction, was composed of several DNA double helices surrounding a branch point (Figure 1.2a). Unlike the naturally existing Holliday junctions (intermediates in genetic recombination)[9], these branched junctions were not designed with sequence symmetry flanking the branch point and thus were immobile and stable. Besides the 4-arm immobile junctions, to demonstrate the versatility, 3-, 5-, 6-, 8-, and 12-arm junctions were also assembled via the similar method.[10–12] It was also proposed that these junctions could be further assembled into high-order periodic lattices by introducing sticky-ended cohesion as shown in Figure 1.2b.[4,7,8,13]

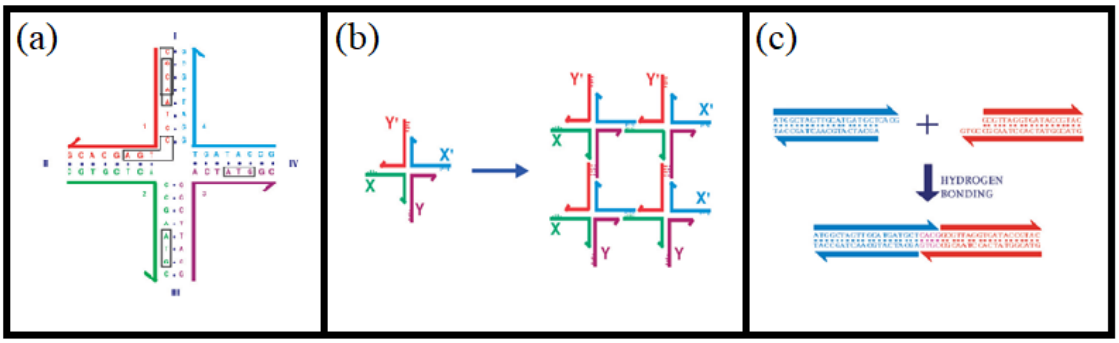

Figure 1.2. (a) A stable branched junction. There is no dyad symmetry flanking the branch point; tetramers, such as the boxed sequences CGCA and GCAA are unique, and there is no TCAG to complement the CTGA flanking the corner. (b) A branched molecule is shown on the left with four sticky ends, X, complementary to X', and Y, complementary to Y'. Four of them are shown to assemble to form a quadrilateral, with further sticky ends on the outside, so that an infinite lattice could be formed by the addition of further components. (c) Affinity in sticky-ended cohesion. Two double-helical strands with complementary overhangs are shown. Under appropriate conditions, they will cohere in a sequence-specific fashion, and can be ligated, if desired.[7]

Sticky ends are complementary single-stranded overhangs protruding from the ends of DNA double helices. Under proper solution conditions, sticky ends can act as

bridges to link two assembly components together to form complex structures (Figure 1.2c). Thus, highly ordered lattices are expected to be constructed with the use of sticky ends and artificially constructed junctions. However, these artificial junctions were relatively flexible and thus were not suitable for assembling higher-order periodic lattices. DNA double crossover (DX) with greater rigidity was then designed and constructed, which contained two 4-arm junctions connected by two double helical arms as shown in Figure 1.3a.[14–16] In 1998, Seeman successfully demonstrated the fabrication of the first two-dimensional (2D) higher-order periodic lattice using the DX molecules (Figure 1.3b).[17] The successful utilization of DX molecules has expanded the constructable variety of DNA 2D crystals with three, four, five, and six arms (Figure 1.3b). [18–20] These crystals were able to serve as templates for the precise arrangement of materials such as nanoparticles,[21] proteins,[22,23] and quantum dots.[24] Since then, the field of structural DNA nanotechnology started to grow rapidly. The fundamental explorations in structural DNA nanotechnology have dramatically enlarged the complexity of DNA-based artificial nanostructures and led to the development of DNA origami.

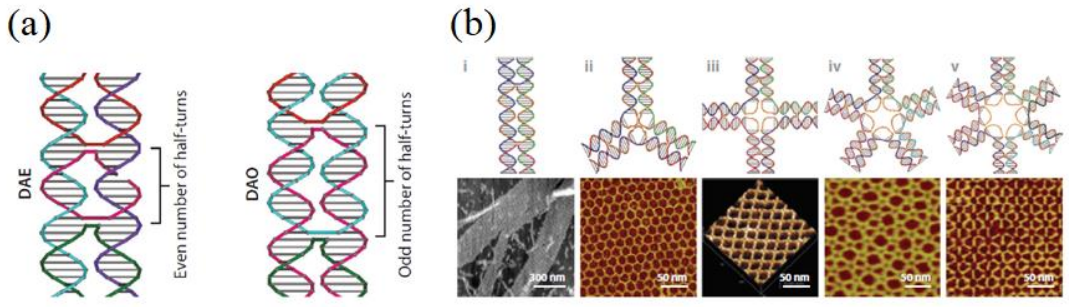

Figure 1.3. (a) Rigid double-crossover structures and (b) Multiarm DNA tiles for two-dimensional (2D) crystals.[15,16]

Origami refers to the Japanese art of folding a flat paper into desired shapes. In structural DNA nanotechnology, DNA origami, as a branch of structural DNA nanotechnology, was firstly introduced by Dr. Rothemund in 2006. It is a process of folding DNA to create arbitrary shapes at the nanoscale, such as squares, rectangles, and stars (Figure 1.4). In this self-folding method, a long circular single-stranded DNA (scaffold), typically M13mp18 phage DNA, is folded into prescribed shapes with the assist of hundreds of short synthetic DNA strands (staple strands) through the arrangement of crossovers (Figure 1.4).[25] The pathway of scaffold can be manipulated by designing the sequences of staple strands and the locations of crossovers. Each of the staples has its unique position and can be further chemically modified with functional groups such as amino groups and thiols. Thus, each of them can serve as a precision positioning point for the assembly of materials including nuclei, proteins, and nanoparticles. In this way, addressable and multifunctional hybrid materials can be realized.[26] More interestingly, besides the static nanostructures, by introducing environment-responsive functional groups, DNA origami could be further modified into dynamic nanostructures. These dynamic DNA origami can be controlled by environmental factors such as temperature, pH, light, etc. In both static and dynamic aspects, the possibility of organizing functional nanomaterials with nanoscale precision and the capability to build switchable nanostructures based on DNA has led to the ever-increasing development in the area of DNA nanotechnology, demonstrating the applications in nanopores, nanolithography, nanorobots, drug delivery, etc. The research background of static DNA origami and dynamic DNA origami will be introduced in Section 1.2 and 1.3, respectively.

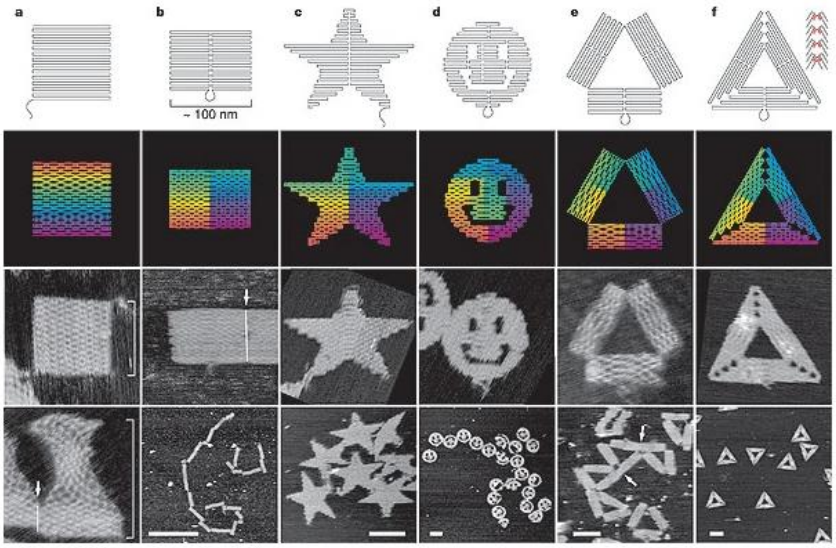

Figure 1.4. DNA Origami. The schematic drawings and AFM images of different origami patterns. From left to right, (a) square, (b) rectangle, (c) star, (d) disk with three holes, (e) triangle with rectangular domains and (f) sharp triangle.[25]

1.2. STATIC DNA ORIGAMI NANOSTRUCTURES

The assembly mechanism of DNA origami has already been introduced. With such mechanism, origami can be designed and fabricated in any desired geometry, such as six-helix bundle nanotubes,[27] gears,[28] boxs,[29] etc. Furthermore, various methods have been investigated to scale up the DNA origami structure assembly. For instance, 2D DNA origami lattices were assembled based on cation-controlled surface diffusion by Woo et al ,[30] sticky-end associations by Liu et al,[31] and using prefolded scaffold frames.[32]

Taking advantage of the precise manipulation of molecules in nanoscale, DNA origami nanostructures have been employed for many applications. For example, DNA origami can be utilized to construct artificial nanodevices to mimic biological systems. In a representative work demonstrated by Dietz and Simmel,[33] synthetic transmembrane channels for lipid bilayers were constructed from DNA origami (Figure 1.5a). A stem

protruding out of the origami was designed, which could penetrate and span into lipid membranes. The origami was also incorporated with 26 cholesterol moieties for attachment to the membrane. It showed gating behavior similar to many natural ion channels. This concept was further developed by Keyser et al.[34] Larger synthetic channels in a lipid membrane were made by using funnel-shaped porin from origami. The cross section of DNA porin was 6 nm, which was wider than natural porins and previous designs. The ionic conductance was subsequently determined by ionic current measurements, indicating the conductance of the DNA porin was at least one order of magnitude greater than that of all previously reported DNA membrane pores.

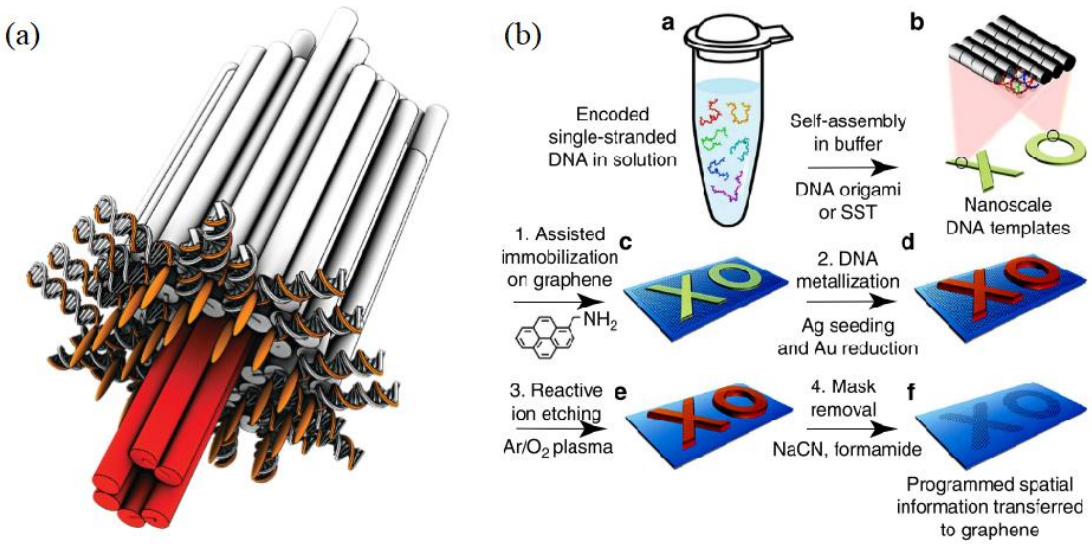

Figure 1.5. (a) Synthetic DNA membrane channels and (b) Nanopatterning of graphene via metallized DNA structures that encode and transfer spatial information.[33,35]

Besides the artificial nanodevices, DNA origami can also be used in nanolithography. Top-down fabrication, such as lithography, is robust for constructing

microscale structures, while it remains a challenge to build nanoscale objects. However, bottom-up self-assembly provides an efficient route to manipulate nanomaterials. Therefore, combining bottom-up self-assembly with top-down lithography can produce hierarchical complex patterns.[36–39] DNA origami, as a bottom-up technique, is an ideal tool for this purpose due to its customizable design of any arbitrary shape and high rigidity. Yin et al. demonstrated the basic idea of utilizing metallized DNA origami as lithographic masks for the transfer of spatial information from DNA nanostructures to graphene nanostructures (Figure 1.5b).[35] The DNA origami was assembled into planar shape and then adsorbed onto graphene surface. The DNA structures were treated with glutaraldehyde to enable seeding with silver, followed by coating with gold. The metallized DNA origami served as lithographic masks. After the removing of unprotected graphene by reactive ion etching and subsequent metal dissolution, the transfer of spatial information was successfully realized.

Moreover, static DNA origami nanostructures can be used as templates for the organization of nanomaterials such as carbon nanotubes, metal nanoparticles , and quantum dots with nanometer-scale precision.[40] Among them, noble metals, such as gold, are most widely studied, especially gold nanoparticles (AuNPs) and gold nanorods (AuNRs). Organizing these gold nanomaterials into nanostructures with well-defined geometry has provided an effective way to construct plasmonic structures with desirable optical properties.[41] For example, in the work reported by Schmidt and co-workers, a six-helix bundle DNA origami nanotubes was fabricated to assemble AuNPs into plasmonic chain waveguides.[42–45] The light propagation losses in these chain waveguides were dramatically decreased from 10 dB per 50 nm to 0.8 dB per 50 nm by minimizing

interparticle spacing (Figure 1.6a).[42] Liu and co-workers demonstrated the utilization of DNA origami for organizing AuNPs into well-ordered 2D networks (Figure 1.6b).[46] A cross-shaped origami with a hole in its center to capture AuNP was fabricated. By introducing sticky-ended cohesion on the four edges of the origami, origami framed AuNPs could be assembled into clusters, as well as 2D arrays. In our group, we employed 3D triangular DNA origami as templates for organizing heterogeneously shaped nanoparticles into plasmonic metamolecules, which exhibited tunable optical properties by controlling the presence or absence of components (Figure 1.6c). Recently, Ke and colleagues reported a rigid and versatile origami hashtag tile for organizing AuNRs into one-dimensional (1D) plasmonic polymers. These plasmonic nanostructures exhibited effective propagations of chiro-optic resonances and magnetic surface plasmonic polaritons both experimentally and theoretically (Figure 1.6d).[47] Similarly, other groups have used origami to fabricate plasmonic nanostructures based on AuNRs, including AuNRs helixes,[48] AuNP rings,[49] AuNR dimers.[50] However, the success of fabricating more complicated and larger-scale plasmonic nanostructures has not yet been realized. In paper III of this dissertation, we reported a facile method for the fabrication of well-aligned 2D arrays of AuNRs through an origami guided approach. DNA functionalized AuNRs were decorated on origami frames which were programmed to generate 2D array through base-stacking interactions on mica surface in buffer solution. These assembled 2D arrays showed great stability with AuNRs well-arranged in predesigned orientation. We further demonstrated that preformed 2D arrays of AuNRs could be intactly transferred from the liquid condition to the dry state through an pattern transfer method for potential applications in nanoplasmonics, nanophotonics and nanoelectronics.[51]

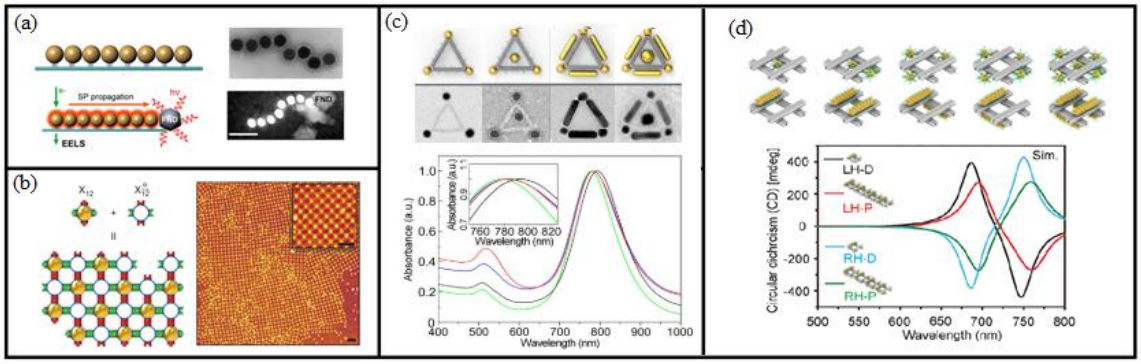

Figure 1.6. DNA origami for fabrication with synthetic materials. (a) Self-assembly of plasmonic waveguides. (b) AFM image of 2D AuNPs arrays. (c) Self-assembled AuNP clusters and corresponding optical characterization. (d) Assembling AuNRs onto hashtag chains and chiro-optic response of AuNRs dimer and polymer.[42,46,47]

1.3. DYNAMIC DNA ORIGAMI NANOSTRUCTURES

In the previous section, we introduced the static assembly of DNA origami and their relevant applications. However, the self-assembly processes that naturally occur in the biological systems are usually more complicated and involve multiple environmental factors in dynamic equilibrium. For example, the assembly of multiple protein subunits into DNA polymerase III holoenzyme, under successive physiological stimuli, is the key ensuring DNA replication in high fidelity and high processivity. In this respect, the construction of dynamic DNA origami nanostructures that are capable of responding to external stimuli is a critical step in the fabrication of intelligent DNA origami-based nanodevices. To address this, extensive research efforts have been devoted to the development of smart and dynamic nanostructures which are responsive to certain external environmental factors such as pH, light, temperature, etc. For example, photo-controlled reversible assembly of DNA origami into designed patterns was accomplished by Suzuki and co-workers as shown in Figure 1.7a.[52] This assembly was realized by utilizing photo-responsive origami composed of photosensitive azobenzene-modified

oligonucleotides (Azo-ODNs). UV-driven conformation changes of Azo-ODNs between trans-form and cis-from resulted in the dissociation and hybridization of origami tiles. Temperature can also be used to control the motion of DNA origami. For instance, Polymer poly(N-isopropylacrylamide) (PNIPAM) is one of thermo-responsive materials. It can switch from hydrophobic to hydrophilic status when temperature is below 32 °C, causing the molecules to relax, while when temperature is above 32 °C, the molecules will contract to a compact globule. By incorporating PNIPAM-modified staple strands into plate-like DNA origami, the origami can adopt opened or closed state by changing temperature (Figure 1.7b).[53] In addition, these dynamic nanostructures can be used for drug delivery. An example of nucleolin targeted drug-delivery vehicles was introduced by Zhao et al (Figure 1.7c). The tubular DNA nanorobots were decorated on the outside with aptamer which could bind nucleolin (a protein expressed on tumor cell) and associated with thrombin within its inner cavity. The nucleolin-targeted aptamer acted as a molecular trigger to open the nanorobot. Then the thrombin was exposed to the surrounding environment and induced coagulation of tumor cells. To explore novel environmental triggers, metal-ion responsive G-quadruplex (G-rich DNA strands) has attracted our interest. It can be easily incorporated into DNA origami systems forming dynamic structures because the G-quadruplex can transform from a secondary structure to a linear structure by exposing to monovalent cations such as potassium (K^+) or sodium (Na^+). In paper I of this dissertation, we demonstrated the G-quadruplex-assisted assembly/disassembly of DNA origami dimers, which was realized by G-quadruplex conformational change, driven by the presence/absence of monovalent cations. Despite these progresses, DNA origami nanostructures reported so far, including our G-

quadruplex dynamic system, are either simple architectures (2-3 origami units) or limited to single-step stimulus between dual-state transitions, which are not sufficient for more sophisticated dynamic systems with multi-step response capabilities. To further realize the scalability of DNA origami nanostructures and multi-step capabilities, in paper II we presented the stepwise assembly of more complex 9-tile origami nanoclusters from two types of pH-sensitive DNA triplexes. We demonstrated the multi-step stimulated formation of DNA nanostructures triggered by varying pH environment. The dynamic process has been characterized by using Atomic Force Microscope (AFM), gel electrophoresis, and Dynamic Light Scattering (DLS).

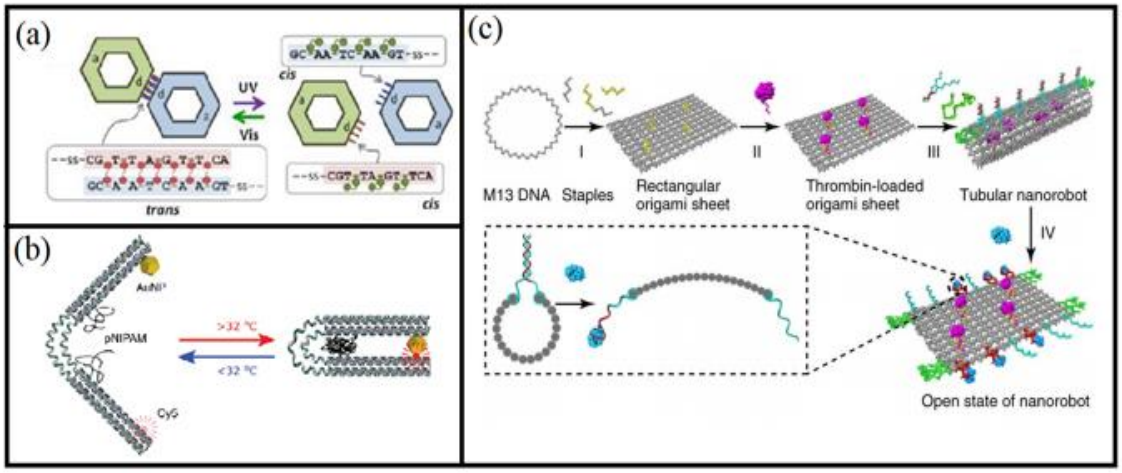

Figure 1.7. (a) Reversible photoregulation for the formation and dissociation of hexagonal dimer under different irradiation conditions. (b) Schematic of DNAo flexor. Above the LCST, the PNIPAM chains on both sides of the hinge become hydrophobic, causing the two arms of origami to fold due to hydrophobic interactions. Once the temperature is lowered below the LCST, PNIPAM rehydrates thereby unfolding the origami structure. (c) Functional DNA origami nanorobot for thrombin delivery.[52,53]

1.4. ORGANIZATION OF DISSERTATION

This dissertation is organized based on three research projects. The first project mainly focused on the study of the metal-ion stimulated assembly/disassembly of DNA origami dimers using G- quadruplexes as dynamic bridges. The second project studied the stepwise assembly of DNA origami nanoclusters via pH stimulation, where structure association and dissociation were controlled by multiple pH-stimulated processes. Whereas in the third project, more complex and larger-scale AuNR array has been fabricated, for the first time, by employing DNA origami as scaffold and assembly on the mica surface. The as-fabricated nanostructures have shown promising applications in nanoelectronics, nanoplasmonics, and nanophotonics.

PAPER

I. METAL-ION RESPONSIVE REVERSIBLE ASSEMBLY OF DNA ORIGAMI DIMERS: G-QUADRUPLEX INDUCED INTERMOLECULAR INTERACTION

Shuo Yang,[a] Wenyan Liu,[b] Rachel Nixon,[a] and Risheng Wang*[a]

[a]Department of Chemistry,
Missouri University of Science and Technology, Rolla, MO 65409, USA

[b]Center of Research in Energy and Environment,
Missouri University of Science and Technology, Rolla, MO 65409, USA

ABSTRACT

We present a novel metal-ion stimulated organization of DNA origami nanostructures by employing G-quadruplexes as stimuli-responsive bridges. The reversible assembly process of DNA origami was the result of conformational changes between the G-quadruplex and its single-strand state induced by monovalent cations. This study might stimulate a new design of responsive DNA-based intelligent nanomaterials.
Key words: G-quadruplex, DNA origami, stimuli-responsive assembly, intermolecular interaction

1. INTRODUCTION

With the development of DNA nanotechnology, DNA origami has been considered as a versatile unit for nanofabrication due to its superior programmability.[1]

The self-assembly of DNA origami units into high-ordered superstructures provides a promising route for organizing multiple and complex functional components with nanometer precision (such as metal nanoparticles,[2, 3] quantum dots,[4-6] and biomolecules).[7, 8] In the past several decades, numerous targeted two dimensional (2D),[9-11] and three dimensional (3D)[12, 13] DNA origami superstructures have been successfully constructed to explore their potential for applications in multidisciplinary fields that cross materials science, biology, electronics, and biomedicine.[7, 14-19] The bottom-up self-assembly of these high-ordered nanostructures has been mainly facilitated by traditional DNA sticky-ended cohesion, in which single-stranded DNA overhangs in one molecule are able to hybridize with their corresponding complementary strands in another molecule, based on Watson-Crick base paring.[20] However, these traditional cohesive end-mediated superstructures are static and could not respond to environmental stimulation by automatically assembling or disassembling. The development of smart and dynamic nanomaterials, which are able to respond to external stimulation, is a critical step towards the fabrication of intelligent drug delivery carriers, nano-robots, and switches for advanced applications.[21, 22]

Fortunately, great progress has been made in DNA fabrication by attaching specific functional oligonucleotides (that are sensitive to external stimulation) to DNA origami structures forming dynamic cohesive ends. For example, Suzuki et al. developed a method to assemble and disassemble hexagonal DNA origami tiles by using photosensitive azobenzene-modified oligonucleotides as sticky-ends;[23] Wu et al. showed the dissociation of DNA origami dimers and trimers by attaching pH-responsive DNA strands,[24] DNAzymes,[25] and aptamer ligands to DNA origami.[26] To avoid complex

chemical synthesis, specific structural design, and extreme environmental variation (such as pH), considerable attention has been recently given to G-quadruplex,[27, 28] a non-canonical secondary DNA motif formed by Hoogsteen hydrogen bonds between guanine bases in G-rich sequences. It is significant because of its facile stimulated responsive capability - reversible conformation changes between G-quadruplex and its single-strand state (which is simply driven by monovalent cations). For example, in the presence of monovalent ions, potassium (K^+) or sodium (Na^+), the linear G-rich DNA strands are capable of forming G-quadruplex structures. Until now, several works have been performed to study G-quadruplex formation[29] and its ion selectivity[30, 31] on DNA origami frames, and G-quadruplex induced shape transition of the origami device.[32] However, G-quadruplex-assisted assembly and disassembly of DNA origami nanostructures has not yet been reported. It has potential to serve as a new type of bridge for self-assembly of high-ordered DNA superstructures with stimuli-responsive capability to make advanced smart materials.

In this study, we demonstrated the metal-ion responsive assembly/disassembly of DNA origami dimers, bridged by nucleic acid duplexes containing encoded G-quadruplex oligonucleotides, for the first time. The dimer structures were associated/dissociated by G-quadruplex conformational change, driven by the presence/absence of monovalent cations. Three types of intra- and intermolecular G-quadruplexes were investigated. The cyclic assembly/disassembly processes were monitored by AFM and gel electrophoresis.

2. EXPERIMENTAL DETAILS

2.1. MATERIALS

All chemicals were purchased from Sigma and used as received without further purification. All chemically synthesized DNA strands were purchased from Integrated DNA Technologies, Inc. (www.Idtdna.com). The unmodified staple strands were ordered in a 96-well plate format, suspended in ultrapure water without purification. All modified strands were purified with PAGE. The DNA origami purification column (100kDa MWCO centrifuge filter) was purchased from Pall, Inc.

2.2. ASSEMBLY/DISASSEMBLY OF DNA ORIGAMI NANOSTRUCTURES

M13mp18 viral DNA and all of the staple strands were mixed together at a 1:5 ratio, in a 1× TAE buffer solution containing 40 mM Tris-HCl, 20 mM of acetic acid, 2 mM of EDTA, and 11.5 mM of magnesium acetate. The mixture was slowly cooled from 90℃ to 15℃ with PCR over 12h. The final concentration of M13mp18 DNA in the solution was 20 nM. The DNA origami was then purified to remove excess DNA strands, using 100kDa MWCO centrifuge filters.

Formation of DNA origami dimer: The prepared DNA origami monomers were mixed at a molar ratio of 1:1 in a 1×TAE buffer containing 11.5 mM of magnesium acetate. Then, the mixture was annealed from 53℃ to 15℃ over varied time course from 2h to 12h to form the corresponding DNA origami dimers (Figure S1). The separation of the origami dimer was accomplished by adding varied concentration of potassium chloride or sodium chloride in the solution of DNA origami dimer and incubating at a

temperature ranging from 53℃ to 15℃ over 12 h time course. A 100kDa MWCO centrifuge filter was used to exchange the reaction buffer.

2.3. AFM IMAGING

The AFM images of the DNA origami dimer and monomer were obtained through spotting the sample (3 μl) onto freshly cleaved muscovite mica (Ted Pella, Inc.) for 15 s. Afer the fixation of targeted structure of DNA origami on mica surface, doubly distilled H_2O (20-30ul) was placed quickly on the mica to remove the buffer salts, the drop was wicked off, and the sample was dried with compressed air. Atomic force imaging was done by utilizing Nanoscope III (Digital Instruments) tapping in air, with ultra-sharp 14 series (NSC 14) tips that had been purchased from NANOANDMORE.

2.4. AGAROSE GEL ELECTROPHORESIS

The samples were loaded into 0.8% agarose gel that contained 5 mM $Mg(CH3COO)_2$, 20 mM KCl or NaCl in a 1×TAE buffer solution under 55V at room temperature. The gel was stained with ethidium bromide for DNA visualization.

3. RESULTS AND DISCUSSION

Figure 1A presents a schematic drawing of a G-quadruplex-assisted formation and dissociation of the DNA origami dimers C1 and C2. Cross-shaped DNA origami tile[9] designed by Liu et al was used in this study (see supporting information for structural and sequence design). The right arm of C1 was attached with four hairpin loops that were

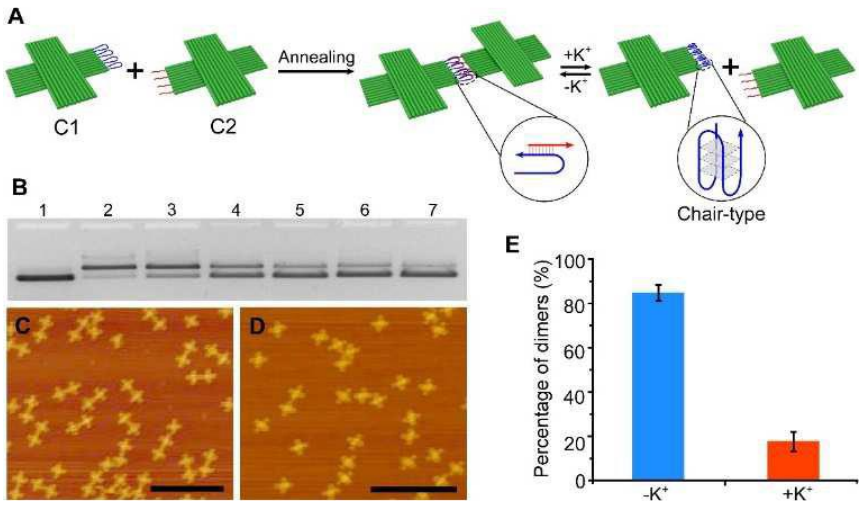

Figure 1. Chair-type G-quadruplex-driven assembly/disassembly of DNA origami dimers. (A) Schematic drawing of cross-shaped DNA origami assembly/disassembly by introducing ion-responsive chair-type G-quadruplexes as sticky-end cohesion. (B) Agarose gel electrophoresis image of dissociation of DNA origami dimer with different concentrations of potassium. Lane 1: DNA origami monomer. Lane 2: DNA origami dimer before K^+ treatment. Lane 3 to Lane 7: DNA origami dimer treated with varied concentrations of K^+, 25 mM, 50 mM, 80 mM, 100 mM, 200 mM, respectively. (C) AFM image of DNA origami dimer before K^+ treatment and after K^+ treatment (100 mM) (D). (E) Statistical analysis of the percent of the DNA origami dimer before K^+ treatment (blue, 85.2 ± 3.5%) and after K^+ treatment (red, 18.0 ± 4.2%). Scale bar, 500nm.

encoded with the 5'-GGGTTAGGGTTAGGGTTAGGG-3' sequence which can fold over forming a chair-type intramolecular G-quadruplex in thepresence of K^+.[27, 33] The left arm of C2 contained four single-stranded DNA, partially complementary to the hairpin loops on C1. Through a thermal annealing process, the hybridization between C1 and C2 resulted in the formation of the origami dimer C1+C2, via Watson-Crick base paring (Figure S1). Please note that the isomer state of DNA origami dimer may exist by forming C1 + inverted C2. While the introduction of K^+ to the DNA origami dimer solution led to the dissociation of the dimer into monomers because of the reconfiguration of the hairpin loops into chair-type G- quadraplexes.[33] Evidently, the

concentration of K^+ is a critical factor in determining the efficiency of assembly and disassembly processes, as such the concentration of K^+ was optimized. The DNA origami dimers were treated with various concentrations of K^+ ranging from 0 to 200 mM. As can be seen from the agarose gel in Figure 1B, with no K^+ treatment, Lane 2 exhibits an intense upper band and a much weaker lower band that correspond to the DNA origami dimer and monomer, respectively. After treatment with different concentrations of K^+, as shown in Lane 3-7, the intensity of the upper bands and lower bands subsequently changed; the higher the concentration of K+ was, the lower the intensity of the upper bands, indicating increased dissociation efficiency (fewer DNA origami dimers present in the solution). Also, notably, the DNA origami dimers treated with 100 mM K^+ (lane 6) and 200 mM K^+ (lane 7) did not exhibit any apparent difference in the bands' intensity. This suggests that the ionic strength of 100 mM K^+ is high enough to induce the hairpin loops to fold into chair-type G-quadruplexes and, thus, to disassemble the DNA origami dimers. Therefore, the K^+ concentration of 100 mM was chosen for subsequent studies. Figure 1C and 1D show representative AFM images of DNA origami dimers and monomers, respectively, before and after treatment with 100 mM K^+. Perhaps because of either aggregation or partial bridging between the origami tiles, it was noted that some origami dimers are not in a linear shape, but a rugged shape (red circle in Figure S2). The statistical analysis of the AFM images (shown in Figure 1E) reveals that ~ 85% of the DNA origami tiles existed in a dimeric form before treatment with K^+. After K^+ treatment, however, a majority of the DNA origami dimers dissociated into monomers, with less than 18% of the DNA origami dimers remaining. This is consistent with the observation obtained from gel electrophoresis (Figure 1B).

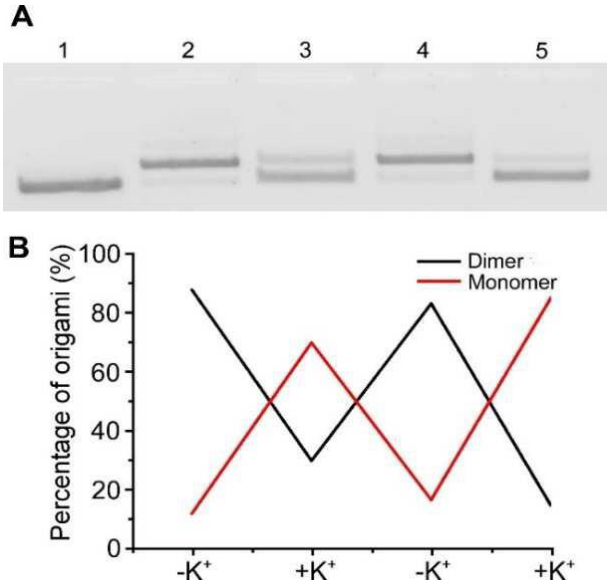

Figure 2. Investigation of the dynamic process of formation and separation of the DNA origami dimer driven by G-quadruplexes. (A) Agarose gel electrophoresis characterization of the reversible process. Lane 1: DNA origami monomer. Lane 2: DNA origami dimer before K^+ treatment. Lane 3: adding 100 mM K^+ to the product in Lane 2. Lane 4: removing K^+ from the product in Lane 3. Lane 5: adding 100 mM K^+ to the product in Lane 4. (B) Working cycles of G-quadruplex-driven DNA origami nanostructures switching between dimer and monomer in response to K^+ stimulation. The quantification of the DNA origami dimer and monomer was based on the intensity of gel electrophoresis.

It is well known that telomeric G-rich sequences not only can response to monovalent cation, K^+, but also to Na^+,[27] thus, further investigation was performed to study the disassembly of DNA origami dimer C1+C2 in the presence of varied concentration of Na+ via gel electrophoresis. Figure S3 shows that the population of DNA origami monomers increased from ~ 32% to ~ 40% with increasing Na+ concentration from 20 mM to 100 mM. Compared with the K^+ induced dissociation of DNA origami dimer, Na^+ exhibited less selectivity. ~ 60% DNA origami dimers did not undergo a topological transition at Na^+ concentration of 100 mM. This is due to the coordination of K^+ into the central ion channel of G-quartets, leading to more stable G-

quadruplexes in K^+ than in Na^+.[34] Therefore, we mainly focused on the K^+ induced G-quadruplex transition for further study. The reversible stimuli-responsive feature is one of the basic requirements for nanomaterials that are used to develop intelligent products. Thereby, we further examined the reversibility of the above K^+-responsive dimer system. The assembly/disassembly of the dimers was controlled by adding/removing K^+, via buffer exchange, and monitored by agarose gel electrophoresis for two cycles. As shown in Figure 2A, the dimer exhibited an effective reversible switching between the dimer and monomer forms upon K^+ stimulus. The gel image analysis reveals that, in two continuous cycles, a very similar population (~90%) of origami tiles existed as dimers.

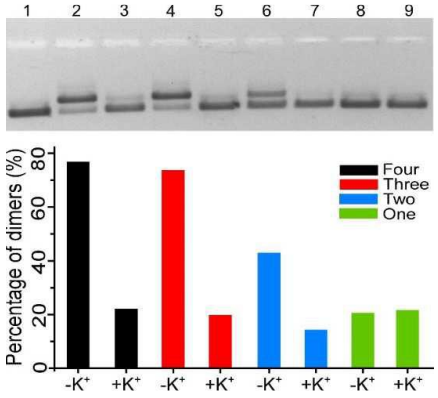

Figure 3. Agarose gel electrophoresis analysis of the effect of the number of G-quadruplex sticky-ends on the efficiency of assembly and disassembly of a DNA origami dimer. Lane 1: DNA origami monomer. Lane 2: DNA origami dimer formed via 4 G-quadruplex sticky-ends. Lane 3: adding 100 mM K^+ to the product in Lane 2. Lanes 4, 6, and 8: DNA origami dimer formed via 3, 2, and 1 G-quadruplex sticky-ends, respectively. Lanes 5, 7, and 9: adding 100 mM K^+ to the products of Lanes 4, 6, and 8, respectively. Statistical analysis of the prevalence of DNA origami dimers with differing numbers of G-quadruplex sticky-ends based on the intensity of gel electrophoresis.

This demonstrated that the reversible assembly/disassembly of DNA origami dimers could be effectively controlled by employing the ion-responsive G-quadruplex for

functional sticky-ended cohesion. Furthermore, we also investigated the effect of the number of G-quadruplex sticky-ends on the efficiency of assembly/disassembly of DNA origami dimers. The DNA origami dimers were annealed under the aforementioned conditions, with various numbers of G-quadruplex sticky-ends, ranging from 1 to 4. Figure 3 shows the agarose gel electrophoresis analysis of the samples. It can be seen that, in the absence of K^+, the intensity of the upper bands (that correspond to the DNA origami dimers) decreased as the number of G-quadruplex sticky-ends decreased. This indicates that the binding affinity of the dimer is strongly dependent on the number of sticky-ends. Moreover, by comparing the population of dimers in each case (before and after treatment with K^+), we found that the number of dimers containing 4, 3, and 2 G-quadruplex sticky-ends had significantly decreased with K^+ treatment. This suggests that these dimers are still sensitive to K^+ stimulation. However, it is evident that the population of dimers that contained 1 Gquadruplex sticky-end remained practically the same before and after the addition of K^+, implying that there was no response to K^+ stimulation. This might be due to the competition between G-quadruplex driven dissociation of DNA origami dimer and the intrinsic stability of the dimers associated through DNA hybridization. This similar phenomenon was also observed in the ATP-driven separation of DNA dimer.[26]

Encouraged by the successful assembly and disassembly of DNA origami dimers, bridged by the chair-type Gquadruplexes, we then investigated the dimer-monomer transitions of DNA origami, guided by propeller-type intramolecular G-quadruplexes. As

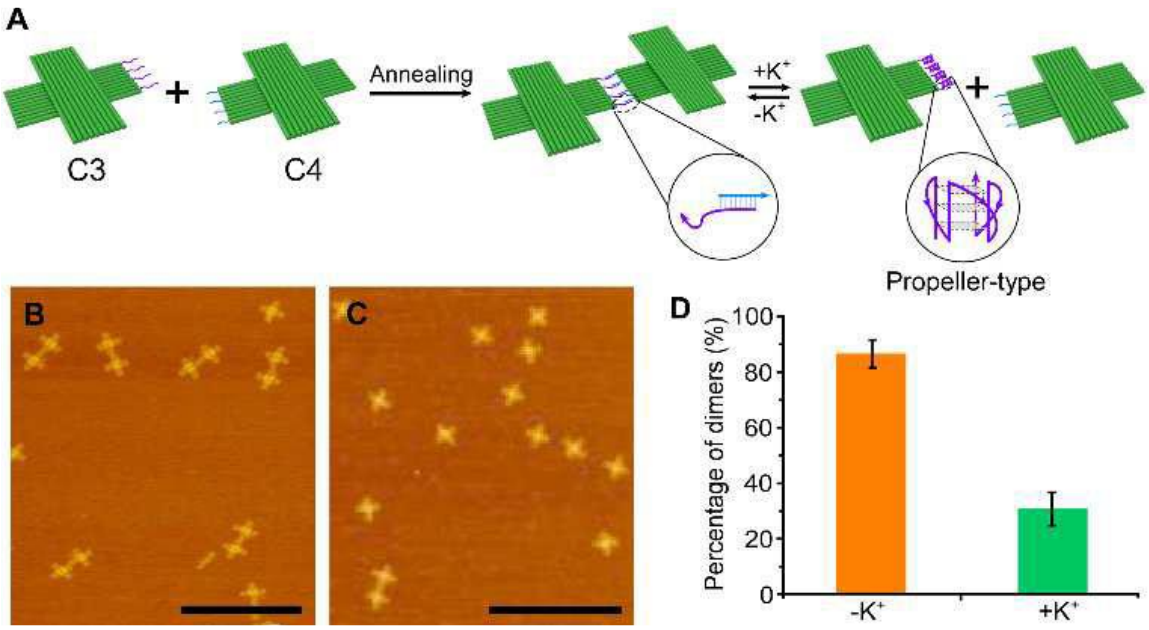

Figure 4. Propeller-type G-quadruplex-driven assembly/disassembly of DNA origami dimers. (A) Schematic drawings of cross-shaped DNA origami assembly/disassembly by introducing propeller-type G-quadruplex as sticky-ended cohesion. (B) AFM images of a DNA origami dimer before K+ treatment and after K+ treatment (C). (D) Statistical analysis of the percent of the DNA origami dimer before K+ treatment (orange, 86.6 ± 4.9%) and after K+ treatment (green, 30.6 ± 6.0%). Scale bar, 500nm.

shown in Figure 4A, four linear oligonucleotides, which can fold into propeller-type intramolecular G-quadruplexes in the presence of K+, 35, 36 were tethered to the right arm of DNA origami C3. Their complementary oligonucleotides were introduced to the left arm of DNA origami C4. Similar to the system shown in Figure 1, without K+ added, tiles C3 and C4 can form dimer structures as a result of formation of DNA duplexes between tethered linear oligonucleotides (Figure S4), while, after addition of 100 mM K+, the dimers separate into monomers due to the K+-induced Gquadruplex folding. Figure 4B and 4C depict the corresponding AFM images of the dimers and monomers. The image analysis, as shown in Figure 4D, reveals that ~87% of DNA origami tiles existed in dimeric form, similar to those in the first system, whereas the treatment of

dimers with K+ caused the dimer population to drop to ~ 30%. This observation was further supported by agarose gel electrophoresis (Figure S5). In addition to the intramolecular G-quadruplexes-assisted separation of DNA dimers, as demonstrated above, we also explored the possibility of using intermolecular G-quadruplexes as bridges to mediate the association and dissociation of DNA origami via K+ stimulation (Figure S6). We attached four hairpin loops on the right arm of origami tile C5 and the left arm of origami tile C6. Upon adding the K+, we expected that corresponding hairpin loop pairs between tiles C5 and C6 would form anti-parallel hairpin dimeric G-quadruplexes, leading to the formation of DNA origami dimer C5+C6, and after removing K^+, the dimer would dissociate into monomers (Figure S6A). We first incorporated sequence 5'-GGGTTAGGG-3' in each loop; however, this sequence did not result in the formation of DNA origami dimers via G-quadruplex structures. This may have been due to hairpin loops that were too short, or because of the steric hindrance of the DNA origami tiles. Then, we extended the G-tract length from 3 to 9, and treated the samples with various concentrations of K^+ (0-300 mM). The gel electrophoresis showed that multiple bands were formed, even without K+ (Figure S6B). AFM imaging confirmed that band 1 corresponds to the DNA origami monomer, band 2 corresponds to dimer, and bands 3 and 4 are DNA origami aggregations. Moreover, this design showed no response to K+ stimulation, perhaps due to the complicated secondary structures formed by long repetitious G sequences. Given the structural diversity of G-quadruplexes, further factors need to be considered for developing intermolecular G-quadruplex-based stimuli-responsive bridges, such as the number and polarity of strands, loop length, sequence, and G-tract length.

4. CONCLUSIONS

In conclusion, we introduced a new type of stimuli-responsive functional sticky-ended cohesion to enhance DNA supramolecular self-assembly capability and diversity. We have demonstrated that the ion-stimulated reversible assembly/disassembly of DNA origami dimers can be realized by employing intramolecular G-quadruplexes as bridges. The conformation switching between G-quadruplex and its single-strand state leads to the association/dissociation of DNA origami dimers. This type of environmental-stimuli responsive cohesion offers a new way to organize, not only small, finite size clusters, but also larger 2D and 3D structures to construct intelligent materials for advanced nanotechnology applications.

ACKNOWLEDGEMENT

This work is supported by University of Missouri Research Board, Material Research Center at Missouri University of Science and Technology and College of arts and Science of Missouri S&T.

SUPPLEMENTARY INFORMATION

METAL-ION RESPONSIVE REVERSIBLE ASSEMBLY OF DNA ORIGAMI DIMERS: G-QUADRUPLEX INDUCED INTERMOLECULAR INTERACTION

Shuo Yang,[a] Wenyan Liu,[b] Rachel Nixon,[a] and Risheng Wang[*a]

[a]Department of Chemistry,
Missouri University of Science and Technology, Rolla, MO 65409, United States

[b]Center for Research in Energy and Environment,
Missouri University of Science and Technology, Rolla, MO 65409, United States
*E-mail: wangri@mst.edu

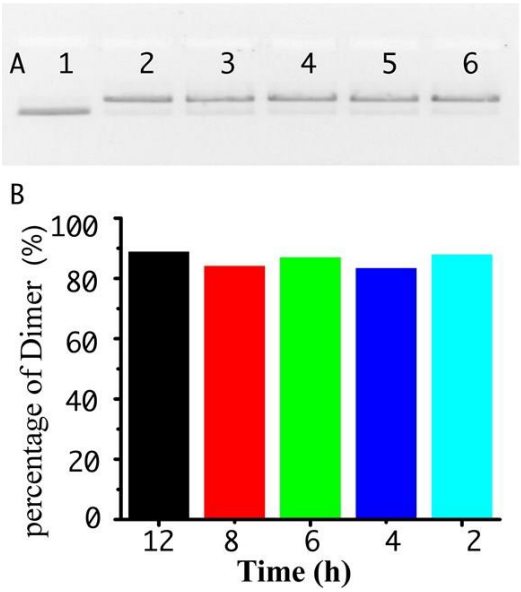

Figure S1. (A) Agarose gel electrophoresis image of assembly of DNA origami dimer with varied annealing period (design corresponding to Figure 1A). Lane 1: DNA origami monomer. Lane 2 to lane 6: corresponding to the annealing period from 12 h, 8 h, 6h, 4h to 2 h respectively. (B) The quantification of band intensity in an agarose gel image (shown in Figure S1A). There is no time-dependence in the formation of DNA origami dimer.

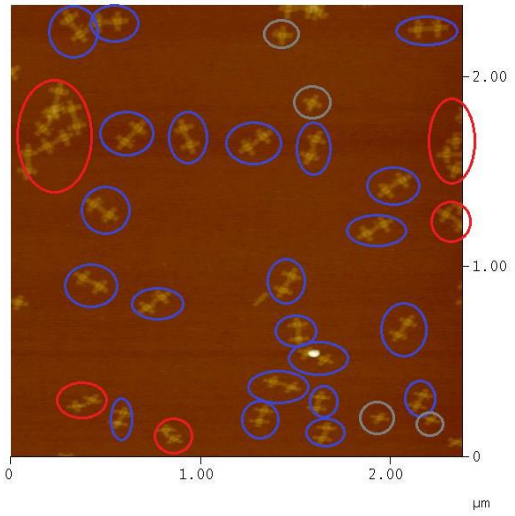

Figure S2. An example of an AFM image used to calculate the yield of a DNA origami dimer with the design shown in Figure 1. The blue circles represent a DNA origami dimer; the grey circles represent DNA origami monomer; and the red circles represent the non-counted DNA origami aggregations. The final yield is the average yield of each image.

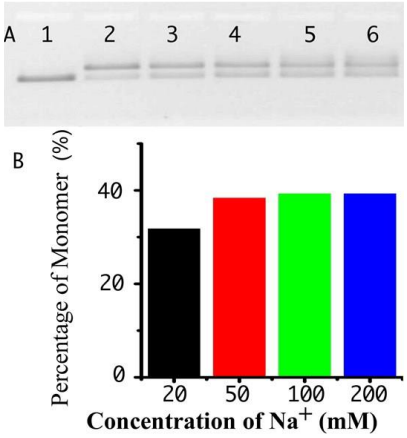

Figure S3. (A) Agarose gel electrophoresis image of dissociation of a DNA origami dimer with different concentrations of Sodium (design corresponding to Figure 1A). Lane 1: DNA origami monomer. Lane 2: DNA origami dimer before Na^+ treatment. Lane 3 to Lane 6: DNA origami dimer treated with varied concentrations of Na^+, 20 mM, 50 mM, 100 mM, 200 mM, respectively. (B) The quantification of band intensity in an agarose gel image (shown in Figure S3A).

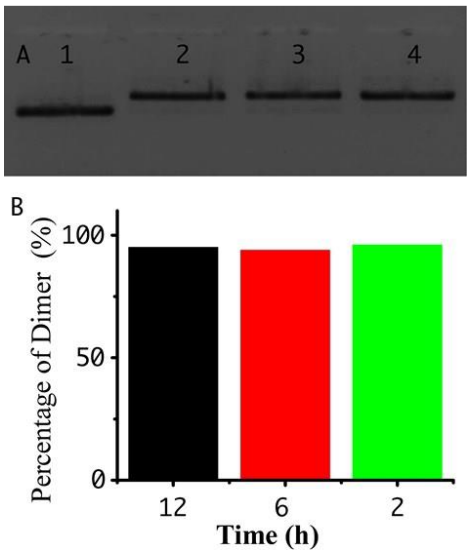

Figure S4. (A) Agarose gel electrophoresis image of assembly of DNA origami dimer with varied annealing period (design corresponding to Figure 4A). Lane 1: DNA origami monomer. Lane 2 to lane 4: corresponding to the annealing period from 12 h, 6h, to 2 h respectively. (B) The quantification of band intensity in an agarose gel image (shown in Figure S4A). There is no time-dependence in the formation of DNA origami dimer.

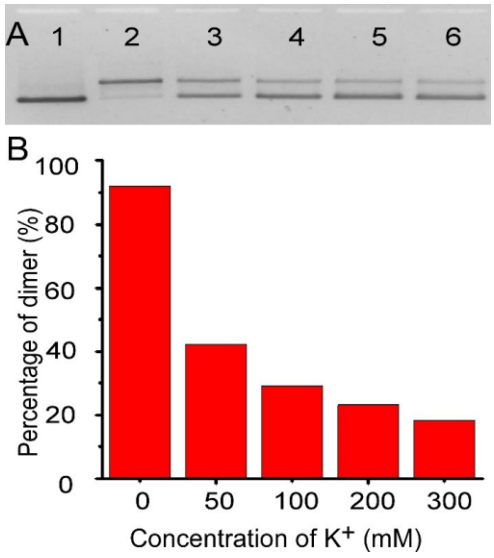

Figure S5. (A) Agarose gel electrophoresis image of dissociation of a DNA origami dimer with different concentrations of potassium (design corresponding to Figure 4A). Lane 1: DNA origami monomer. Lane 2: DNA origami dimer before K^+ treatment. Lane 3 to Lane 6: DNA origami dimer treated with varied concentrations of K^+, 50 mM, 100 mM, 200 mM, 300 mM, respectively. (B) The quantification of band intensity in an agarose gel image (shown in Figure S2A).

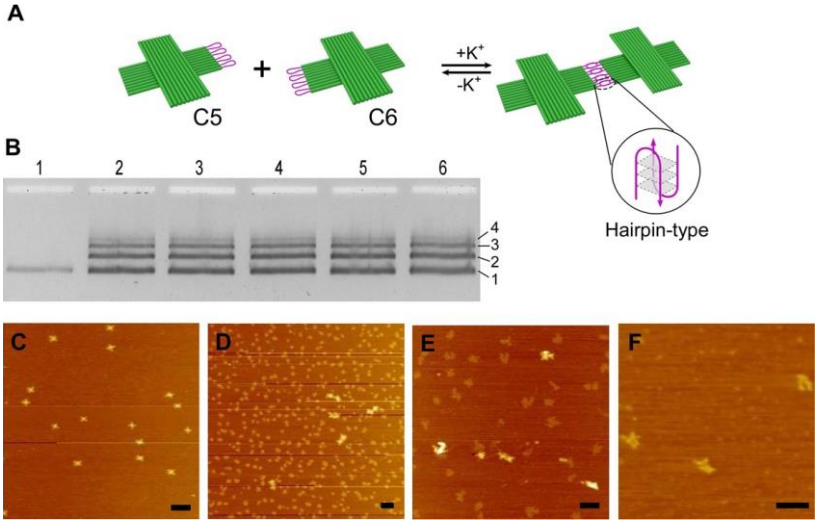

Figure S6. (A) Schematic drawings of a DNA origami assembly/disassembly driven by intermolecular G-quadruplex. (B) Agarose gel electrophoresis image of a DNA origami dimer with different concentrations of potassium. Lane 1: DNA origami monomer. Lane 2 to Lane 6: mixture of DNA origami with varied K^+ concentrations, 0 mM, 50 mM, 100 mM, 200 mM, and 300 mM, respectively. (C)-(F) AFM images corresponding to Band 1 through Band 4, respectively. Scale bar, 200nm.

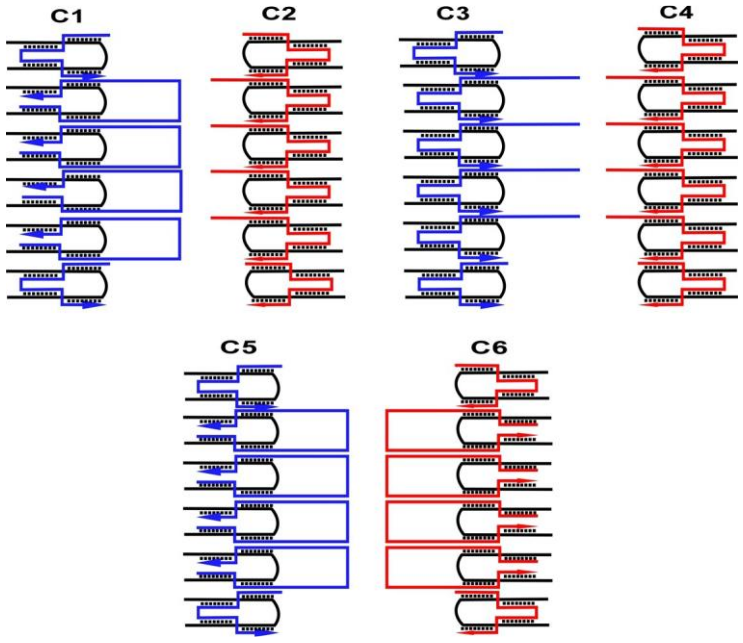

Figure S7. The Stikcy-ends design and sequences of DNA origami.

DNA Sequences:

RC-M1 AGCTAATGCAGAACGCGCCTGTTTTAATATCC

RC-M2 CATCCTAATTTGAAGCCTTAAATCTTTTATCC

RC-M3 TGAATCTTGAGAGATAACCCACAAAACAATGA

RC-M4 AATAGCAATAGATGGGCGCATCGTACCGTATC

RC-M5 GGCCTCAGCTTGCATGCCTGCAGGGAATTCGT

RC-M6 AATCATGGTGGTTTTTCTTTTCACCCGCCTGG

RC-M7 CCCTGAGAGAGTTGCAGCAAGCGGGTATTGGG

RC-M8 CGCCAGGGTCATAGCTGTTTCCTGGACGGCCA

RC-M9 GTGCCAAGGAAGATCGACATCCAGATAGGTTA

RC-M10 CGTTGGTGTAGCTATCTTACCGAATTGAGCGC

RC-M11 TAATATCAACCTTCGCTAACGAGCCCGACTTG

RC-M12 CGGGAGGTTTTACGAGCATGTAGAACATGTTC

RC-M13 CTGTCCAGACGACGACAATAAACAAACCAATC

RC-M14 AATAATCGCGTTTTAGCGAACCTCGTCTTTCC

RC-M15 AGAGCCTACAAAGTCAGAGGGTAAGCCCTTTT

RC-M16 TAAGAAAAGATTGACCGTAATGGGCCAGCTTT

RC-M17 CCGGCACCCACGACGTTGTAAAACTGTGAAAT

RC-M18 TGTTATCCGGGAGAGGCGGTTTGCTCCACGCT

RC-M19 GGTTTGCCCCAGCAGGCGAAAATCAATCGGCC

RC-M20 AACGCGCGGCTCACAATTCCACACCCAGGGTT

RC-M21 TTCCCAGTGCTTCTGGTGCCGGAAGTGGGAAC

RC-M22 AAACGGCGGTAAGCAGATAGCCGAAACTGAAC

RC-M23 ACCCTGAAATTTGCCAGTTACAAATTCTAAGA

RC-M24 ACGCGAGGGCTGTCTTTCCTTATCAAGTAATT

RC-M25 GTACCGACAAAAGGTAATTCCAAG

RC-M26 AACGGGTAGAAGGCTTATCCGGTAATAAACAG

RC-M28 GTCGGATTCTCCACCAGGCA

RC-M30

AGCCGGAAGCCAGCTGCATTAATGCTGTTTGATGGTGTCTTCCTGTAGCCAGC

TTTAATCGATG

RC-M31

GCAAAATTCGGGAAACCTGTCGTGCATAAAGTGTAAAGCGATGTGCT

RC-M32 GCAAGGCGTTCGCCATTCAGGCTGCGCAACTG

RC-M33 GGAAGCGCTTTATCCCAATCCAAAAAGCAAAT

RC-M34

CAGATATATTAAACCATACGGAAATTACCCAAAAGAACTGGCATGATTA

RC-M35 AGGCATTTTCGAGCCAGTACTCATCG

RC-M36 AGAACAAGTACCGCGCCCAATAGCTAAGAAAC

RC-M39 CCTAATGAACTGCCCGCTTTCCAGCCCTTATA

RC-M40 AATCAAAAGAATAGCCCTTTAAATATGCATTCTACTA

RC-M41 GAGATAGGGTTGTCAGGATTAGAGAGTACCTATTCATT

RC-M42 TTGCGCTCGTGAGCTAACTCACATGATAGCCC

RC-M43 TATTACGCGGCGATCGGTGCGGGCGAGGATTT

RC-M44 CAGCCTTTGTTTAACGTCAAAAATTTTCAATT

RC-M45 GGAATCATCAAGCCGTTTTTATTTGTTATATA

RC-M46 TCGCCATATTTAACAACGTTGCGGGGTTTTAAGCCCAA

RC-M47 CCAACAGTGTGTGCCCGTATAAACAGTTAACCAGAGC

RC-M48 ACTATATGCTCCGGCTTAGGTTGGTCATCGTA

RC-M51 TAAAACATCTTTAATGCGCGAACTTAATTGCG

RC-M52 CTATTAGTCGCCATTAAAAATACCATAGATTA

RC-M53 GAGCCGTCTAGACTTTACAAACAATTCGACAA

RC-M54

AATCGCGCAAAAGAAGTTAGTTAGCTTAAACAGCTTGATACGCCCACGC

RC-M55 TTTTTAACTAAATGCTGATGCAAAATTGAGAA

RC-M56 CAAGACAAAAATCATAGGTCTGAGACAAACAT

RC-M59 CACCAGCAGGCACAGATTTAATTTCTCAATCATAAGGGAAC

RC-M60 TGCTGGTAATATCCAGAACAATATAAGCGTAA

RC-M61 GAATACGTGAAGATAAAACAGAGGATCTAAAA

RC-M62 TATCTTTAAAATCCTTTGCCCGAACCGCGACCTGC

RC-M63 CGAAACAAAGTAATAACGGA

RC-M64 TTCGCCTGCAAAATTAATTACATTAATAGTGA

RC-M65

ATTTATCAAGAACGCGAGAAAACTAGTATAAAGCCAATAAAGAATACAC

RC-M66 ATATGCGTTATACAAATTCTTACCTTTTCAAA

RC-M67 TATATTTTGACGCTGAGAAGAGTCTAACAATT

RC-M69 ATTTGTATCATCGCTTCTGAATTACAGTAACA

RC-M71 TCAGTATTAACCCTTCTGACCTGATACCGCCA

RC-M72 GCCATTGCAACAGGAAAAACGCTCTGGCCAAC

RC-M73 AGAGATAGAACACCGCCTGCAACAAAATCAAC

RC-M74 AGTAGAAAAGTTTGAGTAACATTA

RC-M75 TTTGGATTATACCTGATAAATTGTGTCGAAATCGTTATTA

RC-M76 GTACCTTTATTACCTTTTTTAATGCGATAGCT

RC-M77 TAGATTAAAGTTAATTCGATCTTCTTAGTATC

RC-M78 TCATAATTACTAGAAAAAGCCTGTTGACCTAA

RC-M79 ATTTAATGATCCTTGAAAACATAGGAAACAGT

RC-M80 ACATAAATACGTCAGATGAATATATGGAAGGA

RC-M81 ATTGAACCAATATAATCCTGATTGTCATTTTG

RC-M82 CGGAACAATATCTGGTCAGTTGGCGTGCCACG

RC-M83 CTGAGAGCAATAAAAGGGACATTCATGGAAAT

RC-M84 ACCTACATTTTGACGCTCAATCGTCAGTGCGC

RC-M85 CGACCAGTCAGCAGCAAATGAAAATCAAACCC

RC-M86 TCAATCAAAGAAACCACCAGAAGGATGATGGC

RC-M87 AATTCATCAACCATATCAAAATTATAGATTTT

RC-M88 CAGGTTTACAATATATGTGAGTGATTAATTTT

RC-M89 CCCTTAGAGTTTGAAATACCGACCCACCGGAA

RC-M90 AAAAGGGTAAGATTGTATAAGCAAAAATTCGC

RC-M91 AATAACCTTTAGAACCCTCATATAAAAGATTC

RC-M92 GAAAGACTCAATTCTGCGAACGAGAAATGGTC

RC-M93 CATAGTAATGACTATTATAGTCAGGGAAGCCC

RC-M94 TAACAAAGTTAGGAATACCACATTTTACGAGG

RC-M95 GCTGGCTGACCTTCATCAAGAGTAAATCAACG

RC-M96 GTTGAGATCTGCTCATTCAGTGAAGCGCATAG

RC-M97 CTTTACCCGAGCAACACTATCATAATTCATCA

RC-M98 TTGATTCCTCAAATATCGCGTTTTAATCAGGT

RC-M99 AAAAATTTGTTTAGCTATATTTTCTGTAACAG

RC-M100 AAAACAGGGAGAAAGGCCGGAGACGCAAGGAT

RC-M101 GTTAAATTTTTGTTAAATCAGCTCAAGCCCCA

RC-M102 CACCATCACGGTTGATAATCAGAAATTTTTTA

RC-M103 CGCGAGCTAAGCCTTTATTTCAACAGTCAAAT

RC-M104 CTTCAAAGTGGAAGTTTCATTCCAATTTGGGG

RC-M105 TTACCAGAATGACCATAAATCAAAAATTCGAG

RC-M106 GCCCTGACTATTACAGGTAGAAAGACCCTCGT

RC-M107 ACAGATGAACGGTGTACAGACCAGTAAGGCTT

RC-M108 AACAACATGAGAACACCAGAACGAGAAAGAGG

RC-M110 ACGGTGTCCGAACCAGACCGGAAGAGTTCAGA

RC-M112 ATGTACCCATATGATATTCAACCGAATACTTT

RC-M113 ACCAATAGGAACGCCATCAAAAATTCAATCAT

RC-M114

GATAAATTTCGTAAAACTAGCATGAATTCGCGTCTGGCTGTTCCGAAATCG

RC-M115 ATAGTAGTAACATTATGACCCTGTTTCTAGCT

RC-M116

CAAACTCCAACAGTTGAGTGTTGTTCGTAGAAGAACTCAAACTTTGAATGG

RC-M117 GAGGCTTTCTCAAATGCTTTAAAC

RC-M118 TTGGGCTTTACGTTAATAAAACGAAATAGCGA

RC-M119 CGAACTGACCAACTTTGTAGTAAA

RC-M120 GAAAAATCGAGATGGTTCAATATTTATCGGCCT

RC-M123 AACGGTAAAATGCCGGAGAGGGTAAATCGGTT

RC-M124 TTAAATGTGAGCGAGTAACAACTTAAGGAAACCGAGGAAA

RC-M125 CTGGAGCAAACAAGAGCATCAACA

RC-M126

CTGAATCTAAATCATACAGGCAAGTCAGAGCATGAAAGGGGCTGGGGTG

RC-M127

GGTAATAGGCGGAATCGTCATAAATTTAATTGCTCCTTTTCTTAATTG

RC-M128 TCATTGTGTTATACCAGTCAGGACCCAGAGGG

RC-M129 AACGAGGCGCAGACGGAACTTTAA

RC-M130 CTGGCTCAAATTACCTTATGCGATAATGACAA

RC-M132 GCTTAGAGGATAAGAGGTCATTTTTGAAACAT

RC-M134 CTGAGAGTCTACAAAGGCTATCAGACTTGAGC

RC-M135 CATTTGGGATTATCACCGTCACCGGTCATTGC

RC-M136 CTCAGAGCACCGCCACCCTCAGAGATTAAGCA

RC-M137 GAAAGTATTCGGAACCTATTATTCTGCGGATG

RC-M138 CCACAGACACAAACTACAACGCCTGATAGCGT

RC-M139 CAACCATCCGATAGTTGCGCCGACTTTAAGAA

RC-M140

ATAACCGATCATCTTTGACCCCCAGCGATTATACCAAGTTCATGTTACTTAGC

CGG

RC-M142 TGCCTATTTAAGAGGCTGAGACTCGAGTTTCG

RC-M144 AAAGGTGAAATTAGAGCCAGCAAAAGCCGCCA

RC-M145 CGCAATAATAACGGAATATTCATT

RC-M146 TAGCACCAAAATATTGTAGTACCGCAATAAGAGAATATAAA

RC-M147 CGCCGCCAGAACCGCCTCCCTCAGATCACCAG

RC-M148 CTAAAGTTCATGTACCGTAACACTCTCAAGAGAAGGATTAGGATTA

RC-M149

TAAAACACTATATTCGGTCGCTGATTTCGAGGAGAATTTCGTAACGAT

RC-M150

GGGAGTTAAACGAAAGAGGCGTCGCTCAACAGTAGGGCTTATCCAATCG

RC-M153

AGACTCCTTTGAGGGAGGGAAGGTTTACCATTAGCAAGGCACCAGAGC

RC-M154 AGTATGTTAGCAAACGTAGAAAATGCGCCAAA

RC-M155 TCACCAATGGCGACATTCAACCGATATTACGC

RC-M156 TCAGACGAAATCAAAATCACCGGACGGAAACG

RC-M157 CCAGGCGGTTTTAACGGGGTCAGTGAGGCAGG

RC-M158 AATGAATTCATTTTCAGGGATAGCGCTCAGTA

RC-M159 TTTTGCGGGAGCCTTTAATTGTATCGTTAGTA

RC-M160 GCCACTACGAAGGCACCAACCTAAAAGGCCGC

RC-M161 TCCAAAAGGATCGTCACCCTCAGCTACGTAAT

RC-M162 ACCACCCTTTCTGTATGGGATTTTAAAAAGGC

RC-M163 GTAATAAGATAAGTGCCGTCGAGATCAGAGCC

RC-M164 CTTTTCATTTGGCCTTGATATTCAGTGTACTG

RC-M165 GACAAAAGGAAACCATCGATAGCATTTGCCAT

RC-M166 AAAGGTGGCAACATATAAAAGAAACACAATCA

RC-M167 ATCAGTAGTTCATATGGTTTACCAACATACAT

RC-M168 TGGATCTTAGCCCCCTTATTAGCGGCACCGTA

RC-M169 ATAAGTATTTTTGATGATACAGGACAAACGAA

RC-M170 ACTTTCAACTCAGAACCGCCACCCGGGTTGAT

RC-M171 ACAGCATCGTTGAAAATCTCCAAAGCTAAACA

RC-M172 GAAGTTTCCATTAAACGGGTAAAAAGCGAAAG

RC-M173 TTTTTCACGGAACGAGGGTAGCAATTCATGAG

RC-M174 CCGCCACCCAGTTTCAGCGGAGTGATAATAAT

RC-M175 TACATGGCAGCCCGGAATAGGTGTCCTCAGAA

RC-M176 TCGGTCATCATTAAAGCCAGAATGAAGCGTCA

RC-M177 ATAGAAAACGACAGAATCAAGTTTCGGCATTT

RC-M27-AS CCATATTAATTAGACGGGAGAATTACAAAGTTACC

RC-M29-AS AAGCGCCAATTAAGTTGGGTAACGAACATACG

RC-M37-AS GATTTTTTACAGAGAGAATAACATAAAAACAG

RC-M38-AS TTGGGAAGCAGCTGGCTTAAAGCTAGCTATTTTTGAGAGAT

RC-M49-AS ACCTGAGCAGAGGCGAATTATTCAGAAAATAG

RC-M50-AS AGAAGTATAATAGATAATACATTTCTCTTCGC

RC-M57-AS CAAGAAAAATTGCTTTGAATACCAAGTTACAA

RC-M58-AS CTCGTATTGGTGCACTAACAACTAGAACGAAC

RC-M68-AS TGATTTGATACATCGGGAGAAACACAACGGAG

RC-M70-AS ATTTTAAAGGAATTGAGGAAGGTTTGAGGCGG

RC-M109-AS AAACGAGACGACGATAAAAACCAAACTAACGG

RC-M111-AS TGCGGGAGGAAAAGGTGGCATCAAACTAAAGT

RC-M121-AS GAATCCCCTGCAAAAGAAGTTTTGGTTGGGAA

RC-M131-AS CCAATACTTAAAATGTTTAGACTGGTAGCATT

RC-M133-AS ATAAAGCCGCAAAGAATTAGCAAACCACCACC

RC-M141-AS TCACCAGTAGCCCTCATATGATGAAAGACTACC

RC-M143-AS CCCTCAGACGCCACCAGAACCACCATGCCCCC

RC-M122-AS

GTACCAAAAGCATTAACATCCAATGGTGCTGTAGCTCAACATGTTT

RC-M151-AS

TAGGAACCTTGTCGTCTTTCCAGACGGTTTATCAGCTTGCGGCTTGCA

RC-M152-AS

CACCACCGGCATTGACAGGAGGTTGCCTTGAGTAACATAATTTAGGCAG

Modified DNA sequences corresponding to the design of Figure 1:

Loop GQ1

TAACCTTGCTTCTGTTTTTGGGTTAGGGTTAGGGTTAGGGTTTTTAATCGTCGC

TATTAA

Loop GQ2

TAGCACGTAAAACATTTTTGGGTTAGGGTTAGGGTTAGGGTTTTTAATAAAGA

AATTGCG

Loop GQ3

GCGGAATTATCATCTTTTTGGGTTAGGGTTAGGGTTAGGGTTTTTATTCCTGA

TTATCAG

Loop GQ4

TCTAAAGCATCACCTTTTTGGGTTAGGGTTAGGGTTAGGGTTTTTGCTGAACC

TCAAATA

Blunt RE1 TTTTGTTAAATAAGAATAAAGTGTGATAAATAAGGCTTTT

Blunt RE6 TTTTACATTGGCAGATTCACCTGAAATGGATTATTTTTTT

Loop Complementary G1

CCTAACCCTTTTTTGAGTAATGTGTAGGTTTTTAAATGCAATGCCTTTTT

Loop Complementary G2

CCTAACCCTTTTTTATTAGATACATTTCGCTAGATTTAGTTTGACCTTTTT

Loop Complementary G3

CCTAACCCTTTTTTATCAAAAAGATTAAGAAAGCAAAGCGGATTGCTTTTT

Loop Complementary G4

CCTAACCCTTTTTTATAACGCCAAAAGGAACAACTAATGCAGATACTTTTT

Blunt DE1 TTTTCGTTAATATTTTGTTAATATTTAAATTGTAAATTTT

Blunt DE6 TTTTGGATATTCATTACCCAATCTTCGACAAGAACCTTTT

Modified DNA sequences corresponding to the design of Figure 4:

Linear GQ1

GGGTTAGGGTTAGGGTTAGGGTTTTAAATCGTCGCTATTAAATAACCTTGCTT

CTGTTTT

Linear GQ2

GGGTTAGGGTTAGGGTTAGGGTTTTAAATAAAGAAATTGCGTTAGCACGTAA

AACAGTTT

Linear GQ3

GGGTTAGGGTTAGGGTTAGGGTTTTTATTCCTGATTATCAGAGCGGAATTATC

ATCATTT

Linear GQ4

GGGTTAGGGTTAGGGTTAGGGTTTTTGCTGAACCTCAAATAATCTAAAGCATC

ACCTTTT

Linear Complementary G1

CCTAACCCTTTTTTGAGTAATGTGTAGGTTTTTAAATGCAATGCCTTTTT

Linear Complementary G2

CCTAACCCTTTTTATTAGATACATTTCGCTAGATTTAGTTTGACCTTTTT

Linear Complementary G3

CCTAACCCTTTTTATCAAAAAGATTAAGAAAGCAAAGCGGATTGCTTTTT

Linear Complementary G4

CCTAACCCTTTTTATAACGCCAAAAGGAACAACTAATGCAGATACTTTTT

Blunt DE1 TTTTCGTTAATATTTTGTTAATATTTAAATTGTAAATTTT

Blunt DE6 TTTTGGATATTCATTACCCAATCTTCGACAAGAACCTTTT

Blunt RE1 TTTTGTTAAATAAGAATAAAGTGTGATAAATAAGGCTTTT

Blunt RE6 TTTTACATTGGCAGATTCACCTGAAATGGATTATTTTTTT

Modified DNA sequences corresponding to design in Figure S6 (G3):

Blunt RE1 TTTTGTTAAATAAGAATAAAGTGTGATAAATAAGGCTTTT

Short G LEFT1

ATAACCTTGCTTCTGTTTTTTGGGTTAGGGTTTTTAAATCGTCGCTATTAA

Short G LEFT2

TTAGCACGTAAAACAGTTTTTGGGTTAGGGTTTTTAAATAAAGAAATTGCG

Short G LEFT3

AGCGGAATTATCATCATTTTTGGGTTAGGGTTTTTTATTCCTGATTATCAG

Short G LEFT4

ATCTAAAGCATCACCTTTTTTGGGTTAGGGTTTTTTGCTGAACCTCAAATA

Blunt RE6 TTTTACATTGGCAGATTCACCTGAAATGGATTATTTTTTT

Blunt DE1 TTTTCGTTAATATTTTGTTAATATTTAAATTGTAAATTTT

Short G RIGHT1

TTTTAAATGCAATGCCTTTTTGGGTTAGGGTTTTTTGAGTAATGTGTAGGT

Short G RIGHT2

TAGATTTAGTTTGACCTTTTTGGGTTAGGGTTTTTATTAGATACATTTCGC

Short G RIGHT3

AAGCAAAGCGGATTGCTTTTTGGGTTAGGGTTTTTATCAAAAAGATTAAGA

Short G RIGHT4

CAACTAATGCAGATACTTTTTGGGTTAGGGTTTTTATAACGCCAAAAGGAA

Blunt DE6 TTTTGGATATTCATTACCCAATCTTCGACAAGAACCTTTT

Modified DNA sequences corresponding to design in Figure S6 (G9):

Blunt RE1 TTTTGTTAAATAAGAATAAAGTGTGATAAATAAGGCTTTT

Full G LEFT1

ATAACCTTGCTTCTGTTTTGGGGGGGGGTTTTGGGGGGGGGTTTAAATCGTCG

CTATTAA

Full G LEFT2

TTAGCACGTAAAACAGTTTGGGGGGGGGTTTTGGGGGGGGGTTTAAATAAAG

AAATTGCG Full G LEFT3

AGCGGAATTATCATCATTTGGGGGGGGGTTTTGGGGGGGGGTTTTATTCCTGA

TTATCAG

Full G LEFT4

ATCTAAAGCATCACCTTTTGGGGGGGGGTTTTGGGGGGGGGTTTTGCTGAAC

CTCAAATA

Blunt RE6 TTTTACATTGGCAGATTCACCTGAAATGGATTATTTTTTT

Blunt DE1 TTTTCGTTAATATTTTGTTAATATTTAAATTGTAAATTTT

Full G RIGHT1

TTTTAAATGCAATGCCTTTGGGGGGGGGTTTTGGGGGGGGGTTTTGAGTAATG

TGTAGGT

Full G RIGHT2

TAGATTTAGTTTGACCTTTGGGGGGGGGTTTTGGGGGGGGGTTTATTAGATAC

ATTTCGC

Full G RIGHT3

AAGCAAAGCGGATTGCTTTGGGGGGGGGTTTTGGGGGGGGGTTTATCAAAAA

GATTAAGA

Full G RIGHT4

CAACTAATGCAGATACTTTGGGGGGGGGTTTTGGGGGGGGGTTTATAACGCC

AAAAGGAA

Blunt DE6 TTTTGGATATTCATTACCCAATCTTCGACAAGAACCTTTT

REFERENCES

1. P. W. K. Rothemund, Nature, 2006, 440, 297-302.

2. B. Q. Ding, Z. T. Deng, H. Yan, S. Cabrini, R. N. Zuckermann and J. Bokor, J Am Chem Soc, 2010, 132, 3248.

3. R. Schreiber, N. Luong, Z. Y. Fan, A. Kuzyk, P. C. Nickels, T. Zhang, D. M. Smith, B. Yurke, W. Kuang, A. O. Govorov and T. Liedl, Nat Commun, 2013, 4.

4. H. Bui, C. Onodera, C. Kidwell, Y. Tan, E. Graugnard, W. Kuang, J. Lee, W. B. Knowlton, B. Yurke and W. L. Hughes, Nano Lett, 2010, 10, 3367-3372.

5. R. Wang, C. Nuckolls and S. J. Wind, Angew Chem Int Ed Engl, 2012, 51, 11325-11327.

6. S. H. Ko, K. Du and J. A. Liddle, Angew Chem Int Ed Engl, 2013, 52, 1193-1197.

7. S. M. Douglas, I. Bachelet and G. M. Church, Science, 2012, 335, 831-834.

8. J. Fu, Y. R. Yang, S. Dhakal, Z. Zhao, M. Liu, T. Zhang, N. G. Walter and H. Yan, Nat Protoc, 2016, 11, 2243-2273.

9. W. Liu, H. Zhong, R. Wang and N. C. Seeman, Angew Chem Int Ed Engl, 2011, 50, 264-267.

10. F. Zhang, S. Jiang, S. Wu, Y. Li, C. Mao, Y. Liu and H. Yan, Nat Nanotechnol, 2015, 10, 779-784.

11. W. Liu, J. Halverson, Y. Tian, A. V. Tkachenko and O. Gang, Nat Chem, 2016, 8, 867-873.

12. S. M. Douglas, H. Dietz, T. Liedl, B. Hogberg, F. Graf and W. M. Shih, Nature, 2009, 459, 414-418.

13. F. Hong, S. X. Jiang, T. Wang, Y. Liu and H. Yan, Angew Chem Int Edit, 2016, 55, 12832-12835.

14. H. T. Maune, S. P. Han, R. D. Barish, M. Bockrath, W. A. Goddard, P. W. K. Rothemund and E. Winfree, Nature Nanotechnology, 2010, 5, 61-66.

15. X. Shen, C. Song, J. Wang, D. Shi, Z. Wang, N. Liu and B. Ding, J Am Chem Soc, 2012, 134, 146.

16. C. Zhou, X. Duan and N. Liu, Nature Communication, 2015, 6, 8102.

17. E. M. Roller, L. K. Khorashad, M. Fedoruk, R. Schreiber, A. O. Govorov and T. Liedl, Nano Lett, 2015, 15, 1368.

18. P. Wang, S. Gaitanaros, S. Lee, M. Bathe, W. M. Shih and Y. Ke, J Am Chem Soc, 2016, 138, 7733.

19. P. Zhan, P. K. Dutta, P. Wang, G. Song, M. Dai, S. X. Zhao, Z. G. Wang, P. Yin, W. Zhang, B. Ding and Y. Ke, ACS Nano, 2017, 11, 1172.

20. E. Winfree, F. R. Liu, L. A. Wenzler and N. C. Seeman, Nature, 1998, 394, 539-544.

21. C. Mao, W. Sun, Z. Shen and N. C. Seeman, Nature, 1999, 397, 144-146.

22. Z. W. Dai, H. M. Leung and P. K. Lo, Small, 2017, 13.

23. Y. Suzuki, M. Endo, Y. Y. Yang and H. Sugiyama, Journal of the American Chemical Society, 2014, 136, 1714-1717.

24. N. Wu and I. Willner, Nano Letters, 2016, 16, 6650-6655.

25. N. Wu and I. Winner, Nano Letters, 2016, 16, 2867-2872.

26. N. Wu and I. Willner, Nanoscale, 2017, 9, 1416-1422.

27. M. Y. Kim, M. Gleason-Guzman, E. Izbicka, D. Nishioka and L. H. Hurley, Cancer Res, 2003, 63, 3247-3256.

28. R. Hansel-Hertsch, M. Di Antonio and S. Balasubramanian, Nat Rev Mol Cell Bio, 2017, 18, 279-284.

29. M. Endo and H. Sugiyama, Accounts Chem Res, 2014, 47, 1645-1653.

30. L. Olejko, P. J. Cywinski and I. Bald, Angew Chem Int Ed Engl, 2015, 54, 673-677.

31. L. Olejko, P. J. Cywinski and I. Bald, Nanoscale, 2016, 8, 10339-10347.

32. A. Kuzuya, Y. Sakai, T. Yamazaki, Y. Xu and M. Komiyama, Nat Commun, 2011, 2, 449.

33. A. Siddiqui-Jain, C. L. Grand, D. J. Bearss and L. H. Hurley, Proc Natl Acad Sci U S A, 2002, 99, 11593-11598.

34. D. Bhattacharyya, G. Mirihana Arachchilage and S. Basu, Front Chem, 2016, 4, 38.

35. G. N. Parkinson, M. P. Lee and S. Neidle, Nature, 2002, 417, 876-880.

II. CONTROL OF THE STEPWISE ASSEMBLY-DISASSEMBLY OF DNA ORIGAMI NANOCLUSTERS BY PH STIMULI-RESPONSIVE DNA TRIPLEXES

Shuo Yang,[a] Wenyan Liu[a,b] and Risheng Wang[*a]

[a]Department of Chemistry,
Missouri University of Science and Technology, Rolla, MO 65409, USA

[b]Center for Research in Energy and Environment,
Missouri University of Science and Technology, Rolla, MO 65409, USA

ABSTRACT

We present the pH-triggered reversible assembly of DNA origami clusters in a stepwise fashion. The structure formation and dissociation are controlled by a series of consecutive pH-stimulation processes that rely on the triplex-to-duplex transition of DNA triplexes in different pH conditions. This multilevel dynamic assembly strategy brings more structural complexity and provides the possibility of developing intelligent materials for engineering applications.

Key words: DNA triplex, DNA origami, stimuli-responsive assembly

1. INTRODUCTION

Living systems represent the most efficient and adaptable example of the stepwise assembly of functional macromolecules in response to external and internal stimuli and, in some cases, these assemblies can also disassemble into their individual components when triggered by other signals.[1] For example, the stepwise assembly of multiple protein

subunits into DNA polymerase III holoenzyme, under successive physiological stimuli, is a key to ensure that DNA replicates in high fidelity and high processivity.[2] In view of the sophisticated self-assembly process and intriguing functional abilities of biological systems, the mimicking of their stimuli-responsive reversible assembly/disassembly behavior, through use of synthetic biomolecules, has proven to be one of the most promising, yet challenging aspects of nanoscience. Benefited by its superior programmability (as per Watson–Crick base paring), DNA has been widely utilized for the self-assembly of a diversity of pre-designed 2D and 3D DNA nanostructures.[3–12] This makes DNA a well-suited candidate for creating dynamic reconfigurable assembly systems.[13–16] The self-assembly of stimuli-responsive DNA architectures, in a stepwise fashion, could endow conventional static DNA structures with defined geometry, and novel capabilities in sensing, monitoring, and dynamic controls in the areas of nanodevices, matematerials, and nanomedicine.

Recently, extensive research efforts have been devoted to exploring the reversible multimerization of DNA origami nanostructures in response to various external stimuli.[17–25] Examples include the reversible assembly of hexagon-shaped DNA origami controlled by photoirradiation between UV and visible light,[17] and the K^+-ion stimulated assembly of DNA origami dimers by use of G-quadruplexes.[21,25] Recently, the reconfiguration of DNA origami dimers and trimers have been achieved based on pH-sensitive i-motif, and triplex DNA,[18] in which the DNA origami trimers assembled under neutral conditions could transit into a mixture of dimers and monomerswhen the assemblies were subjected to either acidic or basic conditions. Those pioneering studies on the dynamic assembly of DNA structures in response to a single-step stimulus

between a two-state transition have inspired us to design a consecutive multi-step transition system, which was induced by multiple steps of environmental stimulation that is able to reversibly and selectively create complicated and larger DNA nanostructures (>5 units). The realization of such a dynamic and elegant fabrication process will extend our capabilities to synthesize intelligent biomaterials with well-defined structures, which represent one step forward towards the imitation of designs and processes that are found in nature.

In this study, we present the pH-regulated, multistep cyclic self-assembly of DNA origami nanoclusters by employing DNA triplexes as dynamic linkers (Figure 1). The DNA triplex is formed by the interaction between a pH-insensitive Watson–Crick duplex and a single-stranded DNA (ssDNA) through pH-sensitive parallel Hoogsteen base-pairing.[26,27] The triplex-to-duplex (closing-to-opening) transition is strongly pH dependent, and its pH sensitivity can be regulated by manipulating the ratio of C-G·C vs. T-A·T in the DNA sequence because C-G·C triplets prefer acidic pH and T-A·T triplets favor a neutral pH.[27] As such, it is possible to allow the triplex-to-duplex transition to take place in a desired pH range. In an opening state, the ssDNA domain of the DNA triplexes is available for complementary DNA hybridization, linking components together, while refolding the DNA triplex will disrupt this complementary pairing, and lead to dissociation of the components. Compared with the two-state transition of i-motif occurring within a narrow pH range,[18,28] DNA triplexes are more tunable for awide range of pH response, thereby providing opportunities for multiple-step regulation. Here, we tested the selective assembly/disassembly of DNA origami trimers and more complex nine-unit DNA origami clusters, in a stepwise fashion, based on DNA triplexes in

response to three different pH environments. The reversible control of the association/dissociation of the nanoclusters is demonstrated by AFM images and gel analysis.

2. EXPERIMENTAL DETAILS

2.1. MATERIALS

All chemicals including agarose, magnesium acetate, acetic acid, sodium hydroxyl, hydrogen chloride, were purchased from Sigma and used as received without further purification. All chemically synthesized DNA strands were purchased from Integrated DNA Technologies, Inc. (www.Idtdna.com). The unmodified staple DNA strands were ordered in a 96-well plate format, suspended in ultrapure water without purification. All modified strands were purified with PAGE. A circular single-stranded M13mp18 DNA genome was ordered from Bayou Biolabs. The DNA origami purification column (100kDa MWCO centrifuge filter) was purchased from Pall, Inc.

2.2. THE FORMATION OF CROSS-SHAPED DNA ORIGAMI UNIT

The cross-shaped DNA origami was assembled by a slow cooling method. Specifically, M13mp18 viral DNA and all of the staple strands were mixed together at a ratio of 1:5, in a 1×TAE buffer solution containing 40 mM Tris-HCl, 20 mM of acetic acid, 2 mM of EDTA, and 11.5 mM of magnesium acetate. The mixture was slowly cooled from 90℃ to 15℃ over 12h in a thermocycler (BIO-RAD). The final concentration of M13mp18 DNA in the solution was 20 nM. The DNA origami was then purified to remove excess staple strands, using 100kDa MWCO centrifuge filters.

2.3. THE ASSEMBLY-DISASSEMBLY OF DNA ORIGAMI DIMER

The assembly/disassembly of DNA origami dimer (A1/A2) between pH = 5.0 and pH = 7.5: the prepared DNA origami monomers were mixed at a molar ratio of 1:1 in a 1×TAE buffer solution (pH = 5.0) containing 10 mM of magnesium acetate. Then, the mixture was adjusted to pH=7.5, and annealed from 38℃ to 25℃ at a rate of 2.1℃/h to form the corresponding DNA origami dimers. In order to disassembly of DNA origami dimer, the pH value of the dimer solution was adjusted from 7.5 to 5 by column exchange in a 1×TAE buffer with 10 mM Mg^{2+}, then incubated at room temperature for 6h. The assembled/disassembled DNA dimer was directly used for AFM images, and gel electrophoretic characterization without further purification. The association/dissociation of the DNA origami dimer was performed by further buffer exchange following the same incubation step as the aforementioned procedure. The same process was followed for assembly/disassembly of the dimer (A2/A3), except the pH values changed to between pH = 7.5 and pH = 9.0.

2.4. THE ASSEMBLY-DISASSEMBLY OF DNA ORIGAMI TRIMER

Stepwise upstream assembly process of DNA origami trimer (pH: 5.0 -7.5 – 9.0).

The prepared three DNA origami monomers (A1, A2, and A3) were mixed at a molar ratio of 1:1:1 in a 1×TAE buffer solution (pH = 5.0) containing 10 mM of magnesium acetate.

Then the mixture was adjusted to pH=7.5, and annealed from 35℃ to 25℃, at a rate of 0.8/h to form DNA origami dimers by activating the sticky end interaction in DNA triplex set T1.

Next, the centrifuge column was used to exchange the buffer solution to pH = 9.0. Then the mixture was re-annealed from 30℃ to 25℃ at a rate of 0.8℃/h to form a DNA origami trimer through activating the sticky end interaction in DNA triplex set T2 (73%TAT). The assembled DNA origami trimers were then directly imaged by AFM without further purification.

Stepwise downstream disassembly process of DNA origami trimer (pH: 9.0 - 7.5 – 5.0).

The prepared DNA origami monomers were mixed at a molar ratio of 1:1:1 in a 1×TAE buffer solution (pH = 9) containing 10 mM of magnesium acetate.

Then the mixture was annealed from 35℃ to 25℃ at a rate of 0.8℃/h to form DNA origami trimer through activating the sticky end interaction in both DNA triplexes T1 (20%TAT) and T2 (73%TAT). The dissociation of the trimers was allowed to proceed for 6 h at room temperature after changing the pH value to 7.5 through deactivating the sticky end in DNA triplex set T2 (73%TAT) only.

With further adjustment of the pH value to 5 with another 6h incubation at room temperature, the trimers could be totally separated into monomers with the deactivation of sticky end interaction in both DNA triplex T1 (20%TAT), and T2 (73%TAT).

2.5. THE FORMATION OF 9-TILE DNA ORIGAMI

The prepared DNA origami monomers (A4, A5, and A6) were mixed at a molar ratio of 1:4:4 in a 1×TAE buffer solution (pH = 5.0) containing 10 mM of magnesium acetate. Then the mixture was adjusted to pH=7.5, annealed from 50℃ to 25℃ at a rate of 2℃/h by selectively bridging titles A4 and A5 together to form 5-tile DNA origami

through DNA triplex set T1, while keeping DNA title A6 as a monomer. Next, the centrifuge column was used again to exchange the buffer solution to pH = 9.0. The mixture was reannealed from 45℃ to 25℃ at a rate of 3.3℃/h to form a 9-tile DNA origami by bridging title A6 to preformed 5 title units through DNA triplex set T2.

2.6. THE DISASSEMBLY OF 9-TILE DNA ORIGAMI

First, the prepared DNA origami monomers were mixed at a molar ratio of 1:4:4 in a 1×TAE buffer solution (pH = 9) containing 10 mM of magnesium acetate. Then the mixture was annealed from 45℃ to 25℃ at a rate of 1.2℃/h to form 9-tile DNA origami. Second, adjusting the pH value to 7.5, and incubating at room temperature for 6h, 9-tile DNA origami units could be dissociated to 5-tile DNA origami units, and monomer units through deactivating the sticky end cohesion in 73%TAT triplex (T2). By further adjusting the pH value to 5.0, and incubating another 6h at room temperature, the 5-tile DNA origami disassembled to monomers through deactivating the sticky end in 20%TAT DNA triplexes (T1).

2.7. AFM IMAGING

The AFM images of DNA origami were obtained through spotting each sample (3 μl) onto freshly cleaved muscovite mica (Ted Pella, Inc.) for 15 s. After the fixation of the targeted structure of DNA origami on mica surface, doubly distilled H2O (20-30 ul) was placed quickly on the mica to remove the buffer salts, the drop was wicked off, and the sample was dried with compressed air. Atomic force imaging was done by utilizing Nanoscope III (Digital Instruments) tapping in air; with ultra-sharp 14 series (NSC 14) tips that had been purchased from NANOANDMORE.

2.8. AGAROSE GEL ELECTROPHORESIS

For the agarose gel under pH =5.0 and 7.5; the samples were loaded into 0.8% agarose gel with adjusted pH values that contained 5 mM Mg $(CH_3COO)_2$ in a 1×TAE buffer solution under 55V at room temperature. For the agarose gel under pH =9, the concentration of $Mg(CH_3COO)_2$ was changed to 2 mM. The gel was stained with ethidium bromide for visualization.

2.9. DYNAMIC LIGHT SCATTERING

The size distribution of DNA origami nanostructures was measured with a DLS analyzer (Zetasizer ZS90, Malvern, UK). The DNA origami was diluted to 10 nM by a 1× TAE buffer with 10 mM Mg^{2+} and injected into a 70 uL plastic cuvette to measure the size distributions. This procedure was repeated three times.

3. RESULTS AND DISCUSSION

Figure 1 shows a schematic illustration of in situ stepwise assembly/disassembly of DNA origami trimers. Two different types of intramolecular DNA triplexes, which stimulate the proposed multi-state transitions of the DNA origami trimers, are involved. The right arm of tile A1 is modified with four strands of DNA triplex set (T1) containing 20% T-A·T, while the right arm of tile A2 is attached with four strands of DNA triplex set (T2) containing 73% T-A·T (triplex-to-duplex transition occurring at pH = ∼7.5 and pH = ∼9.0 respectively).[26] Both types of DNA triplexes contain sticky ends (dashed line), which are complementary to the ssDNA overhangs, T1’ and T2’, decorated at the left arms of tiles A2 and A3, respectively. The prepared three DNA origami monomers (A1,

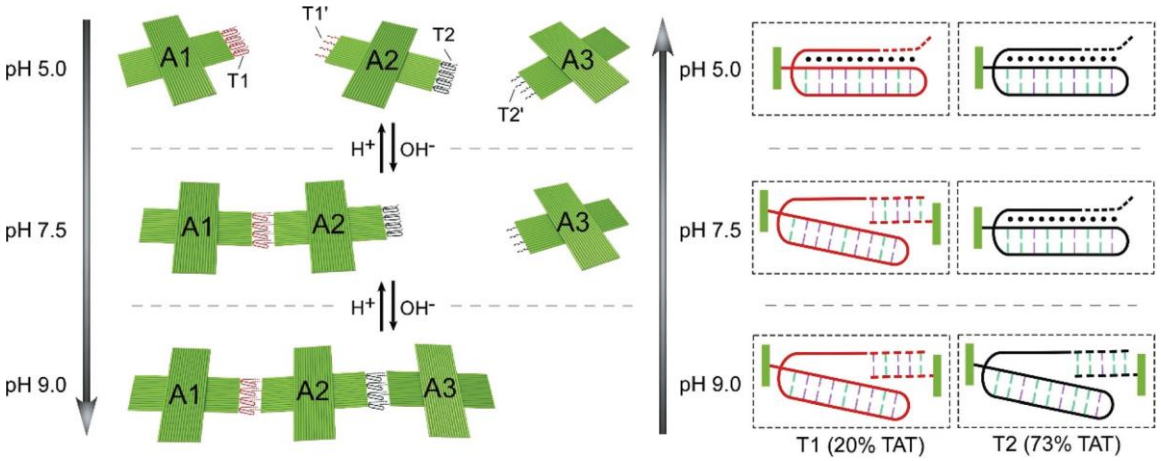

Figure 1. Schematic drawing of the pH-stimulated stepwise assembly/disassembly of DNA origami trimer. The three-state transition of DNA origami (monomer–dimer–trimer) is triggered by the pH-dependent DNA triplexes in response to three different pH environments.

A2, and A3) were mixed at a molar ratio of 1:1:1 in a 1× TAE buffer solution (pH = 5.0) containing 10 mM of magnesium acetate. At pH = 5.0, both T1 and T2 preferentially form intramolecular triplexes (folded state) and limit the cohesion ability of their sticky ends, thereby keeping DNA origami A1, A2, and A3 unhybridized in solution. As the pH value is increased from 5.0 to 7.5, DNA triplex sets T1 and T2 respond differently: T1 dissociates and, thus, releases the sticky ends on tile A1, which then bind to their complementary partners (T1′) on tile A2. This results in the formation of A1/A2 dimers after thermal annealing from 35 °C to 25 °C over 12 h while, on the other hand, T2 still remains folded due to high T-A·T content (73%), leaving the tile A3 monomer alone. When the pH value is further increased to 9.0, A1/A2/A3 trimers can be formed through sticky-end association between dimer A1/A2 and tile A3, that results from the unfolding of DNA triplex T2 and, thereby, causes release of the sticky ends on tile A2. This assembly system can also be reconfigured in reverse via a decrease of pH back to neutral,

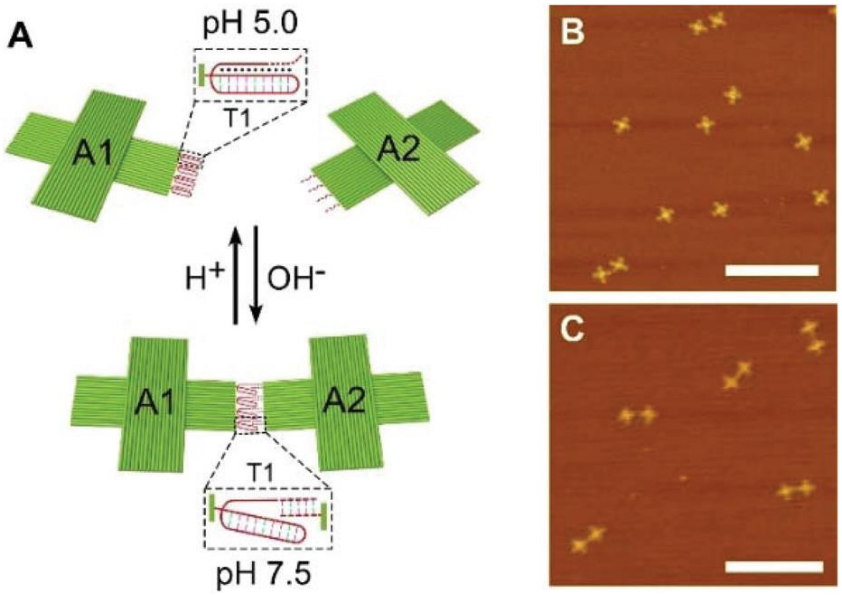

Figure 2. DNA triplexes (20% T-A·T) – driven assembly/disassembly of DNA origami dimer A1/A2. (A) Schematic drawing of the pH-stimulated cyclic assembly of DNA origami dimers through DNA triplex set T1 between pH 5.0 and 7.5. (B) AFM images of DNA origami monomer at pH = 5.0 and dimer at pH = 7.5 (C). Scale bars: 500 nm.

and further to an acidic condition, allowing the origami trimers to dissociate into dimers and further into monomers, once again.

As proof-of-principle, the reversible assembly of two DNA origami dimers (A1/A2 and A2/A3), triggered by DNA triplex sets, T1 and T2, respectively, was first tested. In the case of A1/A2 dimer, as shown in Figure 2, at pH = 5.0, the hybridization between tile A1 and tile A2 is inhibited due to the strong stability of DNA triplex T1. In contrast, changing the pH to 7.5 causes the destabilization of Hoogsteen interactions in the DNA triplexes, thereby, triggering two origami monomers to associate into the dimer structures (A1/A2). Figure 2B and C show the resulting origami monomers and dimers observed at pH 5.0 and pH 7.5, respectively. The statistical analysis of the atomic force microscopy (AFM) images reveals that ~87% DNA origami tiles are present in a dimeric

form at pH 7.5 (see Figure S1 and Table S1†). Similarly, the DNA triplex T2 guided reversible monomer – dimer transition of another origami pair, A2/A3, was also examined. The AFM image analysis, as shown in Figure S2,† presents a reversible transition from the monomer tiles (at pH 7.5) to the dimers (A2/A3, at pH 9.0), with a ~86% of dimer formation yield (Table S2†). In order to increase the targeted dimer yield, the thermal annealing process was employed after the pH triggered unfolding of DNA triplexes. According to our agarose gel analysis, the annealing process enhances the dimer (A1/A2) yield from ~75% to ~89%, when the mixture of A1 and A2 is annealed from 38 °C to 25 °C, instead of incubating at room temperature for 6 h (Figure S3†). However, for the dissociation process, the annealing procedure is not required because of the formation of stabilized DNA triplexes after changing the pH.[29–31] Together, these results confirm that the DNA triplex-assisted assembly of each DNA origami dimer works effectively in response to their corresponding pH environment.

Next, the reversible three-state transition (monomer–dimer–trimer) of a three-tile origami system (A1, A2, and A3), regulated by the conformation change of DNA triplex sets T1 and T2 together, was investigated (Figure 1). Figure 3A–C show the representative AFM images of the resulting productions generated at pH = 5.0, 7.5, and 9.0, respectively. It can be seen that a majority of DNA origami tiles, at pH 5.0, remain as monomers. When the pH increases to 7.5, as expected, a mixture of dimers (A1/A2) and monomers (A3) yields. Upon further increase of pH to 9.0, linear origami trimer structures (A1/A2/A3) start to appear (Figure 3C and Figure S4†). The cross-section analysis of DNA origami monomer, dimer, and trimer are shown in Figure S5†, their corresponding sizes are consistent with our design. The stepwise reversible assembly

process of DNA origami trimers is also demonstrated by gel electrophoresis. As can be seen in Figure 3D, along with an increase in pH, from 5.0 to 7.5, and further to 9.0, the targeted bands exhibit a slower and slower electrophoretic mobility corresponding to the

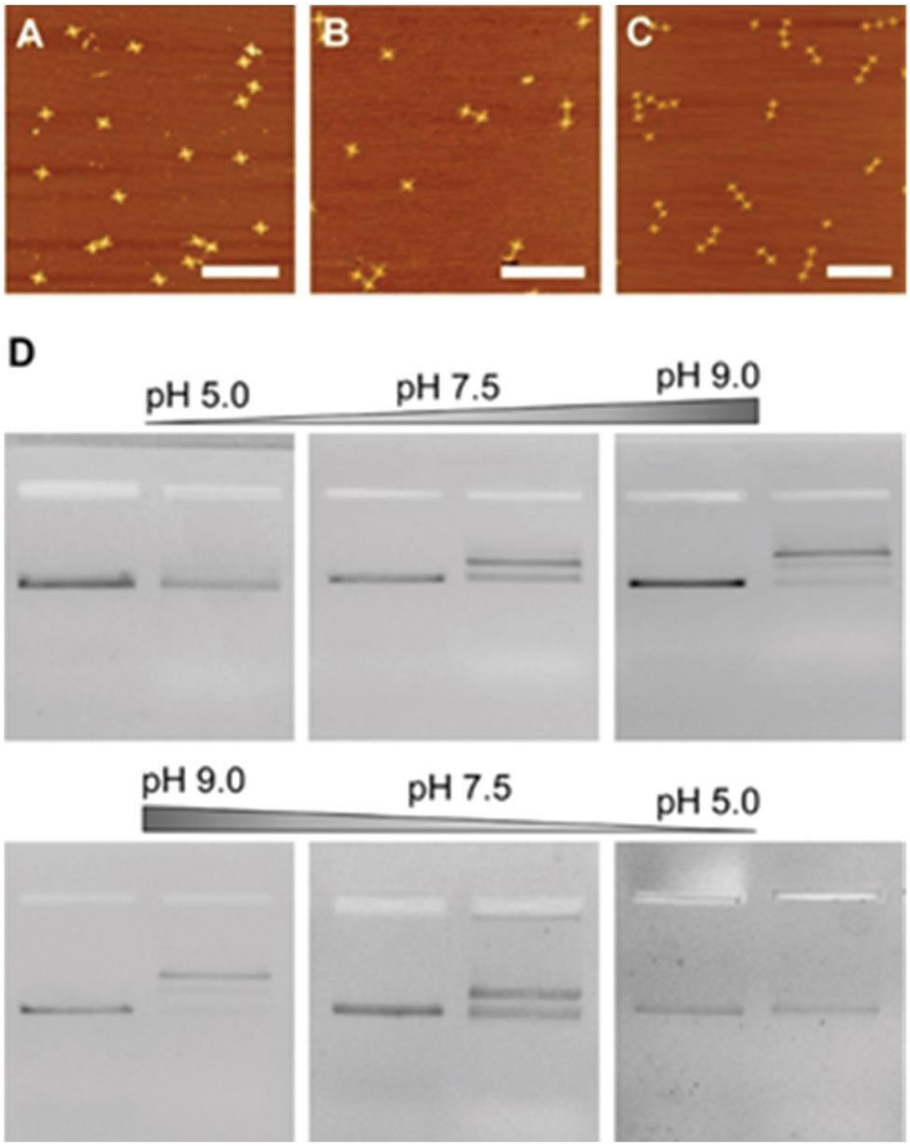

Figure 3. pH-Stimulated stepwise assembly/disassembly of DNA origami trimer. (A–C) AFM images of DNA origami assemblies at pH = 5.0, 7.5, and 9.0, respectively, to show the three-state transitions from monomer to dimer to trimer. (D) Stepwise and reversible assembly of DNA origami trimer demonstrated by agarose gel electrophoresis. Left lane of each image is a DNA origami monomer used as reference control to show the band mobility of targeted dimers and trimers. Scale bars: 500 nm.

formation of dimers and trimers at pH 7.5 and 9.0, respectively. When reducing the pH back, from 9.0 to 7.5, and further to 5.0, the samples result in faster and faster electrophoretic mobility, indicating that the trimers undergo structural dissociation, thereby transitioning to dimers + monomers (A1/A2 + A3), and then further to monomers (A1, A2, and A3). Quantitative analysis of the gel band intensity shows that a majority of DNA tiles stay as monomers at pH 5.0; 55% origami tiles form dimers at pH 7.5; and 72% origami successfully assemble into trimers at pH 9.0. By switching the pH between 5, 7.5, and 9, the system can be further reconfigured multiple times in a fully reversible manner (Figure S6†). These results suggest that the pH-regulated consecutive multistep assembly/disassembly of DNA nanostructures can be achieved by engineering the sequences of DNA triplexes.

To further demonstrate the reversibility of pH-stimulated multiple steps of assembly of DNA origami nanostructures, the dynamic light scattering (DLS) method was used to monitor the assembly processes via detection of the size variations of DNA structures from monomers, dimers, to trimers in response to pH stimulation (Figure S7 and S8†). Two working cycles composed of 9 steps of transition induced by pH changes between pH5 and pH 9 were observed (Figure 4). In this way, the working system can be switched back and forth between the stepwise association and dissociation states controlled by pH stimulation. In addition, the DLS assay was also employed to monitor the dynamic dissociation of DNA origami nanostructures in real-time. After the pH was changed from 9 to 7.5, the size of DNA origami assemblies gradually decreased from ~75 nm to ~60 nm over the time course of 150 min (Figure S9A†), indicating the DNA origami trimers were dissociated to dimers due to the release of tile A3 by refolding of

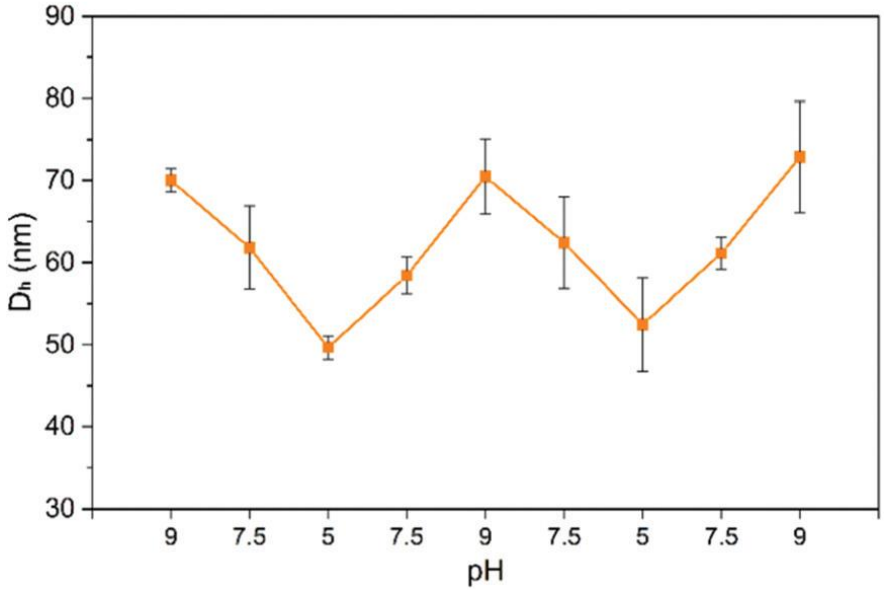

Figure 4. Working cycles of DNA triplex-driven DNA origami nanostructures stepwise assembly/disassembly in response to pH stimulation. The size decreases after pH changing from 9 to 7.5, and keeps decreasing at pH = 5, then increases with pH increasing.

DNA triplexes (73% T-A·T). Figure S9B† shows the decreasing size of DNA origami assemblies from ~60 nm to ~50 nm once the pH further changed from 7.5 to 5, corresponding to the transition from dimers to monomers.

Encouraged by the successful assembly of the DNA origami trimers in a stepwise reversible manner, we further demonstrate the scalability of the controlled formation of more complex 9-tile DNA nanoclusters, based on the same aforementioned approach, as schematically shown in Figure 5A. In this design, three cross-shaped DNA origami tiles, A4 (blue), A5 (green), and A6 (brown), were employed. Each arm of tile A4 was modified with the four ssDNA (red), providing coupling to the complementary sticky-ends in the DNA triplex set T1* containing 20% T-A·T (red) decorated on one arm of tile A5. Two neighboring arms of tile A6 contain the two strands of DNA triplex set T2*

with 73% T- A·T (black), whose sticky-end domains are complementary to the ssDNA (black) attached on the two arms of tile A5. In order to prevent the uncontrolled orientation of origami tiles, distinct sequences of hybridized sticky-ends are designed in a prescribed order (see ESI† for DNA sequences). As demonstrated in previous studies, at pH 5, both DNA triplex sets T1* and T2* are in close states, thereby keeping all of the DNA origami in monomers. Increasing the pH to 7.5 leads to the dissociation of triplex set T1* and, thus, resulting in the appearance of 5-tile origami clusters. As the pH is further increased to pH 9.0, the triplex set T2* on tile A6 is also activated, leading to the

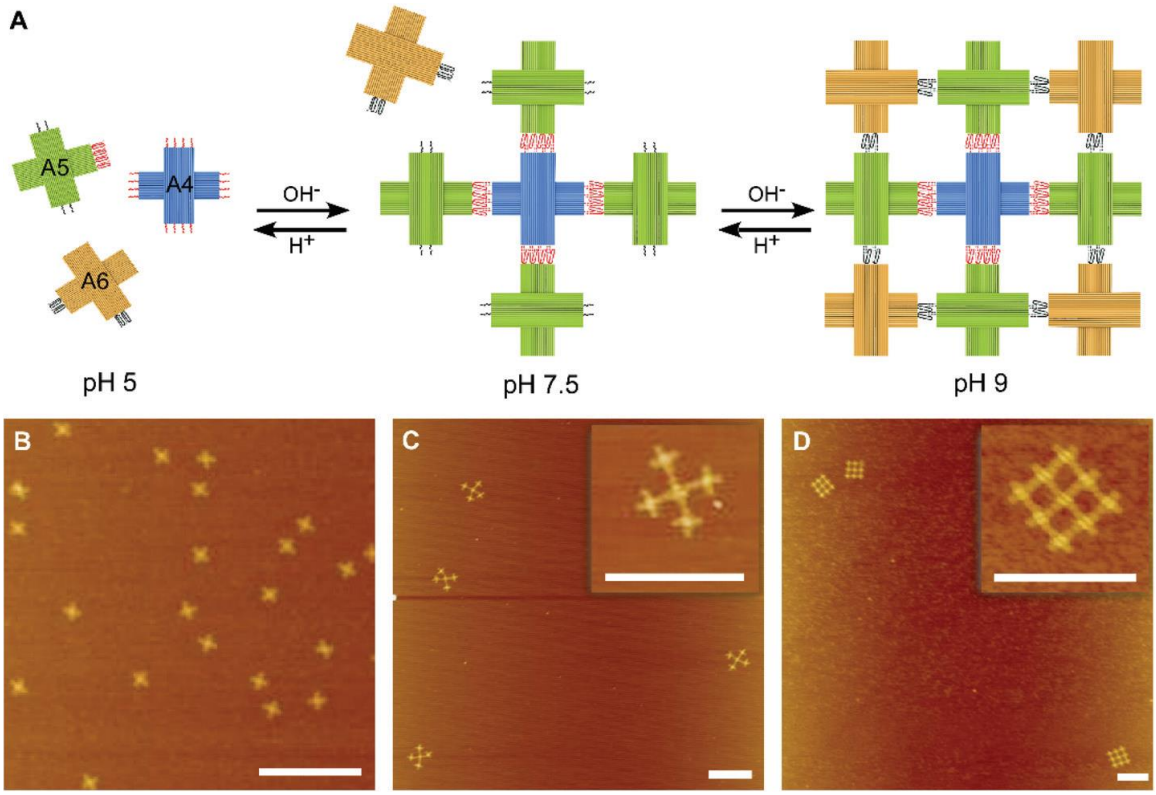

Figure 5. pH-Trigged stepwise assembly/disassembly of 9-tile DNA origami nanoclusters. (A) Schematic drawings of the reversible association of 9-tile DNA origami clusters. (B–D) AFM images of DNA origami at pH = 5 (monomer), pH = 7.5 (5-tile), and pH = 9 (9-title), respectively. Scale bars: 500 nm.

formation of 9-tile nanoclusters. Figure 5B–D, respectively, show the AFM images of resultant assemblies generated at pH 5.0, pH 7.5, and pH 9.0 after gel purification, which are in excellent agreement with our design (Figure S10†). The gel mobility shift assay also confirms that this pH-induced stepwise assembly process is fully reversible (Figure S11†). Due to the flexibility of a cross-shaped DNA origami unit and the incomplete transition of DNA triplexes from triplex-to-duplex states, the partial formation and aggregates of 5-tile and 9-tile clusters can be observed in the absence of previous gel purification, as evidenced by AFM images in Figure S12.† Therefore, optimizing the structural rigidity of DNA units, and improving the pH sensitivity of DNA triplexes, or introducing other robust, and novel dynamic linkers into the system are the key to the scale-up of stepwise self-assembled DNA nanostructures.

4. CONCLUSIONS

We successfully demonstrate a pH-driven stepwise assembly/disassembly of DNA origami nanoclusters with well-defined geometries for each step. Specifically, two types of DNA triplexes, containing 20% and 73% T-A·T, are utilized as the dynamic bridges in controlling the reversible assembly of DNA clusters in response to successive pH-stimulation processes. We show the formation of DNA origami trimers and more complex 9-tile clusters in a stepwise, selective and reversible manner. Our study provides a new and straightforward approach for fabricating well-defined DNA nanostructures regulated by changes in pH value. These multi-level and dynamic assemblies, in particular, may attract biomedical applications due to their specific responses towards

wide ranges of pH environments,[32,33] mimicking the different parts of organelles, for developing pH-responsive drug delivery,[34] gene therapy,[35] and the enzyme cascade reactions.[36] Due to the competition of DNA triplexes at wide range of pH environments, it's also possible to use such structures for DNA computation.[37] Additionally, it is expected that other triggers, such as light, gas, ions, and ligands can be involved to mimic living organisms that can extend our capabilities to create more sophisticated and smart functional nanostructures.

ACKNOWLEDGEMENT

This work was supported by the National Science Foundation under grants CCF-1814797. R. Wang thanks Dr William Shih for his valuable suggestions.

SUPPLEMENTARY INFORMATION

CONTROL OF THE STEPWISE ASSEMBLY-DISASSEMBLY OF DNA ORIGAMI NANOCLUSTERS BY PH STIMULI-RESPONSIVE DNA TRIPLEXES

Shuo Yang,[a] Wenyan Liu,[a,b] and Risheng Wang[*a]

[a]Department of Chemistry,
Missouri University of Science and Technology, Rolla, MO 65409, United States

[b]Center for Research in Energy and Environment,
Missouri University of Science and Technology, Rolla, MO 65409, United States
*E-mail: wangri@mst.edu

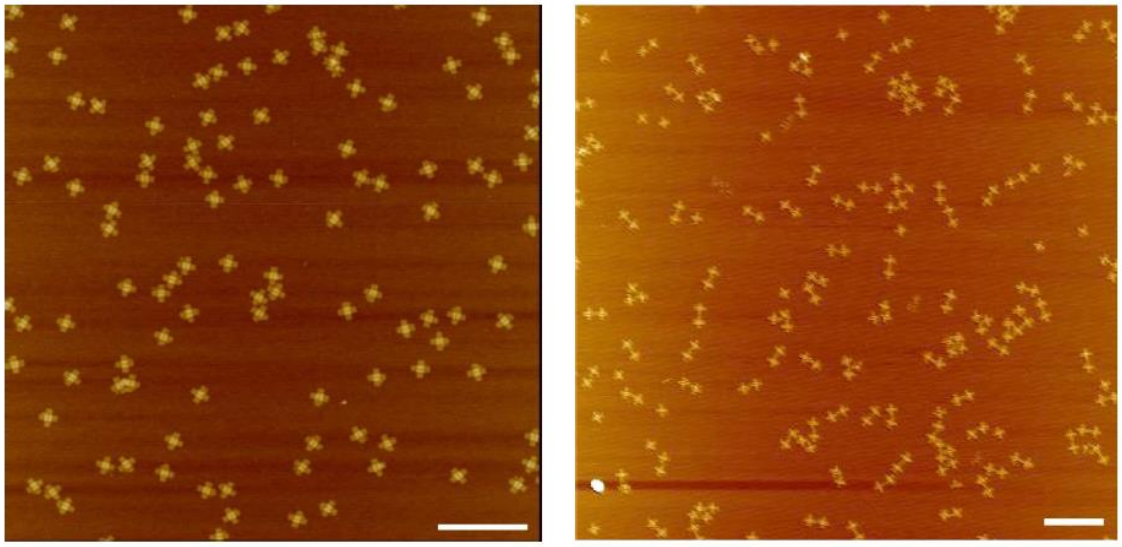

Figure S1. The representative AFM images of DNA origami monomer (A1) (left image) and dimer (A1/A2) (right image) without purification. The calculated yield of dimer is ~87% based on AFM results. Scale bar: 500 nm.

Table S1. The statistical analysis of AFM images of DNA origami monomer and dimer structures generated at pH5 and pH 7.5.

pH values		Monomer (A1, A2)	Dimer (A1/A2)	Total origamis
5.0	Origamis Counted	234	24	258
	Yield (%)	91	9	
7.5	Origamis Counted	44	286	330
	Yield (%)	13	87	

Table S2. The statistical analysis of AFM images of DNA origami monomer and dimer structures generated at pH 7.5 and pH 9.0.

pH values		Monomer (A2, A3)	Dimer (A2/A3)	Total origamis
7.5	Origamis Counted	144	18	162
	Yield (%)	89	11	
9.0	Origamis Counted	27	162	189
	Yield (%)	14	86	

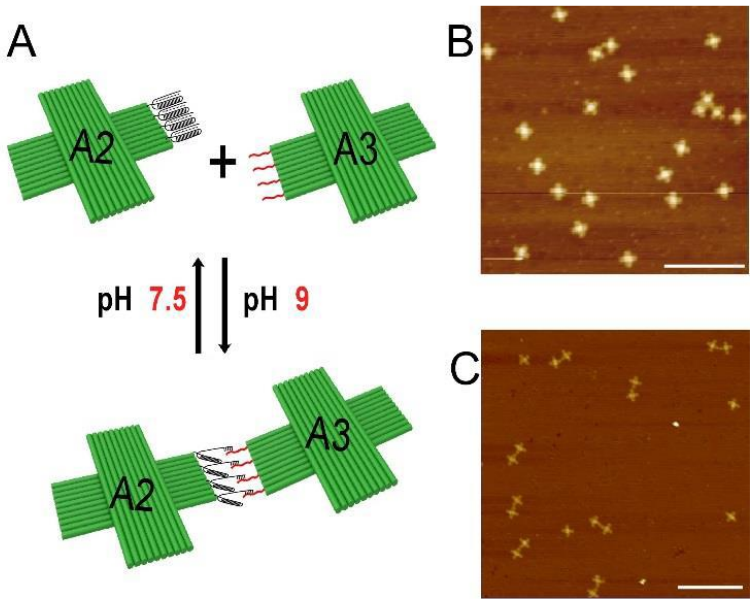

Figure S2. DNA triplexes (73% T-A·T) -driven assembly/disassembly of DNA origami dimer A2/A3. (A) Schematic drawing of the pH-stimulated cyclic assembly of DNA origami dimers through duplextriplex transition of DNA triplexes between pH 7.5 and 9. (B) AFM images of DNA origami monomer at pH=7.5 and dimer at pH=9.0 (C). Scale bars: 500 nm.

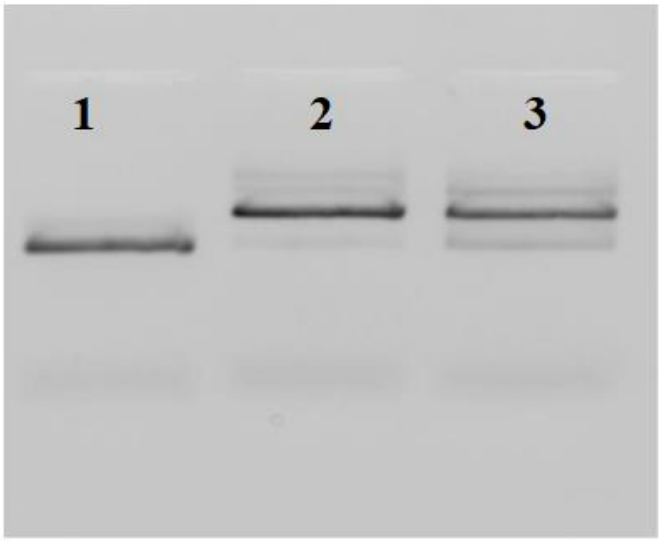

Figure S3. Gel electrophoresis used to compare the yield of dimer at pH 7.5 with and without thermal annealing process. Lane 1: DNA origami monomer control. Lane 2: Self-assembled dimer A1/A2 annealed from 38℃ to 25℃ over 6h. Lane 3: Assembled dimer A1/A2 incubated at room temperature. The dimer yield of lane 2 and lane 3 are 89%, and 75%, respectively.

Table S3. The statistical analysis of AFM images of DNA origami monomer, dimer and trimer structures generated at pH 5.0, pH 7.5 and pH 9.0.

pH values		Monomer (A1, A2, A3)	Dimer (A1/A2, A3)	Trimer (A1/A2/A3)	Total origami
5.0	Origamis Counted	158	12	0	170
	Yield (%)	93	7	0	
7.5	Origamis Counted	68	90	15	173
	Yield (%)	39	52	9	
9.0	Origamis Counted	33	22	126	181
	Yield (%)	18	12	70	

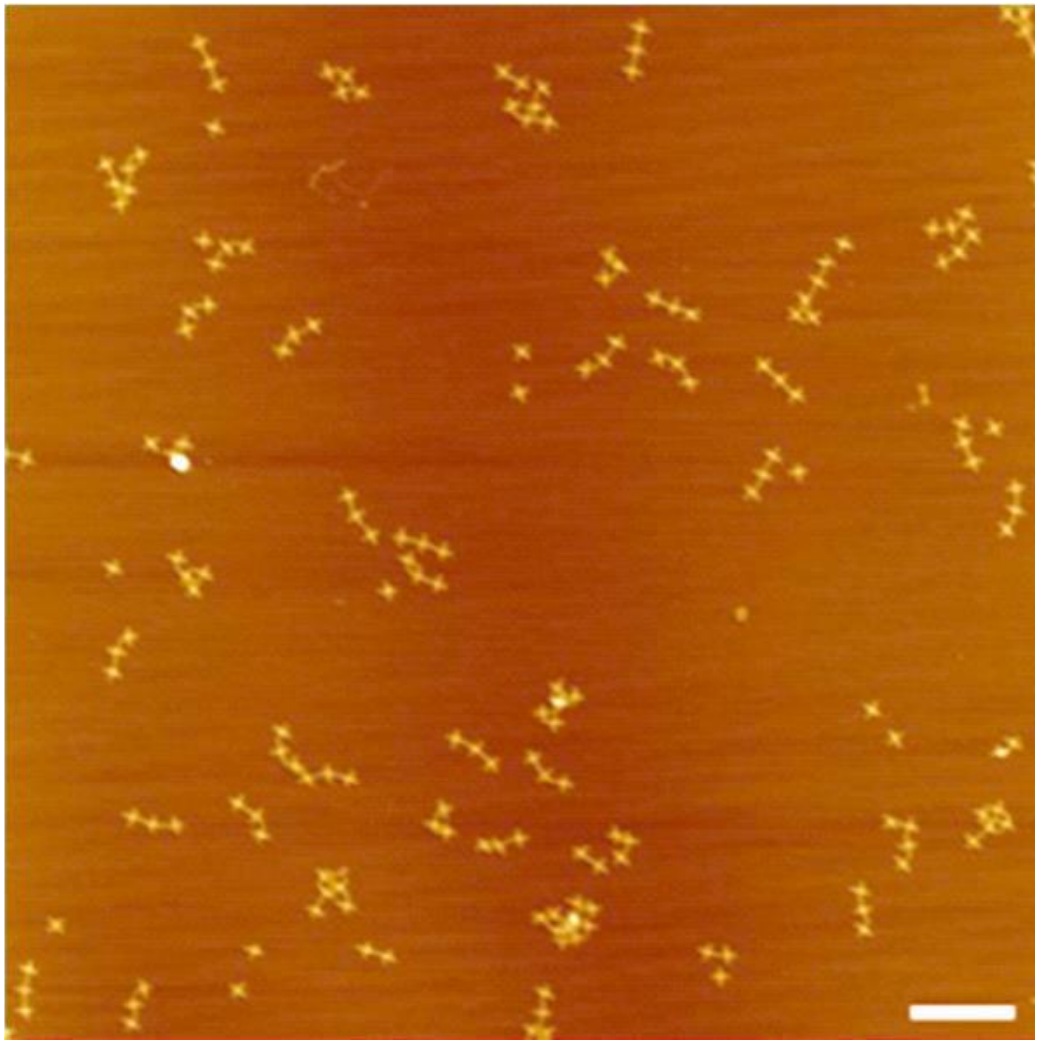

Figure S4. A representative AFM image of DNA origami timer (A1/A2/A3) without purification. The calculated trimer yield was ~70% based on AFM results. Scale bar: 500nm.

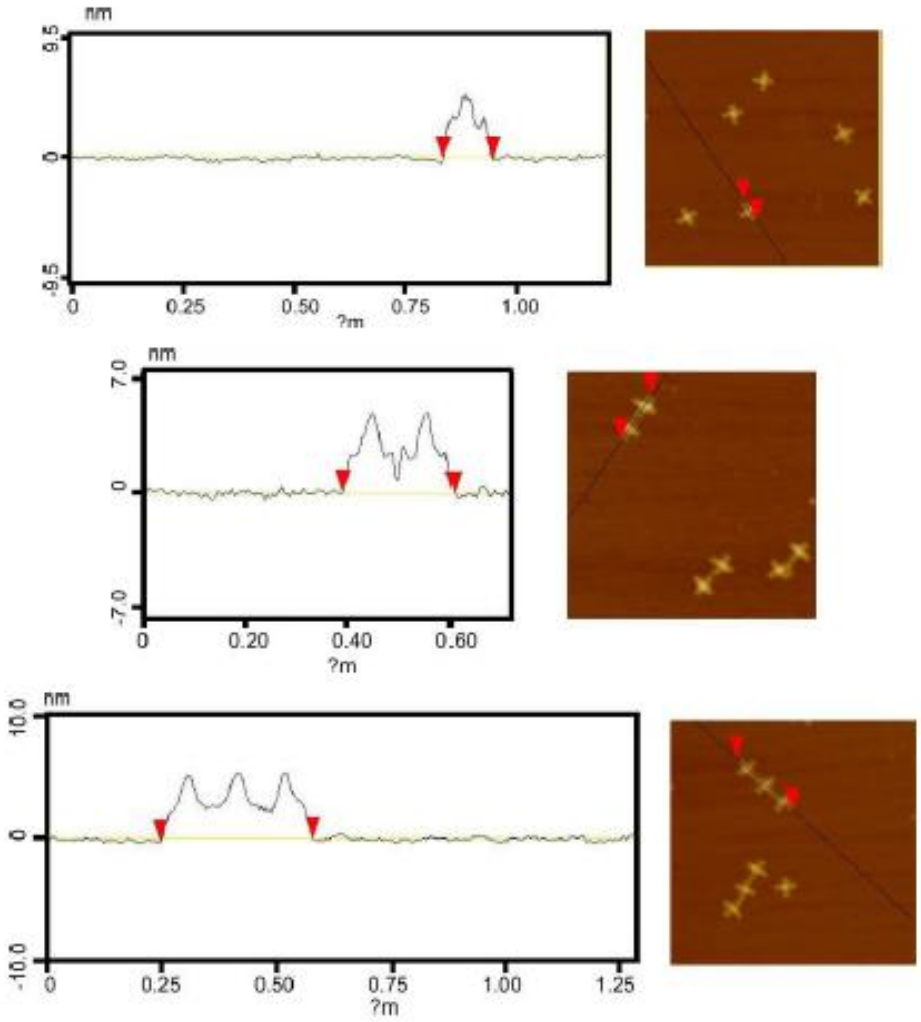

Figure S5. Cross-section analysis of self-assembled DNA origami monomer, dimer, and trimer. The size of monomer is ~ 100 nm, dimer is ~200 nm, and trimer is ~300 nm, which is consistent with design.

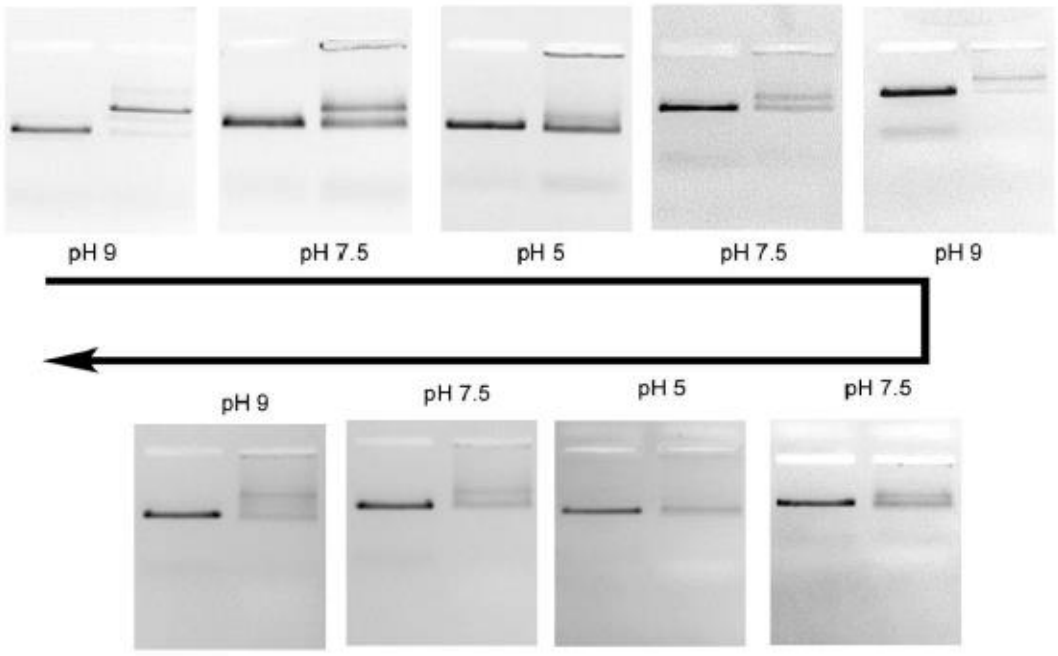

Figure S6. Gel electrophoresis to show the reversible, multistep assembly of DNA origami nanostructures driven by DNA triplexes in response to pH. For each image, the left lane and right lane represent DNA origami monomer control and sample, respectively. For each of the two working cycles, the DNA trimer (pH=9) dissociates to dimer (pH=7.5) and further to monomer (pH=5), and the process reverses when the pH increases.

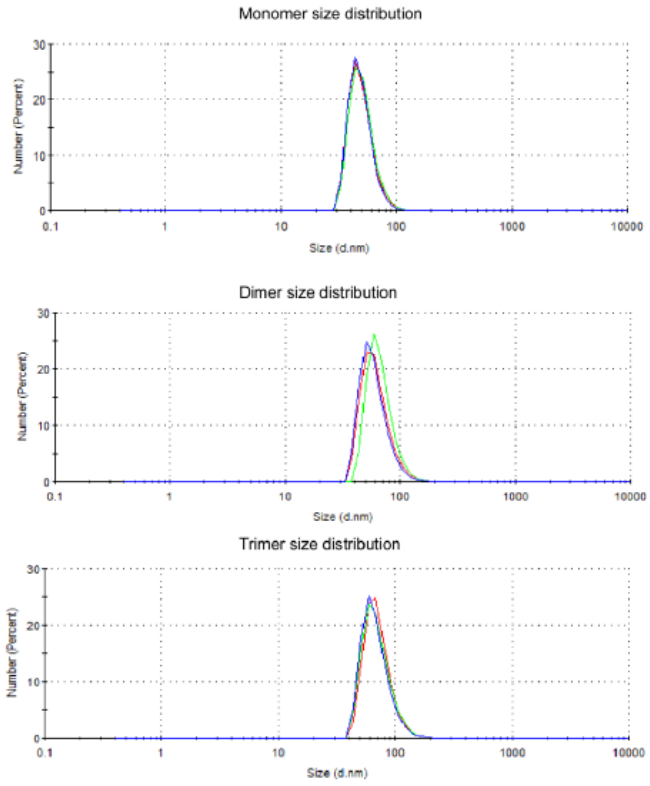

Figure S7. Hydrodynamic size distribution of the DNA origami nanostructures from DLS measurements. The three different colored (red, green, and blue) lines represent the three runs. The average size of monomer, dimer, and trimer is 49.43 ± 0.90 nm, 62.73 ± 3.81 nm, and 70.03 ± 1.39 nm, respectively.

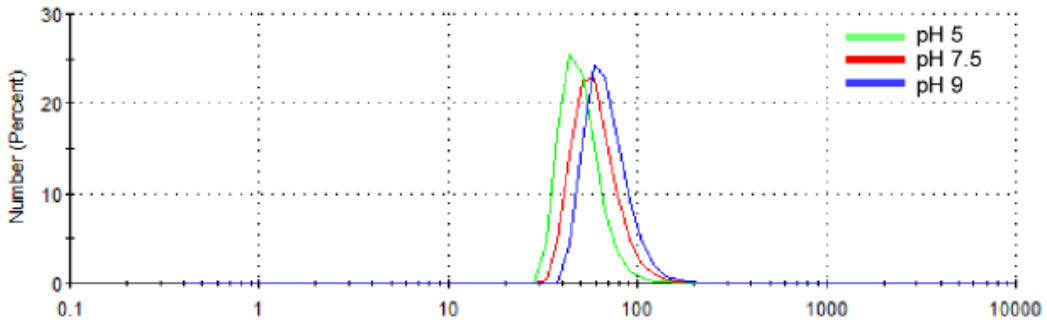

Figure S8. DLS measurements to show the size variations of DNA origami nanostructures induced by pH titration. The size distribution shifted to the left when the pH changed from pH 9, pH 7.5, to pH 5, corresponding to the sizes of DNA origami trimers, dimers, and monomers, respectively, which is consistent with our design.

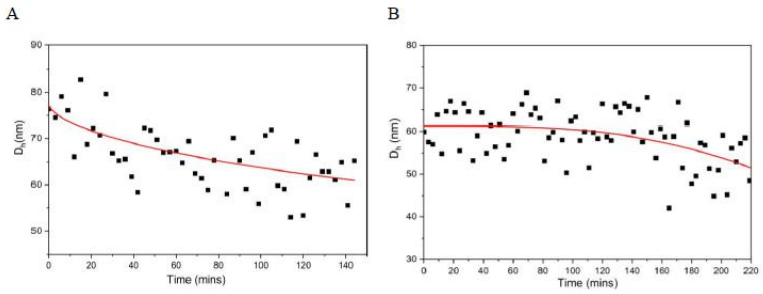

Figure S9. Time-dependent DLS study of the dynamic dissociation of DNA origami nanostructures driven by DNA triplexes. A) The DNA origami trimers dissociated to dimers when the pH was changed from 9 to 7.5. B) The DNA origami dimers dissociated to monomers when the pH was changed from 7.5 to 5.

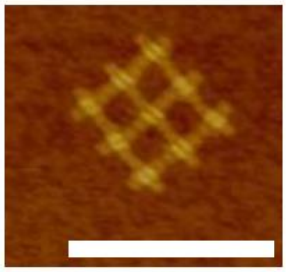

Figure S10. AFM image of assembled 9-tile DNA origami. Rotation of the origami units exactly followed our theoretical design. Scale bar: 500nm.

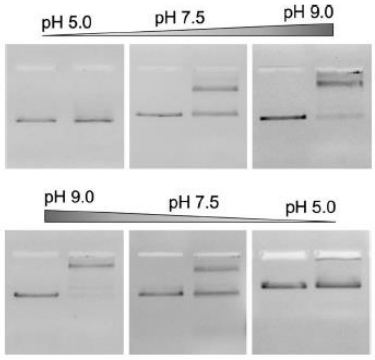

Figure S11. Stepwise and reversible assembly of DNA origami 9-tile clusters demonstrated by agarose gel electrophoresis. Left lane of each image is DNA origami monomer, used as reference control, to show the bands mobility of targeted 5-titles and 9-titles. The yield of the 5-tile structure is 66.9%, while the yield of 9-tile is 72.8% based on gel electrophoresis.

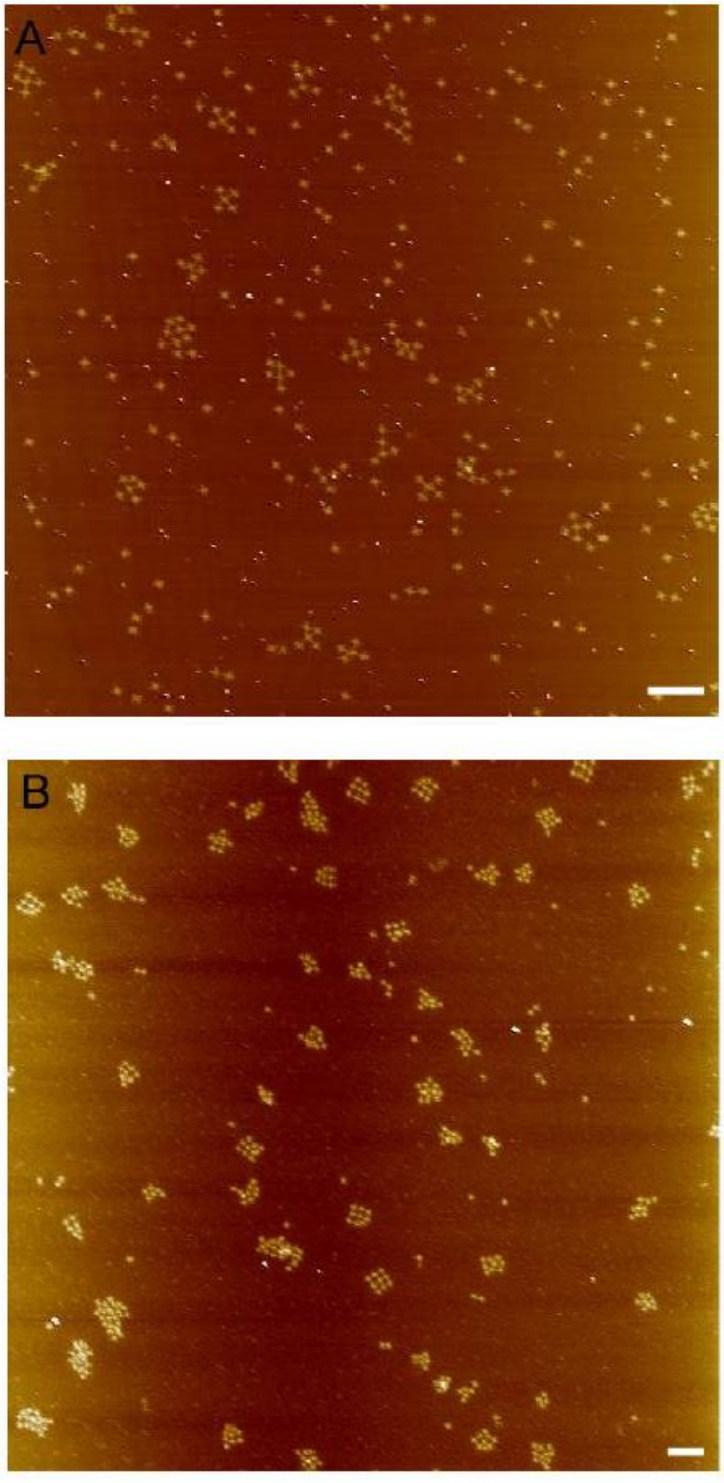

Figure S12. AFM images of unpurified 5-tile and 9-tile DNA origami. A) A representative 5-tile DNA origami. B) A representative 9-tile DNA origami. Aggregation and partial formation of DNA origami coexist with targeted structures. Scale bar: 500 nm.

DNA Sequences:

Modified DNA Sequences used for the formation of DNA origami trimer:

20%TAT Triplex

Triplex-A1R1 GTGTGATAAATAAGGCTTTTT

Triplex-A1R2 ATAACCTTGCTTCTGTTTTTT

Triplex-A1R4 AGCGGAATTATCATCATTTTT

Triplex-A1R5 ATCTAAAGCATCACCTTTTTT

Triplex-A1R1G

CTCATGCCTCCCCTCCCCTCCGTTTCCCTCCCCTCCCCTCCATTTGGAGGGGAG

GGGAGGTTTTTTTTGTTAAATAAGAATAAA

Triplex-A1R2G

CTCATGCCTCCCCTCCCCTCCGTTTCCCTCCCCTCCCCTCCATTTGGAGGGGAG

GGGAGGTTTTTTTTAAATCGTCGCTATTAA

Triplex-A1R4G

CTCATGCCTCCCCTCCCCTCCGTTTCCCTCCCCTCCCCTCCATTTGGAGGGGAG

GGGAGGTTTTTTTTTATTCCTGATTATCAG

Triplex-A1R5G

CTCATGCCTCCCCTCCCCTCCGTTTCCCTCCCCTCCCCTCCATTTGGAGGGGAG

GGGAGGTTTTTTTTTGCTGAACCTCAAATA

Blunt RE3 TTTTAAATAAAGAAATTGCGTTAGCACGTAAAACAGTTTT

Blunt RE6 TTTTACATTGGCAGATTCACCTGAAATGGATTATTTTTTT

Triplex-A2L1

GGGAGGCATGAGTTTTTTTTTCCTGAACAAGAAAAAATCAACAATAGATAAG

TTTTT

Triplex-A2L2

GGGAGGCATGAGTTTTTTTTTTGCACCCAGCTACAAAAGATTAGTTGCTATTT

TTTT

Triplex-A2L4

GGGAGGCATGAGTTTTTTTTGTTTGAGGGGACGACGAACCGTGCATCTGCCAT

TTTT

Triplex-A2L5

GGGAGGCATGAGTTTTTTTTCCCGGGTACCGAGGTCTCGACTCTAGAGGATCT

TTTT

Blunt LE3 TTTTAATAATAAGAGCAAGAGAATTGAGTTAAGCCCTTTT

Blunt LE6 TTTTAGCTGATTGCCCTTCACAGTGAGACGGGCAACTTTT

73%TAT Triplex

Triplex-A1R1 GTGTGATAAATAAGGCTTTTT

Triplex-A1R2 ATAACCTTGCTTCTGTTTTTT

Triplex-A1R4 AGCGGAATTATCATCATTTTT

Triplex-A1R5 ATCTAAAGCATCACCTTTTTT

Triplex-A2R1

TCGTATTTCTTCTTCTTTCTTGTTTCTTCTTTCTTCTTCTTATTTAAGAAGAAGA

AAGAATTTTTTTTGTTAAATAAGAATAAA

Triplex-A2R2

TCGTATTTCTTCTTCTTTCTTGTTTCTTCTTTCTTCTTCTTATTTAAGAAGAAGA

AAGAATTTTTTTTAAATCGTCGCTATTAA

Triplex-A2R4

TCGTATTTCTTCTTCTTTCTTGTTTCTTCTTTCTTCTTCTTATTTAAGAAGAAGA

AAGAATTTTTTTTTATTCCTGATTATCAG

Triplex-A2R5

TCGTATTTCTTCTTCTTTCTTGTTTCTTCTTTCTTCTTCTTATTTAAGAAGAAGA

AAGAATTTTTTTTTGCTGAACCTCAAATA

Blunt RE3 TTTTAAATAAAGAAATTGCGTTAGCACGTAAAACAGTTTT

Blunt RE6 TTTTACATTGGCAGATTCACCTGAAATGGATTATTTTTTT

Triplex-A3L1

GAAGAAATACGATTTTTTTTTCCTGAACAAGAAAAAATCAACAATAGATAAG

TTTTT

Triplex-A3L2

GAAGAAATACGATTTTTTTTTTGCACCCAGCTACAAAAGATTAGTTGCTATTT

TTTT

Triplex-A3L4

GAAGAAATACGATTTTTTTTGTTTGAGGGGACGACGAACCGTGCATCTGCCAT

TTTT

Triplex-A3L5

GAAGAAATACGATTTTTTTTCCCGGGTACCGAGGTCTCGACTCTAGAGGATCT

TTTT

Blunt LE3 TTTTAATAATAAGAGCAAGAGAATTGAGTTAAGCCCTTTT

Blunt LE6 TTTTAGCTGATTGCCCTTCACAGTGAGACGGGCAACTTTT

Modified DNA Sequences used for the formation of 9-tile origami:

pH-A4-Left-linearSE1

GGGAGGCATGAGTTTTTTTTTCCTGAACAAGAAAAAATCAACAATAGATAAG

TTTTT

pH- A4-Left-linearSE2

GGGAGGTCTCAATTTTTTTTTTGCACCCAGCTACAAAAGATTAGTTGCTATTT

TTTT

pH- A4-Left-linearSE4

GGGAGGATACATTTTTTTTTGTTTGAGGGGACGACGAACCGTGCATCTGCCAT

TTTT

pH- A4-Left-linearSE5

GGGAGGTAGTCATTTTTTTTCCCGGGTACCGAGGTCTCGACTCTAGAGGATCT

TTTT

pH-A4-Right-linearSE6

GGGAGGCATGAGTTTTTTTTACATTGGCAGATTCACCTGAAATGGATTATTTT

TTTT

pH-A4-Right-linearSE5

GGGAGGTCTCAATTTTTTTTTGCTGAACCTCAAATAATCTAAAGCATCACCTT

TTTT

pH-A4-Right-linearSE3

GGGAGGATACATTTTTTTTTAAATAAAGAAATTGCGTTAGCACGTAAAACAG

TTTTT

pH-A4-Right-linearSE2

GGGAGGTAGTCATTTTTTTTAAATCGTCGCTATTAAATAACCTTGCTTCTGTTT

TTT

pH-A4-Down-linearSE1

GGGAGGCATGAGTTTTTTTTCGTTAATATTTTGTTAATATTTAAATTGTAAATT

TTTTTT

pH-A4-Down-linearSE2

GGGAGGTCTCAATTTTTTTTTGAGTAATGTGTAGGTTTTTAAATGCAATGCCT

TTTT

pH-A4-Down-linearSE4

GGGAGGATACATTTTTTTTTATCAAAAAGATTAAGAAAGCAAAGCGGATTGC

TTTTT

pH-A4-Down-linearSE5

GGGAGGTAGTCATTTTTTTTATAACGCCAAAAGGAACAACTAATGCAGATAC

TTTTT

pH-A4-Top-linearSE6

GGGAGGCATGAGTTTTTTTTGAGGACTAAAGACTTTCGGCTACAGAGGCTTTT

TTTT

pH-A4-Top-linearSE5

GGGAGGTCTCAATTTTTTTTACTAAAGGAATTGCGAAGAATAGAAAGGAACA

TTTTT

pH-A4-Top-linearSE3

GGGAGGATACATTTTTTTTTAATTTACCGTTCCAGTGAAAGCGCAGTCTCTGT

TTTT

pH-A4-Top-linearSE2

GGGAGGTAGTCATTTTTTTTTGTAGCGCGTTTTCATGCCTTTAGCGTCAGACTT

TTT

pH-A5-Right-Triplex SE1

CTCATGCCTCCCCTCCCCTCCGTTTCCCTCCCCTCCCCTCCATTTGGAGGGGAG

GGGAGGTTTTTTTTGTTAAATAAGAATAAA

pH-A5-Right-Triplex SE2

TTGAGACCTCCCCTCCCCTCCGTTTCCCTCCCCTCCCCTCCATTTGGAGGGGA

GGGGAGGTTTTTTAAATCGTCGCTATTAAATAACCTT

pH-A5-Right-Triplex SE4

ATGTATCCTCCCCTCCCCTCCGTTTCCCTCCCCTCCCCTCCATTTGGAGGGGAG

GGGAGGTTTTTTTATTCCTGATTATCAGAGCGGAAT

pH-A5-Right-Triplex SE5

TGACTACCTCCCCTCCCCTCCGTTTCCCTCCCCTCCCCTCCATTTGGAGGGGA

GGGGAGGTTTTTTTGCTGAACCTCAAATAATCTAAAG

pH-A5-TOP-linearSE2

GAAGAAACGATTTTTTTTTTTGTAGCGCGTTTTCATGCCTTTAGCGTCAGACTT

TTT

pH-A5-TOP-linearSE4

GAAGAACTACCGTTTTTTTTTGGTTTAGTACCGCCACATCACCGTACTCAGGAT

TTTT

pH-A5-Down-linearSE2

GAAGAAGATGACTTTTTTTTTGAGTAATGTGTAGGTTTTTAAATGCAATGCCT

TTTT

pH-A5-Down-linearSE4

GAAGAACCTCGATTTTTTTTATCAAAAAGATTAAGAAAGCAAAGCGGATTGC

TTTTT

pH-A6-TOP-TriplexS2

GTCATCTTCTTCTTCTTTCTTGTTTCTTCTTTCTTCTTCTTATTTAAGAAGAAGA

AAGAATTTTTTTGTAGCGCGTTTTCATGCCTTTAG

pH-A6-TOP-TriplexS4

TCGAGGTTCTTCTTCTTTCTTGTTTCTTCTTTCTTCTTCTTATTTAAGAAGAAGA

AAGAATTTTTTGGTTTAGTACCGCCACATCACCGT

pH-A6-Right-TriplexS3

CGGTAGTTCTTCTTCTTTCTTGTTTCTTCTTTCTTCTTCTTATTTAAGAAGAAGA

AAGAATTTTTTAAATAAAGAAATTGCGTTAGCACG

pH-A6-Right-TriplexS5

AATCGTTTCTTCTTCTTTCTTGTTTCTTCTTTCTTCTTCTTATTTAAGAAGAAGA

AAGAATTTTTTTGCTGAACCTCAAATAATCTAAAG

REFERENCES

1. Y. Bai, Q. Luo and J. Liu, Chem. Soc. Rev., 2016, 45, 2756–2767.

2. B. P. Glover and C. S. McHenry, Cell, 2001, 105, 925–934.

3. E. Winfree, F. R. Liu, L. A. Wenzler and N. C. Seeman, Nature, 1998, 394, 539–544.

4. D. R. Han, S. Pal, Y. Yang, S. X. Jiang, J. Nangreave, Y. Liu and H. Yan, Science, 2013, 339, 1412–1415.

5. W. Y. Liu, H. Zhong, R. S. Wang and N. C. Seeman, Angew. Chem., Int. Ed., 2011, 50, 264–267.

6. P. Wang, S. Gaitanaros, S. Lee, M. Bathe, W. M. Shih and Y. Ke, J. Am. Chem. Soc., 2016, 138, 7733–7740.

7. J. Zheng, J. J. Birktoft, Y. Chen, T. Wang, R. Sha, P. E. Constantinou, S. L. Ginell, C. Mao and N. C. Seeman, Nature, 2009, 461, 74–77.

8. S. M. Douglas, H. Dietz, T. Liedl, B. Hogberg, F. Graf and W. M. Shih, Nature, 2009, 459, 414–418.

9. D. R. Han, S. Pal, J. Nangreave, Z. T. Deng, Y. Liu and H. Yan, Science, 2011, 332, 342–346.

10. C. J. Serpell, T. G. Edwardson, P. Chidchob, K. M. Carneiro and H. F. Sleiman, J. Am. Chem. Soc., 2014, 136, 15767–15774.

11. Y. G. Ke, L. L. Ong, W. Sun, J. Song, M. D. Dong, W. M. Shih and P. Yin, Nat. Chem., 2014, 6, 994–1002.

12. E. Benson, A. Mohammed, J. Gardell, S. Masich, E. Czeizler, P. Orponen and B. Hogberg, Nature, 2015, 523, 441–444.

13. E. Kopperger, J. List, S. Madhira, F. Rothfischer, D. C. Lamb and F. C. Simmel, Science, 2018, 359, 296–301.

14. A. E. Marras, L. Zhou, H. J. Su and C. E. Castro, Proc. Natl. Acad. Sci. U. S. A., 2015, 112, 713–718.

15. J. Song, Z. Li, P. Wang, T. Meyer, C. Mao and Y. Ke, Science, 2017, 357, eaan3377.

16. Z. Shi, C. E. Castro and G. Arya, ACS Nano, 2017, 11, 4617–4630.

17. Y. Yang, M. Endo, K. Hidaka and H. Sugiyama, J. Am. Chem. Soc., 2012, 134, 20645–20653.

18. N. Wu and I. Willner, Nano Lett., 2016, 16, 6650–6655.

19. L. N. Green, A. Amodio, H. K. K. Subramanian, F. Ricci and E. Franco, Nano Lett., 2017, 17, 7283–7288.

20. J. Wang, Z. Zhou, L. Yue, S. Wang and I. Willner, Nano Lett., 2018, 18, 2718–2724.

21. S. Yang, W. Liu, R. Nixon and R. Wang, Nanoscale, 2018, 10, 3626–3630.

22. N. Wu and I. Willner, Nano Lett., 2016, 16, 2867–2872.

23. N. Wu and I. Willner, Nanoscale, 2017, 9, 1416–1422.

24. Y. Hu, A. Cecconello, A. Idili, F. Ricci and I. Willner, Angew. Chem., Int. Ed., 2017, 56, 15210–15233.

25. J. Wang, L. Yue, S. Wang and I. Willner, ACS Nano, 2018, 12, 12324–12336.

26. S. Rhee, Z. Han, K. Liu, H. T. Miles and D. R. Davies, Biochemistry, 1999, 38, 16810–16815.

27. A. Idili, A. Vallee-Belisle and F. Ricci, J. Am. Chem. Soc., 2014, 136, 5836–5839.

28. L. Heinen and A. Walther, Chem. Sci., 2017, 8, 4100–4107.

29. J. Volker, S. E. Osborne, G. D. Glick and K. J. Breslauer, Biochemistry, 1997, 36, 756–767.

30. M. S. Searle and D. H. Williams, Nucleic Acids Res., 1993, 21, 2051–2056.

31. G. E. Plum, Y. W. Park, S. F. Singleton, P. B. Dervan and K. J. Breslauer, Proc. Natl. Acad. Sci. U. S. A., 1990, 87, 9436– 9440.

32. S. Mura, J. Nicolas and P. Couvreur, Nat. Mater., 2013, 12, 991–1003.

33. F. Muhammad, M. Guo, W. Qi, F. Sun, A. Wang, Y. Guo and G. Zhu, J. Am. Chem. Soc., 2011, 133, 8778–8781.

34. Y. Dong, Z. Yang and D. Liu, Acc. Chem. Res., 2014, 47, 1853–1860.

35. A. Bacolla, G. Wang and K. M. Vasquez, PLoS Genet., 2015, e1005696, 1–12.

36. V. Linko, M. Eerikainen and M. A. Kostiainen, ChemComm, 2015, 51, 5351–5354.

37. G. Seelig, D. Soloveichik, D. Y. Zhang and E. Winfree, Science, 2006, 314, 1585–1588.

III. BOTTOM-UP FABRICATION OF LARGE-SCALE GOLD NANOROD ARRAYS BY SURFACE DIFFUSION-MEDIATED DNA ORIGAMI ASSEMBLY

Shuo Yang,[a] Wenyan Liu,[a, b] Yuwei Zhang,[a] and Risheng Wang[*a]

[a] Department of Chemistry,
Missouri University of Science and Technology, Rolla, MO 65409, USA

[b] Center for Research in Energy and Environment,
Missouri University of Science and Technology, Rolla, MO 65409, USA

ABSTRACT

Plasmonic metal nanoparticles consisting of gold, silver, and platinum have attracted great attention due to their unique physiochemical properties and broad applications in catalysis, molecular imaging, and disease therapy. Self-assembly of plasmonic metal nanoparticles from unorganized monomers to well-ordered and large-scale patterns could serve as an effective bottom-up route for the nanofabrication of novel artifacts. Highly programmable DNA origami has provided a robust method for the spatial arrangement of nanoparticles with advantages of high yield, superior controllability, and precise positioning with nanometer scale resolution. In this work, we utilized cross-shaped DNA origami tiles as binding frames for the spatial arrangement of gold nanorods (AuNRs) by cation-controlled surface diffusion strategy. The AuNRs were able to polymerize into one-dimensional (1D) and two-dimensional (2D) arrays guided by DNA origami tiles on the solid and liquid interface through π-π stacking interactions. In order to facilitate the further manipulation of those patterns, a novel pattern transfer method was introduced for the first time to transfer the assembled arrays of AuNRs from

liquid environment to dry ambient environment with high yield and minor structural damage. The obtained results have demonstrated the successful DNA origami-assisted, large-scale assembly of AuNRs for constructing complex 1D and 2D superstructures with potential applications in the nanofabrication of plasmonic and electronic devices.

Key words: cation-controlled surface diffusion strategy, DNA origami, π-π stacking interactions, gold nanorod arrays

1. INTRODUCTION

DNA-directed self-assembly of nanomaterials has shown great potentials as a powerful tool for the fabrication of nanostructures with ultra-fine resolution at a reasonable cost.[1,2] This technique is based on base-pairing properties of DNA and is capable of controlled arrangement of functional biomolecules or nanomaterials. As an appealing class of self-assembly methods, DNA origami[3] has served as the templates for the assembly of various functional materials due to advantages of high yield, superior addressability and precise positioning, and has been employed for many applications such as biosensing,[4,5] nanomedicine,[6–8] and nanoelectronics.[9–11] Of particular, extensive research has been focusing on utilizing DNA origami as building blocks for the assembly of plasmonic metallic nanostructures, such as gold nanoparticles (AuNPs) and gold nanorods (AuNRs). For example, self-assembly of AuNPs into linear arrays by origami nanotubes can be used to fabricate plasmonic waveguides.[12,13] AuNRs that are precisely arranged into one-dimensional (1D) plasmonic polymers are capable of transporting plasmonic angular momentum and magnetic surface plasmonic polaritons.[14] Besides, the

dynamic tuning of AuNRs helixes by V-shaped DNA origami can produce plasmonic chiral superstructures with switchable chirality.[15] Other examples include dynamic walker,[16] reconfigurable AuNRs tripod,[17] as well as plasmonic rings.[18]

For most of above-mentioned nanostructures, mishybridization between DNA origami units is one of the major technical obstacles during the fabrication process, which leads to disordered aggregates and lowered productive yield. Besides that, these nanostructures are generally formed in a test tube, then deposited onto substrates for characterization and further processes, which inevitably leads to structural distortion and damage during deposition.[19,20] To address these issues, an effective strategy is to utilize surface diffusion-mediated assembly.[21–24] In such process, origami units are dynamically reorganized on the interface of liquid and substrates such as mica[23,24] by controlling the concentrations of divalent and monovalent ions, and lipid[25,26] into ordered superstructures. However, to the best of our knowledge, this strategy has not yet been used to assemble origami framed plasmonic nanomaterials in large scale. In this study, we combined the surface diffusion-mediated assembly method with a pattern transfer method to fabricate well-aligned 2D arrays of AuNRs. DNA functionalized AuNRs were decorated on origami frames and programmed to assemble into 2D arrays through base-stacking interactions in buffer solution. These assembled 2D arrays exhibited great stability against aggregation and high yield with AuNRs well arranged in predesigned orientation. However, the further utilization of these patterns to fabricate nanoelectronic or plasmonic devices was limited as pattern was formed in wet condition. Furthermore, we demonstrated that preformed 2D arrays of AuNRs were intactly transferred from liquid environment to dry ambient environment in the pattern transfer process. More

complex and larger-scale AuNR arrays were fabricated, for the first time, by assembling on the mica surface with DNA origami as scaffold. In general, the results represented critical progress toward the large-scale, high-yield, and precise fabrication of plasmonic and electronic nanostructures by DNA origami.

2. EXPERIMENTAL DETAILS

2.1. MATERIALS

All chemicals were purchased from Sigma and used as received without further purification. All chemically synthesized DNA strands were purchased from Integrated DNA Technologies, Inc. (www.Idtdna.com). The unmodified staple strands were ordered in a 96-well plate format, suspended in ultrapure water without purification.

2.2. PREPARATION OF DNA ORIGAMI

According to the Rothermund method[1], M13mp18 viral DNA and all of the staple strands were mixed together at a ratio of 1:5, in a 1×TAE buffer solution containing 40 mM Tris-HCl, 20 mM of acetic acid, 2 mM of EDTA, and 11.5 mM of magnesium acetate. The mixture was slowly cooled from 90℃ to 15℃ with thermal cycler (PCR) over 12h. The final concentration of M13mp18 DNA in the solution was 20 nM.

2.3. SYNTHESIS OF GOLD NANORODS

Gold nanorods were prepared according to the seed mediated growth method described by EI-Sayed et al.[2]

2.3.1 AuNRs Seed Solution. 5 mL of 0.5 mM of HAuCl4 solution was mixed with 5 mL of 0.2 M of CTAB solution. Under vigorous stirring, 0.6 mL of 10 mM freshly prepared, ice-cold NaBH4 was added into the mixture. The color of the solution quickly changes to brown-yellow and the mixture was kept under vigorous stirring for 2 minutes. The resulting AuNR seed solution acted as nucleation sites for AuNRs growth.

2.3.2 AuNRs Seed Solution. In a 250 mL Erlenmeyer flash, 1.2 mL of AgNO3 solution (10 mM) was added into 200 mL of CTAB solution (0.1 M) with stirring. After 10 min, 5 mL of HAuCl4·3H2O solution (10 mM) was added into the flask. After another 3 min, 0.6 mL of L-ascorbic acid solution (0.1M) was added the above mixture with gentle stirring until the solution color changed to colorless. Then 400 µL of seed solution was added into the flask under vigorous stirring for 30s and left undisturbed at 27ºC overnight for AuNRs growth.

2.4. PREPARATION OF DNA FUNCTIONALIZED GOLD NANORODS

Gold nanorods were functionalized with thiolated DNA. Prior to use, the SH-DNA was cleaved by the addition of TCEP and incubated at room temperature for 1 hour. The cleaved oligonucleotides were purified using a G-25 column. Freshly cleaved oligonucleotides were added to gold nanorod solutions with molar ratios 500:1. 0.01% sodium dodecyl sulfate (SDS) was added to gold nanorods solutions. The oligonucleotide/gold nanorods solution was allowed to incubate at room temperature for 1 hour. The concentration of NaCl was increased to 50mM, using 2M NaCl, 0.01 M PBS, during a 12-hour period of time. To remove excess DNA, the gold nanoparticles were centrifuged, and the supernatant was removed, leaving a pellet of gold nanoparticles at the bottom. The particles were then suspended in a PBS buffer containing 25 mM of

NaCl. This washing process was repeated three times, and then the gold nanoparticles were dispersed in a PBS buffer and measured by UV-vis.

2.5. FORMATION OF ORIGAMI FRAMED AUNRS

The prepared origami frames were mixed with AuNRs at a molar ratio of 1:3 in a 1xTAE buffer contained 11.5 mM of magnesium acetate, followed by annealing from 50℃ to 30℃ over 12h time course.

2.6. FORMATION OF ORIGAMI FRAMED AUNRS

5ul of origami stock solution with concentration of 20nM were diluted with 100 ul 1xTAE buffer contained 11.5 mM of magnesium acetate and 450mM sodium chloride and deposited on freshly cleaved mica. The sample was incubated for 12h at room temperature in a sealed container. After incubation, samples were imaged by AFM.

2.7. PATTERN TRANSFER METHOD

100 ul origami sample with concentration of 1nM in 1xTAE buffer contained 11.5 mM of magnesium acetate and 450mM NaCl was deposited on freshly cleaved mica for substrate-assisted self-assembly and stored in a sealed container to keep humidity for 6 hours. After incubation, remaining buffer on mica was gently wick off by a piece of Kimwipe (critical step), 150 ul of 1xTAE with 20 mM of magnesium acetate was placed on mica to immobilize preformed structures. After incubation for 30s, the solutions were wicked off. Next, doubly distilled H_2O (50ul) was placed quickly on the mica to remove the buffer salts, the drop was wicked off. The rinsing step was repeated three times. Last the sample was dried with compressed air.

2.8. AFM IMAGING

The AFM images were obtained using Bruker Dimension Icon instrument.

For samples in dried conditions, spotting the sample (3 μl) onto freshly cleaved muscovite mica (Ted Pella, Inc.) for 15 s. After the fixation of targeted structure of DNA origami on mica surface, doubly distilled H_2O (50ul) was placed quickly on the mica to remove the buffer salts, the drop was wicked off, and the sample was dried with compressed air. Atomic force imaging was done by utilizing Scanasyst mode in air, with ultra-sharp 14 series (NSC 14) tips that had been purchased from NANOANDMORE.

For samples in liquid conditions, 5ul of sample solution were mixed with 100 ul 1xTAE buffer contained 450mM NaCl and deposited on freshly cleaved mica for mica-assisted self-assembly. Atomic force imaging was done by utilizing ScanAsyst-fluid mode with ScanAsyst-fluid probes from Bruker.

2.9. AGAROSE GEL ELECTROPHORESIS

For the agarose gel, the samples were loaded into 0.8% agarose gel that contained 5 mM $Mg(CH_3COO)_2$ in a 1×TAE buffer solution under 55V at room temperature. The gel was stained with ethidium bromide for visualization. filters.

2.10. REFERENCES

1. Rothemund, P. W. K. Folding DNA to create nanoscale shapes and patterns. Nature 440, 297–302 (2006).
2. Nikoobakht, B. & El-Sayed, M. A. Preparation and growth mechanism of gold nanorods (NRs) using seed-mediated growth method. Chem. Mater. 15, (2003).

3. RESULTS AND DISCUSSION

Scheme 1 shows an illustration of the strategy for assembling of AuNRs into well-controlled two-dimensional (2D) arrays on solid surface (mica) by the surface diffusion-mediated DNA origami assembly followed by a pattern transfer step. The cross-shaped DNA origami frame[27] developed by Liu et al was initially constructed by folding a long circular single-stranded DNA (M13mp18) using hundreds of shorts staple stands. The origami frame has four edges with each edge decorated with blunt-ends for stacking interactions between the origami frames. To introduce the staking interactions with uniform strength on the four edges, all the blunt-ends were designed with GC base pairs. The structural design is shown in supporting information. On the center of each origami frame, it was designed with one set of ten single-stranded DNA (ssDNA, red color) as binding sites to anchor AuNRs. Thiolated ssDNA which had complementary sequences to the ssDNA on origami frame were decorated on the surface of AuNRs by a salting-aging process.[28,29] The hybridization between binding strands on the origami frame and its complementary ssDNA on AuNRs led to the formation of origami framed AuNRs. The resulting nanostructures were characterized by atomic force microscopy (AFM) and agarose gel electrophoresis (Figure 1). Figure 1a represented the AFM image of the cross-shaped origami, indicating the successful construction of predesigned structure. Figure 1b shows the gel image, in which lane 1 represented the AuNRs as a control while lane 2 exhibited an intense upper band with slower mobility compared to the extra AuNRs band (bottom band) suggesting the successful fabrication of AuNRs on origami frame. In order to further determine the morphology of origami framed AuNRs, the band

was extracted and then examined by AFM, as shown in Figure 1c. Comparison between the AFM images of the origami frames (Figure 1a) and the AuNRs on origami frames (Figure 1c) confirmed that AuNRs were successfully decorated on the origami frames which was consistent with the result from gel image. However, some AuNRs seemed to be shifted off from the desired binding position, which was very likely coming from the partially hybridization between binding strands on origami frames and ssDNA coated on AuNRs. The section profiles along the origami frame (A-B in Figure 1a) and AuNRs on origami frame (C-D in Figure 1c) are shown in Figure 1d and 1e, respectively. As seen from the results, the height of the profile was increased from 4 nm to 13 nm indicating the attachment of AuNRs.

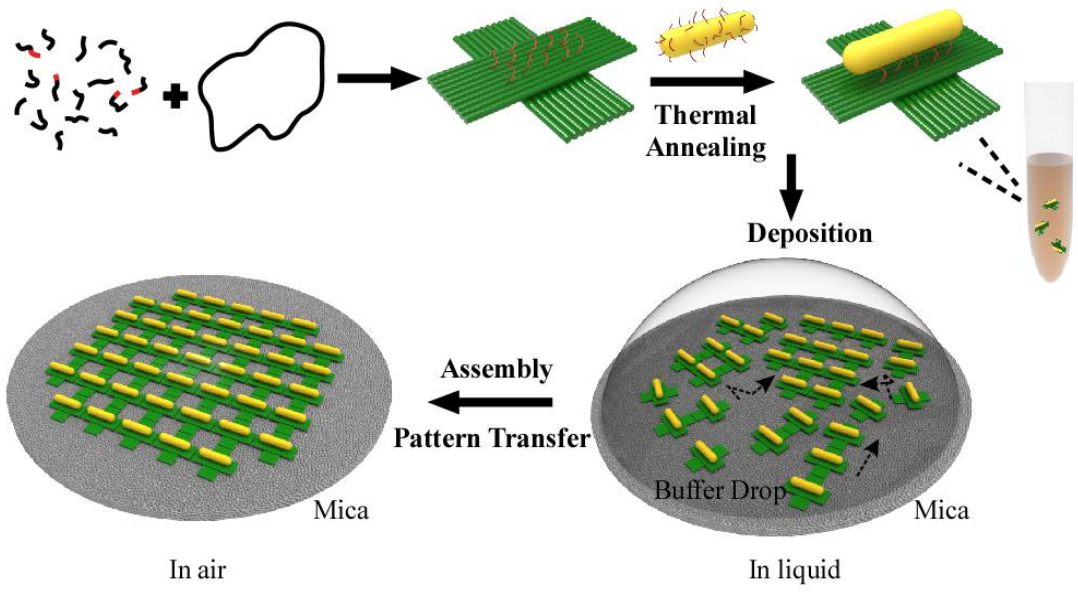

Scheme 1. A schematic illustration of the strategy for constructing origami framed AuNRs and assembling AuNRs into form 2D nanostructures.

To obtain the origami framed AuNRs into well-ordered 2D arrays in dry ambient environment, two major steps were conducted. In the first step called surface diffusion-mediated assembly, origami framed AuNRs were assembled into arrays on mica surface in liquid environment by carefully adjusting the ratio between Mg^{2+} and Na^{+}. Then, in the second step called pattern transfer process, the preformed AuNRs arrays were transferred from wet to dry environment without disturbing the pattern when the balance of cation-controlled interaction was interrupted.

In the first step, rather than using sticky-strand hybridization between origami frames, we employed blunt-end stacking interactions. This type of interactions was weaker, and thus allowed reorganization of origami units to grow into larger nanostructures during the surface diffusion-mediated assembly process. The assembly was achieved by controlling the surface mobility of DNA origami frames in liquid environment through manipulating the concentration of divalent (Mg^{2+}) and monovalent (Na^{+}) cations.[30–32] Under liquid conditions (typically 1xTris-acetate-EDTA buffer), DNA origami frames were immobile with strong adhesion to the mica substrate, as was mediated by divalent cation Mg^{2+}. When the monovalent cation Na^{+} was introduced, DNA origami frames became mobile.[30] The origami units with mobility were able to move around on the mica surface and associate into well-ordered arrays. In the assembly process, the concentration of Na^{+} played a critical role in the formation of arrays. In order to investigate the optimized concentration of Na^{+}, origami frames were treated with solutions containing varied concentrations of Na^{+} from 0 mM to 600 mM. As seen from the results in Figure S1, [NaCl]= 450 mM was the optimized concentration leading to large 2D arrays and was thus chosen for the following studies.

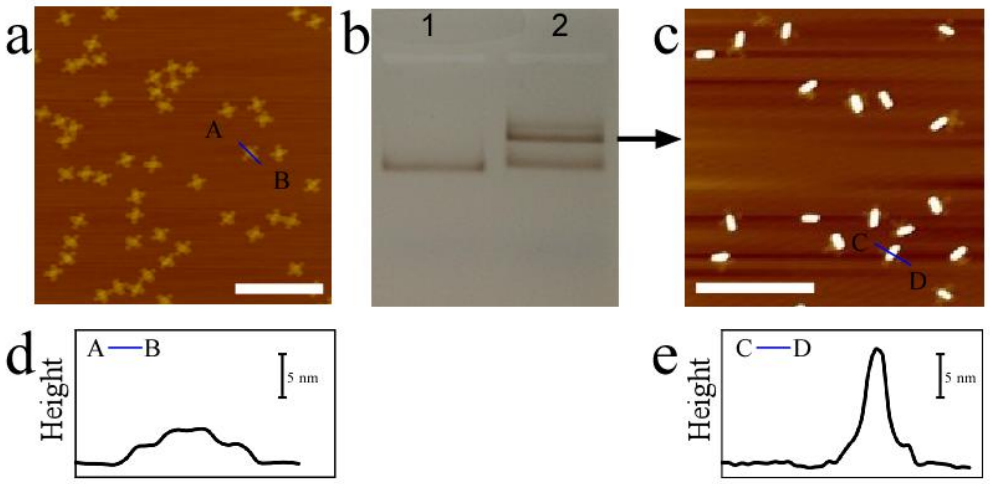

Figure 1. Formation of AuNRs on DNA origami frame. (a,c) AFM images of DNA origami frames before and after AuNRs attachment and corresponding section profiles along lines A-B (d) and C-D (e). (b) Agarose gel electrophoresis image of AuNRs on origami frame. Scale bar, 500 nm.

After the assembly process, the preformed arrays of origami framed AuNRs with designed pattern in liquid environment need to be transferred to dry ambient environment. In this pattern transfer step, any disturbing of the preestablished cation balance will damage the formed structures. Therefore, stronger interactions between mica and origami frames were desired to prevent the AuNRs from structural damage during the removal of buffer. This was achieved by adding extra Mg^{2+} to stabilize the arrays before rinsing.

To optimize the yield of arrays in the pattern transfer step, we tested how the concentration of Mg^{2+} affected the structure of the 1D arrays of origami framed AuNRs during the pattern transfer (Figure 2). The structural design of the 1D arrays of AuNRs is shown in the schematic drawings of Figure 2a and Figure S2. GC pair blunt ends were only designed on the opposite edges (red color) of origami frames while leaving the

scaffold loop on the other two sides unpaired (grey color). Such design enabled the stacking interactions only occurring in linear direction between the origami frames. After sample deposition and following incubation on mica, the 1D arrays of origami framed AuNRs formed in liquid environment and exhibited with blurring shadow in Figure S3 because of the unstable nature of AuNR arrays during liquid AFM scanning. In order to increase the binding affinity between AuNR pattern and mica surface while not disturbing the preformed arrays, then, various concentrations of Mg^{2+} from 5 mM to 40 mM were added to treat the samples for immobilization and pattern transfer processes. As seen from the results, no linear arrays of AuNRs were found after treatment with 1xTAE containing 5 mM Mg^{2+}, suggesting that 5 mM Mg^{2+} was not sufficient to immobilize the formed AuNRs array structures on mica surface during pattern transfer process (Figure 2b). When the concentration of Mg^{2+} was increased to 10 mM, AuNRs were assembled into shorter linear array with tile number less than 5 (Figure 2c), indicating 10 mM Mg^{2+} started to improve the immobility of the formed arrays. As the concentration of Mg^{2+} was further increased to 20 mM and 40 mM, much longer AuNRs linear arrays were observed, indicating the concentration of Mg^{2+} was high enough to stabilize the formed arrays with their structures maintained during the pattern transfer process (Figure 2d, 2e). Since no significant difference in the results by 20 mM Mg^{2+} and 40 mM Mg^{2+} was observed, it was determined that Mg^{2+} concentration of 20 mM was sufficient to provide high yield in the pattern transfer process and was thus used for subsequent studies.

With the optimized surface diffusion-mediated assembly and pattern transfer processes, many different types of AuNR arrays were constructed and transferred. First, AuNRs dimers in both end-to-end and side-by-side configurations were designed by

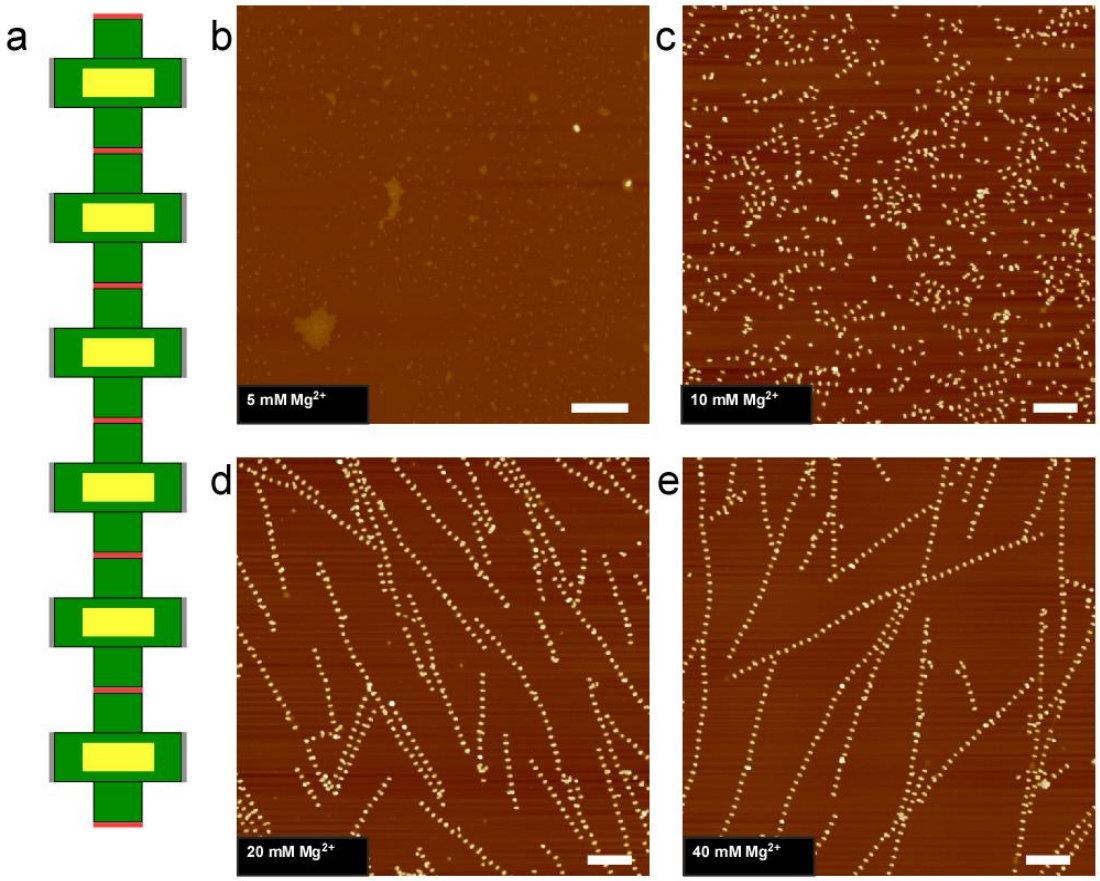

Figure 2. 1D arrays of AuNRs as a function of varying Mg^{2+} concentration during pattern transfer. (a-d) AFM images with different Mg^{2+} concentration: (a) 5 mM (b) 10 mM (c) 20 mM (d) 40 mM. Scale bar, 500 nm.

placing GC pair blunt ends on the one side (red color) of origami frames while leaving the scaffold loop on other three sides unpaired (grey color) as shown in the schematic drawings in Figure 3a and 3b. Dimer AuNRs were successfully assembled and visualized by AFM. It is worth noting that electrostatic repulsion between DNA-functionalized AuNRs in end-to-end configuration was stronger than that in side-by-side configuration, which leaded to the low yield of dimer formation in end-to-end configuration (Figure S4). The electrostatic repulsion can be moderated by controlling divalent cations, such as

Mg^{2+} in buffer.[33] Besides that, it is known that the base stacking interactions between origami frames would enhance with higher salt concentration. Thus, concentration of Mg^{2+} in the assembly process was modified to 15mM to moderate the electrostatic repulsion and increase stacking interaction. With this modification, the AuNRs dimers in end-to-end configuration were successfully formed with high yield as demonstrated in Figure 3b. Besides AuNRs dimer, complex AuNRs nanoclusters were also constructed, including 1D arrays of AuNRs in both end-to-end and side-by-side configurations and ladder arrays of AuNRs. Interestingly, 1D arrays of AuNRs in side-by-side configuration formed longer 1D arrays with high yield (Figure 2), while the AuNRs in end-to-end configuration assembled into 1D arrays in shorter length even with modified Mg^{2+} concentration (Figure 3c). This may also be attributed from the electrostatic repulsion between DNA-functionalized AuNRs. For AuNRs ladder arrays, three neighboring sides of origami frames were designed with GC pair blunt ends (red color) as shown in the schematic drawing in Figure 3d. Ladder arrays of AuNRs were assembled and visualized as shown in the AFM image in Figure 3d. Overall, the results revealed the versatility of proposed method in the assembly of AuNRs.

Encouraged by the formation of various patterns of AuNRs by substrate-assisted self-assembly method, we also explored the feasibility of large-scale assembly of 2D arrays of origami-framed AuNRs. It is already known that the strength of the stacking interactions would vary according to the binding energy of different sequences in the blunt-ends: with GC pair of -2.17 kcal/mol versus AT pair of -0.19 kcal/mol.[34] Herein, we investigated whether the strength of staking interactions would affect the orientation

of the self-assembly of origami-framed AuNRs by designing different sequences in the blunt-ends.

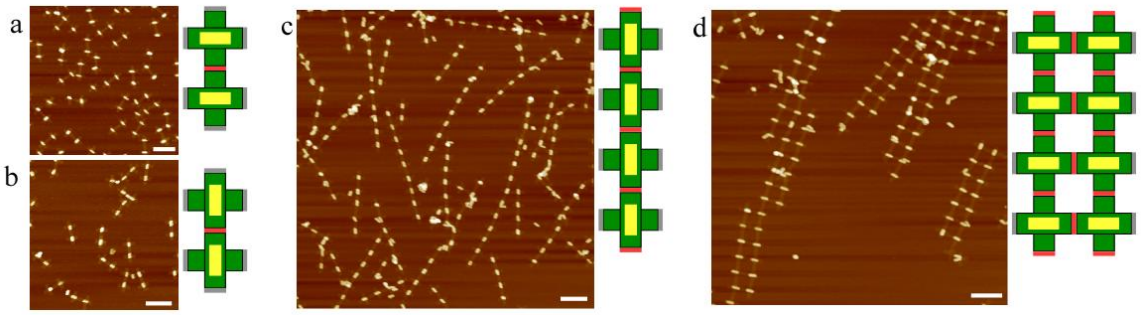

Figure 3. AuNRs dimers and complex AuNRs clusters. (a) AuNRs dimers in end-to-end and (b) side-by-side configurations. (c) 1D arrays of AuNRs in end-to-end configuration. (d) AuNRs ladder arrays. Scale bar, 200 nm.

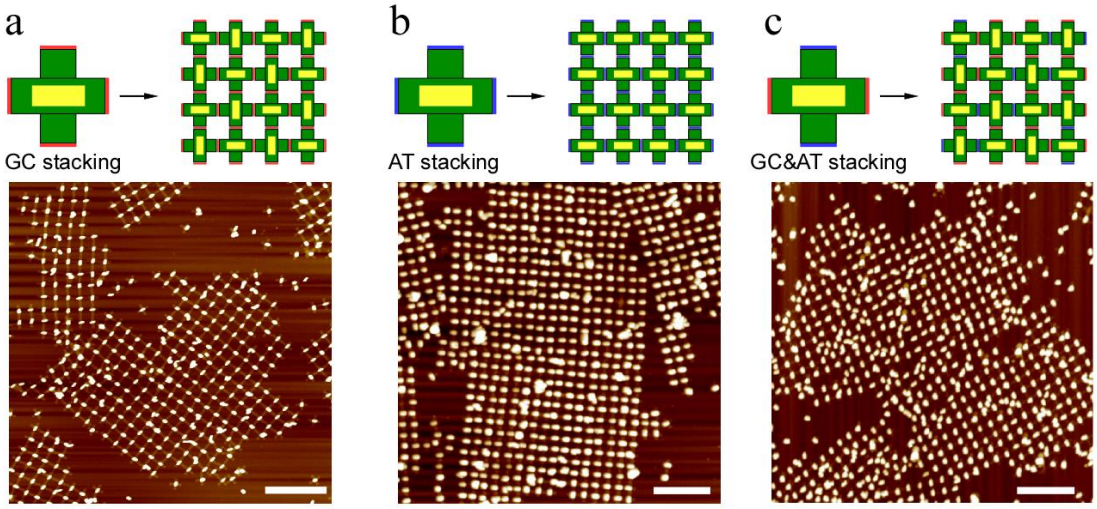

Figure 4. AuNR 2D arrays formed by origami frames with GC stacking (a), AT stacking (b), and both GC stacking and AT stacking (c). Scale bar 500 nm.

Firstly, the structural design of origami frames for AuNR 2D arrays is shown in the schematic drawings in Figure 4a and Figure S5. The four edges of origami frames

were fully designed with GC pair blunt ends (red color). Such design enabled the stacking interactions occurring in four directions between the origami frames. As a result, AuNRs were aligned into random pattern due to strong stacking interactions between GC pair as seen in the AFM image in Figure 4a. Orientation of the formed AuNR arrays was highlighted as shown in Figure S6. Besides the random pattern, well-ordered 2D arrays of AuNRs were also constructed. The four edges of origami frames were modified with weaker blunt-end stacking interactions (AT pair blunt ends).[34] Figure 4b showed the corresponding AFM image of well-ordered 2D arrays of AuNRs. In order to figure out the underlying mechanism of the different assembly configurations in Figure 4a and 4b, we modified the AT pair blunt ends on the left and right sides of origami frames to GC pair blunt ends (Figure 4c). It was found that random pattern rather than well-ordered 2D arrays was formed. The results revealed that by increasing strength of staking interactions on the origami frames, stronger electrostatic repulsion between DNA-functionalized AuNRs was moderated, which led to the configuration transformation from well-ordered 2D arrays to random pattern.

4. CONCLUSIONS

In summary, we demonstrated a novel surface diffusion-mediated DNA origami assembly method for the fabrication of plasmonic nanomaterials into well-ordered structures. Highly ordered 1D and 2D arrays of AuNRs were constructed by employing DNA origami frames as scaffold with the surface mobility of DNA origami frames in liquid environment manipulated by the concentration of divalent (Mg^{2+}) and monovalent

(Na^+) cations. The assembled 1D and 2D arrays of AuNRs were successfully transferred from liquid environment to dry ambient environment with high yield with optimized Mg^{2+} concentration. The successful assembly of AuNRs dimers, 1D arrays, and ladder arrays of AuNRs in both end-to-end and side-by-side configurations revealed the versatility of proposed method in the assembly of AuNRs. Well-ordered and micrometer-sized 2D superstructures with AuNRs arranged in predesigned orientation demonstrated the scalability of the proposed method. The origami-assisted assembly could provide a cost-effective and reliable method for organizing AuNRs with promising applications in nanoelectronics and nanoplasmonics.

ACKNOWLEDGEMENT

This work was supported by National Science Foundation under grants CCF-1814797.

SUPPLEMENTARY INFORMATION

BOTTOM-UP FABRICATION OF LARGE-SCALE GOLD NANOROD ARRAYS BY SURFACE DIFFUSION-MEDIATED DNA ORIGAMI ASSEMBLY

Shuo Yang,[a] Wenyan Liu,[a, b] Yuwei Zhang,[a] and Risheng Wang*[a]

[a] Department of Chemistry,
Missouri University of Science and Technology, Rolla, MO 65409, United States

[b] Center for Research in Energy and Environment,
Missouri University of Science and Technology, Rolla, MO 65409, United States
*E-mail: wangri@mst.edu

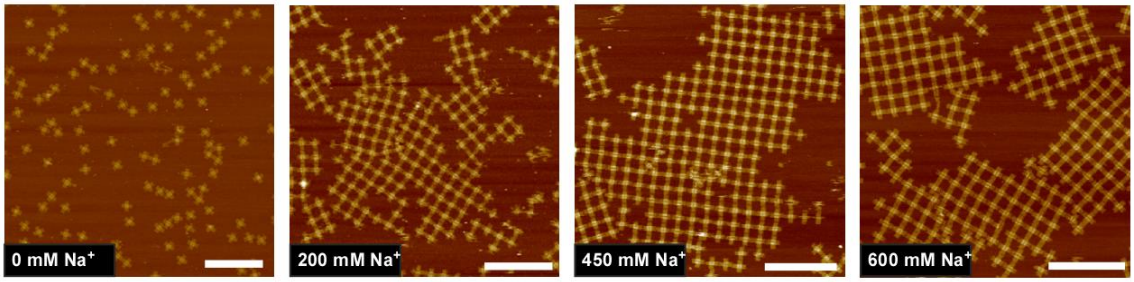

Figure S1. AFM image of origami arrays with varied concentrations of Na^+, 0 mM, 200 mM, 450 mM, 600 mM, respectively.

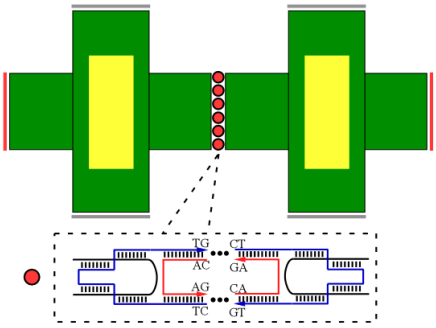

Figure S2. Schematic drawing of 1D arrays of origami framed AuNRs

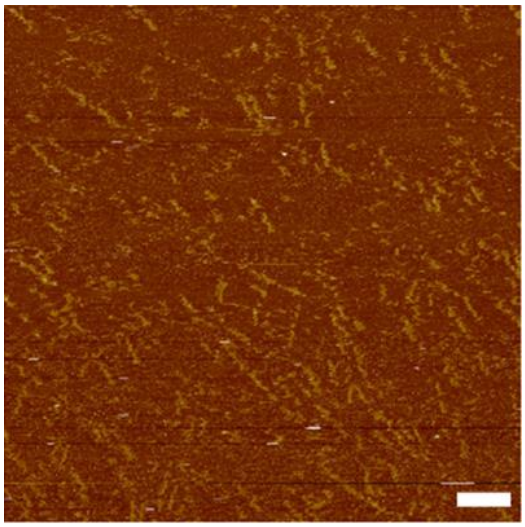

Figure S3. 1D arrays of origami framed AuNRs formed in liquid environment. Scale bar, 500 nm

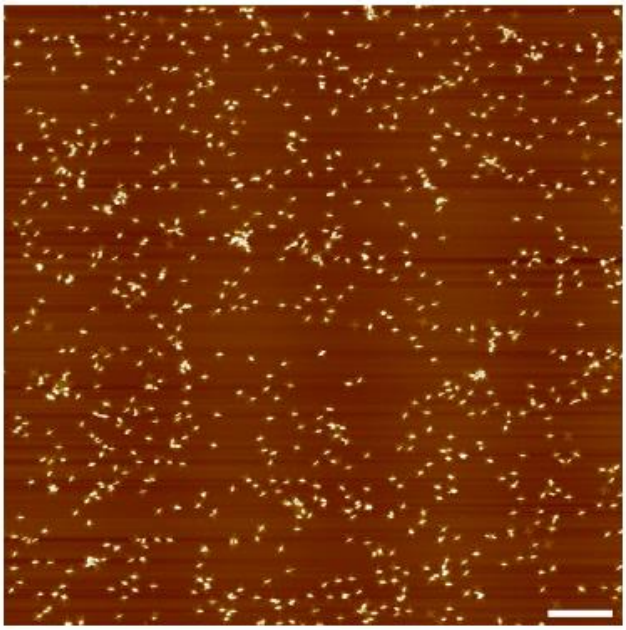

Figure S4. Dimer AuNRs in end-to-end configuration at low yield. Scale bar, 500 nm

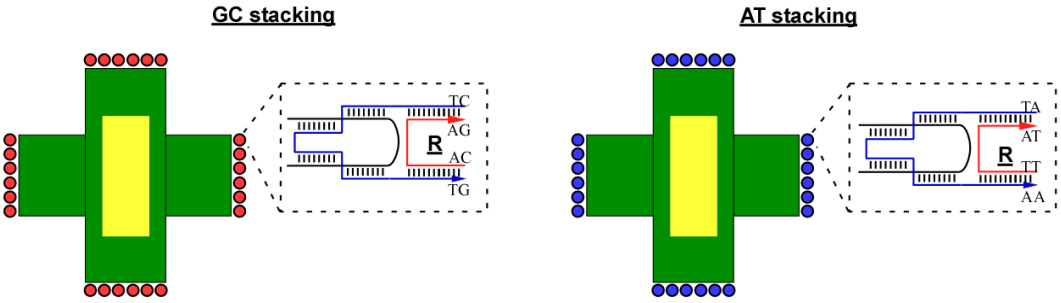

Figure S5. Schematic drawing of the stacking interaction on origami frames with all GC stacking (left) and all AT stacking (right)

DNA Sequences:

RC-M1 AGCTAATGCAGAACGCGCCTGTTTTAATATCC

RC-M2 CATCCTAATTTGAAGCCTTAAATCTTTTATCC

RC-M3 TGAATCTTGAGAGATAACCCACAAAACAATGA

RC-M4 AATAGCAATAGATGGGCGCATCGTACCGTATC

RC-M5 GGCCTCAGCTTGCATGCCTGCAGGGAATTCGT

RC-M6 AATCATGGTGGTTTTTCTTTTCACCCGCCTGG

RC-M7 CCCTGAGAGAGTTGCAGCAAGCGGGTATTGGG

RC-M8 CGCCAGGGTCATAGCTGTTTCCTGGACGGCCA

RC-M9 GTGCCAAGGAAGATCGACATCCAGATAGGTTA

RC-M10 CGTTGGTGTAGCTATCTTACCGAATTGAGCGC

RC-M11 TAATATCAACCTTCGCTAACGAGCCCGACTTG

RC-M12 CGGGAGGTTTTACGAGCATGTAGAACATGTTC

RC-M13 CTGTCCAGACGACGACAATAAACAAACCAATC

RC-M14 AATAATCGCGTTTTAGCGAACCTCGTCTTTCC

RC-M15 AGAGCCTACAAAGTCAGAGGGTAAGCCCTTTT

RC-M16 TAAGAAAAGATTGACCGTAATGGGCCAGCTTT

RC-M17 CCGGCACCCACGACGTTGTAAAACTGTGAAAT

RC-M18 TGTTATCCGGGAGAGGCGGTTTGCTCCACGCT

RC-M19 GGTTTGCCCCAGCAGGCGAAAATCAATCGGCC

RC-M20 AACGCGCGGCTCACAATTCCACACCCAGGGTT

RC-M21 TTCCCAGTGCTTCTGGTGCCGGAAGTGGGAAC

RC-M22 AAACGGCGGTAAGCAGATAGCCGAAACTGAAC

RC-M23 ACCCTGAAATTTGCCAGTTACAAATTCTAAGA

RC-M24 ACGCGAGGGCTGTCTTTCCTTATCAAGTAATT

RC-M25 GTACCGACAAAAGGTAATTCCAAG

RC-M26 AACGGGTAGAAGGCTTATCCGGTAATAAACAG

RC-M28 GTCGGATTCTCCACCAGGCA

RC-M30

AGCCGGAAGCCAGCTGCATTAATGCTGTTTGATGGTGTCTTCCTGTAGCCAGC

TTTAATCGATG

RC-M31

GCAAAATTCGGGAAACCTGTCGTGCATAAAGTGTAAAGCGATGTGCT

RC-M32 GCAAGGCGTTCGCCATTCAGGCTGCGCAACTG

RC-M33 GGAAGCGCTTTATCCCAATCCAAAAAGCAAAT

RC-M34

CAGATATATTAAACCATACGGAAATTACCCAAAAGAACTGGCATGATTA

RC-M35 AGGCATTTTCGAGCCAGTACTCATCG

RC-M36 AGAACAAGTACCGCGCCCAATAGCTAAGAAAC

RC-M39 CCTAATGAACTGCCCGCTTTCCAGCCCTTATA

RC-M40 AATCAAAAGAATAGCCCTTTAAATATGCATTCTACTA

RC-M41 GAGATAGGGTTGTCAGGATTAGAGAGTACCTATTCATT

RC-M42 TTGCGCTCGTGAGCTAACTCACATGATAGCCC

RC-M43 TATTACGCGGCGATCGGTGCGGGCGAGGATTT

RC-M44 CAGCCTTTGTTTAACGTCAAAAATTTTCAATT

RC-M45 GGAATCATCAAGCCGTTTTTATTTGTTATATA

RC-M46 TCGCCATATTTAACAACGTTGCGGGGTTTTAAGCCCAA

RC-M47 CCAACAGTGTGTGCCCGTATAAACAGTTAACCAGAGC

RC-M48 ACTATATGCTCCGGCTTAGGTTGGTCATCGTA

RC-M51 TAAAACATCTTTAATGCGCGAACTTAATTGCG

RC-M52 CTATTAGTCGCCATTAAAAATACCATAGATTA

RC-M53 GAGCCGTCTAGACTTTACAAACAATTCGACAA

RC-M54

AATCGCGCAAAAGAAGTTAGTTAGCTTAAACAGCTTGATACGCCCACGC

RC-M55 TTTTTAACTAAATGCTGATGCAAAATTGAGAA

RC-M56 CAAGACAAAAATCATAGGTCTGAGACAAACAT

RC-M59 CACCAGCAGGCACAGATTTAATTTCTCAATCATAAGGGAAC

RC-M60 TGCTGGTAATATCCAGAACAATATAAGCGTAA

RC-M61 GAATACGTGAAGATAAAACAGAGGATCTAAAA

RC-M62 TATCTTTAAAATCCTTTGCCCGAACCGCGACCTGC

RC-M63 CGAAACAAAGTAATAACGGA

RC-M64 TTCGCCTGCAAAATTAATTACATTAATAGTGA

RC-M65

ATTTATCAAGAACGCGAGAAAACTAGTATAAAGCCAATAAAGAATACAC

RC-M66 ATATGCGTTATACAAATTCTTACCTTTTCAAA

RC-M67 TATATTTTGACGCTGAGAAGAGTCTAACAATT

RC-M69 ATTTGTATCATCGCTTCTGAATTACAGTAACA

RC-M71 TCAGTATTAACCCTTCTGACCTGATACCGCCA

RC-M72 GCCATTGCAACAGGAAAAACGCTCTGGCCAAC

RC-M73 AGAGATAGAACACCGCCTGCAACAAAATCAAC

RC-M74 AGTAGAAAAGTTTGAGTAACATTA

RC-M75 TTTGGATTATACCTGATAAATTGTGTCGAAATCGTTATTA

RC-M76 GTACCTTTATTACCTTTTTTAATGCGATAGCT

RC-M77 TAGATTAAAGTTAATTCGATCTTCTTAGTATC

RC-M78 TCATAATTACTAGAAAAAGCCTGTTGACCTAA

RC-M79 ATTTAATGATCCTTGAAAACATAGGAAACAGT

RC-M80 ACATAAATACGTCAGATGAATATATGGAAGGA

RC-M81 ATTGAACCAATATAATCCTGATTGTCATTTTG

RC-M82 CGGAACAATATCTGGTCAGTTGGCGTGCCACG

RC-M83 CTGAGAGCAATAAAAGGGACATTCATGGAAAT

RC-M84 ACCTACATTTTGACGCTCAATCGTCAGTGCGC

RC-M85 CGACCAGTCAGCAGCAAATGAAAATCAAACCC

RC-M86 TCAATCAAAGAAACCACCAGAAGGATGATGGC

RC-M87 AATTCATCAACCATATCAAAATTATAGATTTT

RC-M88 CAGGTTTACAATATATGTGAGTGATTAATTTT

RC-M89 CCCTTAGAGTTTGAAATACCGACCCACCGGAA

RC-M90 AAAAGGGTAAGATTGTATAAGCAAAAATTCGC

RC-M91 AATAACCTTTAGAACCCTCATATAAAAGATTC

RC-M92 GAAAGACTCAATTCTGCGAACGAGAAATGGTC

RC-M93 CATAGTAATGACTATTATAGTCAGGGAAGCCC

RC-M94 TAACAAAGTTAGGAATACCACATTTTACGAGG

RC-M95 GCTGGCTGACCTTCATCAAGAGTAAATCAACG

RC-M96 GTTGAGATCTGCTCATTCAGTGAAGCGCATAG

RC-M97 CTTTACCCGAGCAACACTATCATAATTCATCA

RC-M98 TTGATTCCTCAAATATCGCGTTTTAATCAGGT

RC-M99 AAAAATTTGTTTAGCTATATTTTCTGTAACAG

RC-M100 AAAACAGGGAGAAAGGCCGGAGACGCAAGGAT

RC-M101 GTTAAATTTTTGTTAAATCAGCTCAAGCCCCA

RC-M102 CACCATCACGGTTGATAATCAGAAATTTTTTA

RC-M103 CGCGAGCTAAGCCTTTATTTCAACAGTCAAAT

RC-M104 CTTCAAAGTGGAAGTTTCATTCCAATTTGGGG

RC-M105 TTACCAGAATGACCATAAATCAAAAATTCGAG

RC-M106 GCCCTGACTATTACAGGTAGAAAGACCCTCGT

RC-M107 ACAGATGAACGGTGTACAGACCAGTAAGGCTT

RC-M108 AACAACATGAGAACACCAGAACGAGAAAGAGG

RC-M110 ACGGTGTCCGAACCAGACCGGAAGAGTTCAGA

RC-M112 ATGTACCCATATGATATTCAACCGAATACTTT

RC-M113 ACCAATAGGAACGCCATCAAAAATTCAATCAT

RC-M114

GATAAATTTCGTAAAACTAGCATGAATTCGCGTCTGGCTGTTCCGAAATCG

RC-M115 ATAGTAGTAACATTATGACCCTGTTTCTAGCT

RC-M116

CAAACTCCAACAGTTGAGTGTTGTTCGTAGAAGAACTCAAACTTTGAATGG

RC-M117 GAGGCTTTCTCAAATGCTTTAAAC

RC-M118 TTGGGCTTTACGTTAATAAAACGAAATAGCGA

RC-M119 CGAACTGACCAACTTTGTAGTAAA

RC-M120 GAAAAATCGAGATGGTTCAATATTTATCGGCCT

RC-M123 AACGGTAAAATGCCGGAGAGGGTAAATCGGTT

RC-M124 TTAAATGTGAGCGAGTAACAACTTAAGGAAACCGAGGAAA

RC-M125 CTGGAGCAAACAAGAGCATCAACA

RC-M126

CTGAATCTAAATCATACAGGCAAGTCAGAGCATGAAAGGGGCTGGGGTG

RC-M127

GGTAATAGGCGGAATCGTCATAAATTTAATTGCTCCTTTTCTTAATTG

RC-M128 TCATTGTGTTATACCAGTCAGGACCCAGAGGG

RC-M129 AACGAGGCGCAGACGGAACTTTAA

RC-M130 CTGGCTCAAATTACCTTATGCGATAATGACAA

RC-M132 GCTTAGAGGATAAGAGGTCATTTTTGAAACAT

RC-M134 CTGAGAGTCTACAAAGGCTATCAGACTTGAGC

RC-M135 CATTTGGGATTATCACCGTCACCGGTCATTGC

RC-M136 CTCAGAGCACCGCCACCCTCAGAGATTAAGCA

RC-M137 GAAAGTATTCGGAACCTATTATTCTGCGGATG

RC-M138 CCACAGACACAAACTACAACGCCTGATAGCGT

RC-M139 CAACCATCCGATAGTTGCGCCGACTTTAAGAA

RC-M140

ATAACCGATCATCTTTGACCCCCAGCGATTATACCAAGTTCATGTTACTTAGC

CGG

RC-M142 TGCCTATTTAAGAGGCTGAGACTCGAGTTTCG

RC-M144 AAAGGTGAAATTAGAGCCAGCAAAAGCCGCCA

RC-M145 CGCAATAATAACGGAATATTCATT

RC-M146 TAGCACCAAAATATTGTAGTACCGCAATAAGAGAATATAAA

RC-M147 CGCCGCCAGAACCGCCTCCCTCAGATCACCAG

RC-M148 CTAAAGTTCATGTACCGTAACACTCTCAAGAGAAGGATTAGGATTA

RC-M149

TAAAACACTATATTCGGTCGCTGATTTCGAGGAGAATTTCGTAACGAT

RC-M150

GGGAGTTAAACGAAAGAGGCGTCGCTCAACAGTAGGGCTTATCCAATCG

RC-M153

AGACTCCTTTGAGGGAGGGAAGGTTTACCATTAGCAAGGCACCAGAGC

RC-M154 AGTATGTTAGCAAACGTAGAAAATGCGCCAAA

RC-M155 TCACCAATGGCGACATTCAACCGATATTACGC

RC-M156 TCAGACGAAATCAAAATCACCGGACGGAAACG

RC-M157 CCAGGCGGTTTTAACGGGGTCAGTGAGGCAGG

RC-M158 AATGAATTCATTTTCAGGGATAGCGCTCAGTA

RC-M159 TTTTGCGGGAGCCTTTAATTGTATCGTTAGTA

RC-M160 GCCACTACGAAGGCACCAACCTAAAAGGCCGC

RC-M161 TCCAAAAGGATCGTCACCCTCAGCTACGTAAT

RC-M162 ACCACCCTTTCTGTATGGGATTTTAAAAAGGC

RC-M163 GTAATAAGATAAGTGCCGTCGAGATCAGAGCC

RC-M164 CTTTTCATTTGGCCTTGATATTCAGTGTACTG

RC-M165 GACAAAAGGAAACCATCGATAGCATTTGCCAT

RC-M166 AAAGGTGGCAACATATAAAAGAAACACAATCA

RC-M167 ATCAGTAGTTCATATGGTTTACCAACATACAT

RC-M168 TGGATCTTAGCCCCCTTATTAGCGGCACCGTA

RC-M169 ATAAGTATTTTTGATGATACAGGACAAACGAA

RC-M170 ACTTTCAACTCAGAACCGCCACCCGGGTTGAT

RC-M171 ACAGCATCGTTGAAAATCTCCAAAGCTAAACA

RC-M172 GAAGTTTCCATTAAACGGGTAAAAAGCGAAAG

RC-M173 TTTTTCACGGAACGAGGGTAGCAATTCATGAG

RC-M174 CCGCCACCCAGTTTCAGCGGAGTGATAATAAT

RC-M175 TACATGGCAGCCCGGAATAGGTGTCCTCAGAA

RC-M176 TCGGTCATCATTAAAGCCAGAATGAAGCGTCA

RC-M177 ATAGAAAACGACAGAATCAAGTTTCGGCATTT

Blunt ends for stacking interactions:

RC-A-L1-BE: TCCTGAACAAGAAAAAATCAACAATAGATAAG

RC-A-L2-BE: TTGCACCCAGCTACAAAAGATTAGTTGCTATT

RC-A-L3-BE: AATAATAAGAGCAAGAGAATTGAGTTAAGCCC

RC-A-L4-BE: GTTTGAGGGGACGACGAACCGTGCATCTGCCA

RC-A-L5-BE: CCCGGGTACCGAGGTCTCGACTCTAGAGGATC

RC-A-L6-BE: AGCTGATTGCCCTTCACAGTGAGACGGGCAAC

RC-A-R1-BE: GTTAAATAAGAATAAAGTGTGATAAATAAGGC

RC-A-R2-BE: AAATCGTCGCTATTAAATAACCTTGCTTCTGT

RC-A-R3-BE: AAATAAAGAAATTGCGTTAGCACGTAAAACAG

RC-A-R4-BE: TATTCCTGATTATCAGAGCGGAATTATCATCA

RC-A-R5-BE: TGCTGAACCTCAAATAATCTAAAGCATCACCT

RC-A-R6-BE: ACATTGGCAGATTCACCTGAAATGGATTATTT

RC-A-D1-BE: CGTTAATATTTTGTTAATATTTAAATTGTAAA

RC-A-D2-BE: TGAGTAATGTGTAGGTTTTTAAATGCAATGCC

RC-A-D3-BE: ATTAGATACATTTCGCTAGATTTAGTTTGACC

RC-A-D4-BE: ATCAAAAAGATTAAGAAAGCAAAGCGGATTGC

RC-A-D5-BE: ATAACGCCAAAAGGAACAACTAATGCAGATAC

RC-A-D6-BE: GGATATTCATTACCCAATCTTCGACAAGAACC

RC-A-U1-BE: AATAAGTTTATTTTGTCGCAAAGACACCACGG

RC-A-U2-BE: TGTAGCGCGTTTTCATGCCTTTAGCGTCAGAC

RC-A-U3-BE: AATTTACCGTTCCAGTGAAAGCGCAGTCTCTG

RC-A-U4-BE: GGTTTAGTACCGCCACATCACCGTACTCAGGA

RC-A-U5-BE: ACTAAAGGAATTGCGAAGAATAGAAAGGAACA

RC-A-U6-BE: GAGGACTAAAGACTTTCGGCTACAGAGGCTTT

Modified DNA sequences to anchor AuNRs:

RC-M27-AS

AGCACATAGGAAGAGTTTCCATATTAATTAGACGGGAGAATTACAAAGTTAC

C

RC-M29-AS

AGCACATAGGAAGAGTTTAAGCGCCAATTAAGTTGGGTAACGAACATACG

RC-M37-AS

AGCACATAGGAAGAGTTTGATTTTTTACAGAGAGAATAACATAAAAACAG

RC-M38-AS

AGCACATAGGAAGAGTTTTTGGGAAGCAGCTGGCTTAAAGCTAGCTATTTTT

GAGAGAT

RC-M49-AS

AGCACATAGGAAGAGTTTACCTGAGCAGAGGCGAATTATTCAGAAAATAG

RC-M50-AS

AGCACATAGGAAGAGTTTAGAAGTATAATAGATAATACATTTCTCTTCGC

RC-M57-AS

AGCACATAGGAAGAGTTTCAAGAAAAATTGCTTTGAATACCAAGTTACAA

RC-M58-AS

AGCACATAGGAAGAGTTTCTCGTATTGGTGCACTAACAACTAGAACGAAC

RC-M68-AS

AGCACATAGGAAGAGTTTTGATTTGATACATCGGGAGAAACACAACGGAG

RC-M70-AS

AGCACATAGGAAGAGTTTATTTTAAAGGAATTGAGGAAGGTTTGAGGCGG

Sequence of the thiolated strands used to functionalize gold nanorods:

5'-CTCTTCCTATGTGCTTTATT/3ThiolMC3-D/-3'

Modified DNA Sequences on four edges of origami frames for GC stacking:

RC-A-L1-GCpair

CTACGACTGATTCCTGAACAAGAAAAAATCAACAATAGATAAGTGAGACACC

TG

RC-A-L2-GCpair

CTACGACTGATTTGCACCCAGCTACAAAAGATTAGTTGCTATTTGAGACACCT

G

RC-A-L3-GCpair

CTACGACTGATAATAATAAGAGCAAGAGAATTGAGTTAAGCCCTGAGACACC

TG

RC-A-L4-GCpair

CTACGACTGATGTTTGAGGGGACGACGAACCGTGCATCTGCCATGAGACACC

TG

RC-A-L5-GC pair

CTACGACTGATCCCGGGTACCGAGGTCTCGACTCTAGAGGATCTGAGACACC

TG

RC-A-L6-GC pair

CTACGACTGATAGCTGATTGCCCTTCACAGTGAGACGGGCAACTGAGACACC

TG

RC-A-R1-GC pair

CTACGACTGATGTTAAATAAGAATAAAGTGTGATAAATAAGGCTGAGACACC

TG

RC-A-R2-GC pair

CTACGACTGATAAATCGTCGCTATTAAATAACCTTGCTTCTGTTGAGACACCT

G

RC-A-R3-GC pair

CTACGACTGATAAATAAAGAAATTGCGTTAGCACGTAAAACAGTGAGACACC

TG

RC-A-R4-GC pair

CTACGACTGATTATTCCTGATTATCAGAGCGGAATTATCATCATGAGACACCT

G

RC-A-R5-GC pair

CTACGACTGATTGCTGAACCTCAAATAATCTAAAGCATCACCTTGAGACACCT

G

RC-A-R6-GC pair

CTACGACTGATACATTGGCAGATTCACCTGAAATGGATTATTTTGAGACACCT

G

RC-A-D1-GC pair

CTACGACTGATCGTTAATATTTTGTTAATATTTAAATTGTAAAGATGAGATAA

A

RC-A-D2-GC pair

CTACGACTGATTGAGTAATGTGTAGGTTTTTAAATGCAATGCCTGAGACACCT

G

RC-A-D3-GC pair

CTACGACTGATATTAGATACATTTCGCTAGATTTAGTTTGACCTGAGACACCT

G

RC-A-D4-GC pair

CTACGACTGATATCAAAAAGATTAAGAAAGCAAAGCGGATTGCTGAGACACC

TG

RC-A-D5-GC pair

CTACGACTGATATAACGCCAAAAGGAACAACTAATGCAGATACTGAGACACC

TG

RC-A-D6-GC pair

CTACGACTGATGGATATTCATTACCCAATCTTCGACAAGAACCTGAGACACCT

G

RC-A-U1-GC pair

CTACGACTGATAATAAGTTTATTTTGTCGCAAAGACACCACGGTGAGACACC

TG

RC-A-U2-GC pair

CTACGACTGATTGTAGCGCGTTTTCATGCCTTTAGCGTCAGACTGAGACACCT

G

RC-A-U3-GC pair

CTACGACTGATAATTTACCGTTCCAGTGAAAGCGCAGTCTCTGTGAGACACCT

G

RC-A-U4-GC pair

CTACGACTGATGGTTTAGTACCGCCACATCACCGTACTCAGGATGAGACACC

TG

RC-A-U5-GC pair

CTACGACTGATACTAAAGGAATTGCGAAGAATAGAAAGGAACATGAGACAC

CTG

RC-A-U6-GC pair

CTACGACTGATGAGGACTAAAGACTTTCGGCTACAGAGGCTTTTGAGACACC

TG

GC pair Complementary strand CAGGTGTCTCAATCAGTCGTAG

Modified DNA Sequences on four edges of origami frames for AT stacking:

RC-A-L1-AT pair

ATGAACTAAGCTCCTGAACAAGAAAAAATCAACAATAGATAAGGATGAGAT

AAA

RC-A-L2-AT pair

ATGAACTAAGCTTGCACCCAGCTACAAAAGATTAGTTGCTATTGATGAGATA

AA

RC-A-L3-AT pair

ATGAACTAAGCAATAATAAGAGCAAGAGAATTGAGTTAAGCCCGATGAGAT

AAA

RC-A-L4-AT pair

ATGAACTAAGCGTTTGAGGGGACGACGAACCGTGCATCTGCCAGATGAGATA

AA

RC-A-L5-AT pair

ATGAACTAAGCCCCGGGTACCGAGGTCTCGACTCTAGAGGATCGATGAGATA

AA

RC-A-L6-AT pair

ATGAACTAAGCAGCTGATTGCCCTTCACAGTGAGACGGGCAACGATGAGATA

AA

RC-A-R1-AT pair

ATGAACTAAGCGTTAAATAAGAATAAAGTGTGATAAATAAGGCGATGAGAT

AAA

RC-A-R2-AT pair

ATGAACTAAGCAAATCGTCGCTATTAAATAACCTTGCTTCTGTGATGAGATAA

A

RC-A-R3-AT pair

ATGAACTAAGCAAATAAAGAAATTGCGTTAGCACGTAAAACAGGATGAGAT

AAA

RC-A-R4-AT pair

ATGAACTAAGCTATTCCTGATTATCAGAGCGGAATTATCATCAGATGAGATA

AA

RC-A-R5-AT pair

ATGAACTAAGCTGCTGAACCTCAAATAATCTAAAGCATCACCTGATGAGATA

AA

RC-A-R6-AT pair

ATGAACTAAGCACATTGGCAGATTCACCTGAAATGGATTATTTGATGAGATA

AA

RC-A-D1-AT pair

ATGAACTAAGCCGTTAATATTTTGTTAATATTTAAATTGTAAAGATGAGATAA

A

RC-A-D2-AT pair

ATGAACTAAGCTGAGTAATGTGTAGGTTTTTAAATGCAATGCCGATGAGATA

AA

RC-A-D3-AT pair

ATGAACTAAGCATTAGATACATTTCGCTAGATTTAGTTTGACCGATGAGATAA

A

RC-A-D4-AT pair

ATGAACTAAGCATCAAAAAGATTAAGAAAGCAAAGCGGATTGCGATGAGAT

AAA

RC-A-D5-AT pair

ATGAACTAAGCATAACGCCAAAAGGAACAACTAATGCAGATACGATGAGAT

AAA

RC-A-D6-AT pair

ATGAACTAAGCGGATATTCATTACCCAATCTTCGACAAGAACCGATGAGATA

AA

RC-A-U1-AT pair

ATGAACTAAGCAATAAGTTTATTTTGTCGCAAAGACACCACGGGATGAGATA

AA

RC-A-U2-AT pair

ATGAACTAAGCTGTAGCGCGTTTTCATGCCTTTAGCGTCAGACGATGAGATA

AA

RC-A-U3-AT pair

ATGAACTAAGCAATTTACCGTTCCAGTGAAAGCGCAGTCTCTGGATGAGATA

AA

RC-A-U4-AT pair

ATGAACTAAGCGGTTTAGTACCGCCACATCACCGTACTCAGGAGATGAGATA

AA

RC-A-U5-AT pair

ATGAACTAAGCACTAAAGGAATTGCGAAGAATAGAAAGGAACAGATGAGAT

AAA

RC-A-U6-AT pair

ATGAACTAAGCGAGGACTAAAGACTTTCGGCTACAGAGGCTTTGATGAGATA

AA

AT pair Complementary strand TTTATCTCATCGCTTAGTTCAT

REFERENCES

1. Vittala, S. K. & Han, D. DNA-Guided Assemblies toward Nanoelectronic Applications. ACS Appl. Bio Mater. 3, 2702–2722 (2020).

2. Seeman, N. C. & Sleiman, H. F. DNA nanotechnology. Nat. Rev. Mater. 3, (2017).

3. Rothemund, P. W. K. Folding DNA to create nanoscale shapes and patterns. Nature 440, 297–302 (2006).

4. Raveendran, M., Lee, A. J., Sharma, R., Wälti, C. & Actis, P. Rational design of DNA nanostructures for single molecule biosensing. Nat. Commun. 11, 1–9 (2020).

5. Han, S., Liu, W., Yang, S. & Wang, R. Facile and Label-Free Electrochemical Biosensors for MicroRNA Detection Based on DNA Origami Nanostructures. ACS Omega 4, 11025–11031 (2019).

6. Schüller, V. J. et al. Cellular immunostimulation by CpG-sequence-coated DNA origami structures. ACS Nano 5, 9696–9702 (2011).

7. Douglas, S. M., Bachelet, I. & Church, G. M. A Logic-Gated Nanorobot for Targeted Transport of Molecular Payloads. Science. 335, 831 LP – 834 (2012).

8. Zeng, Y. et al. Time-lapse live cell imaging to monitor doxorubicin release from DNA origami nanostructures. J. Mater. Chem. B 6, 1605–1612 (2018).

9. Liu, J. et al. Metallization of branched DNA origami for nanoelectronic circuit fabrication. ACS Nano 5, 2240–2247 (2011).

10. Ye, J., Helmi, S., Teske, J. & Seidel, R. Fabrication of Metal Nanostructures with Programmable Length and Patterns Using a Modular DNA Platform. Nano Lett. 19, 2707–2714 (2019).

11. Bayrak, T. et al. DNA-Mold Templated Assembly of Conductive Gold Nanowires. Nano Lett. 18, 2116–2123 (2018).

12. Klein, W. P. et al. Multiscaffold DNA origami nanoparticle waveguides. Nano Lett. 13, 3850–3856 (2013).

13. Gür, F. N. et al. DNA-Assembled Plasmonic Waveguides for Nanoscale Light Propagation to a Fluorescent Nanodiamond. Nano Lett. 18, 7323–7329 (2018).

14. Wang, P. et al. DNA Origami Guided Self-Assembly of Plasmonic Polymers with Robust Long-Range Plasmonic Resonance. Nano Lett. 20, 8926–8932 (2020).

15. Lan, X. et al. DNA-Guided Plasmonic Helix with Switchable Chirality. J. Am. Chem. Soc. 140, 11763–11770 (2018).

16. Zhou, C., Duan, X. & Liu, N. A plasmonic nanorod that walks on DNA origami. Nat. Commun. 6, 8102 (2015).

17. Zhan, P. et al. Reconfigurable Three-Dimensional Gold Nanorod Plasmonic Nanostructures Organized on DNA Origami Tripod. ACS Nano 11, 1172–1179 (2017).

18. Roller, E.-M. et al. DNA-assembled nanoparticle rings exhibit electric and magnetic resonances at visible frequencies. Nano Lett. 15, 1368–1373 (2015).

19. Liu, W., Li, L., Yang, S., Gao, J. & Wang, R. Self-Assembly of Heterogeneously Shaped Nanoparticles into Plasmonic Metamolecules on DNA Origami. Chem. - A Eur. J. 23, 14177–14181 (2017).

20. Yang, S., Liu, W. & Wang, R. Control of the stepwise assembly–disassembly of DNA origami nanoclusters by pH stimuli-responsive DNA triplexes. Nanoscale 11, 18026–18030 (2019).

21. Sun, X., Hyeon Ko, S., Zhang, C., Ribbe, A. E. & Mao, C. Surface-Mediated DNA Self-Assembly. J. Am. Chem. Soc. 131, 13248–13249 (2009).

22. Hamada, S. & Murata, S. Substrate-Assisted Assembly of Interconnected Single-Duplex DNA Nanostructures. Angew. Chemie 121, 6952–6955 (2009).

23. Aghebat Rafat, A., Pirzer, T., Scheible, M. B., Kostina, A. & Simmel, F. C. Surface-assisted large-scale ordering of DNA origami tiles. Angew. Chemie - Int. Ed. 53, 7665–7668 (2014).

24. Woo, S. & Rothemund, P. W. K. Self-assembly of two-dimensional DNA origami lattices using cation-controlled surface diffusion. Nat. Commun. 5, 4889 (2014).

25. Suzuki, Y., Endo, M. & Sugiyama, H. Lipid-bilayer-assisted two-dimensional self-assembly of DNA origami nanostructures. Nat. Commun. 6, 1–9 (2015).

26. Kocabey, S. et al. Membrane-Assisted Growth of DNA Origami Nanostructure Arrays. ACS Nano 9, 3530–3539 (2015).

27. Liu, W., Zhong, H., Wang, R. & Seeman, N. C. Crystalline two-dimensional DNA-origami arrays. Angew. Chemie - Int. Ed. 50, 264–267 (2011).

28. Liu, J. & Lu, Y. Preparation of aptamer-linked gold nanoparticle purple aggregates for colorimetric sensing of analytes. Nat. Protoc. 1, 246–252 (2006).

29. Hill, H. D. & Mirkin, C. A. The bio-barcode assay for the detection of protein and nucleic acid targets using DTT-induced ligand exchange. Nat. Protoc. 1, 324–336 (2006).

30. Pastré, D. et al. Adsorption of DNA to mica mediated by divalent counterions: A theoretical and experimental study. Biophys. J. 85, 2507–2518 (2003).

31. Pastré, D. et al. Anionic polyelectrolyte adsorption on mica mediated by multivalent cations: A solution to DNA imaging by atomic force microscopy under high ionic strengths. Langmuir 22, 6651–6660 (2006).

32. Bezanilla, M., Manne, S., Laney, D. E., Lyubchenko, Y. L. & Hansma, H. G. Adsorption of DNA to Mica, Silylated Mica, and Minerals: Characterization by Atomic Force Microscopy. Langmuir 11, 655–659 (1995).

33. Misra, V. K. & Draper, D. E. The interpretation of Mg2+ binding isotherms for nucleic acids using Poisson-Boltzmann theory. J. Mol. Biol. 294, 1135–1147 (1999).

34. Protozanova, E., Yakovchuk, P. & Frank-Kamenetskii, M. D. Stacked-unstacked equilibrium at the nick site of DNA. J. Mol. Biol. 342, 775–785 (2004).

SECTION

2. CONCLUSION

In this dissertation, both dynamic and static DNA origami-based nanostructures have been demonstrated, such as metal-ion stimulated DNA origami nanostructures, pH-triggered DNA origami nanostructures, and DNA-origami-assisted spatial arrangement of AuNRs.

In the first part of this dissertation, reversible assemblies of DNA origami nanostructures triggered by two types of stimuli, metal ion and pH, were introduced. These two new types of dynamic and environmentally responsive bridges increased the diversity of stimuli-responsive systems. The first project presented the metal-ion stimulated reversible assembly of DNA origami dimers. The assembly/disassembly were achieved by using G-quadruplexes as dynamic bridges because of the stimulated responsive capability-reversible conformation changes between G-quadruplex and its single-strand state driven by metal-ion, such as potassium (K^+). AFM was performed to investigate the assembly/disassembly process. The statistical analysis of the AFM images revealed that ~85% of the DNA origami tiles existed in a dimeric form before the treatment with K^+. However, after the K^+ treatment, a majority of the DNA origami dimers dissociated into monomers, with less than 18% of the DNA origami dimers remaining. Gel electrophoresis were performed to understand the reversibility of this K^+-responsive system. The gel image showed that in two continuous cycles, the dimer origami exhibited an effective stimuli-responsive capability. The second project

described a pH-driven stepwise assembly/disassembly of DNA origami nanoclusters. Two types of DNA triplexes were used as pH responsive bridges in controlling the reversible association of DNA clusters. Gel electrophoresis results showed that with an increase in pH, from 5.0 to 7.5, and further to 9.0, the targeted bands exhibit a slower and slower electrophoretic mobility corresponding to the formation of 5-tile and 9-tile origami nanoclusters. DLS method was used to monitor the reversibility of assembly of DNA origami clusters via detection of the size variations of DNA structures from monomers, dimers, to trimers in response to pH stimulation. Results showed that in two working cycles, the dynamic system can be switched between association and dissociation states controlled by pH stimulation. This dynamic DNA origami structure brought intriguing functions to the current technology of self-assembled DNA origami.

In the second part of this dissertation, a novel method for the fabrication of plasmonic nanomaterials into well-ordered structures was introduced. Through a surface assisted assembly method, the AuNRs on the DNA origami tiles self-organized into highly ordered 1D and 2D arrays on the mica surface by optimizing the concentration of divalent (Mg^{2+}) and monovalent (Na^{+}) cations in the assembly solution. AFM was performed to investigate how the concentration of Mg^{2+} affected the structure of the 1D arrays of origami framed AuNRs during the pattern transfer. AFM images showed that as the concentration of Mg^{2+} was increased to 20 mM and 40 mM, much longer AuNRs linear arrays were observed, indicating Mg^{2+} concentration of 20 mM was sufficient to provide high yield in the pattern transfer process. AFM results also showed the successful assembly of AuNRs into dimers, ladder arrays, 1D arrays and 2D arrays, indicating the versatility of proposed method in the assembly of AuNRs and other nanomaterials.

BIBLIOGRAPHY

1. Whitesides, G. M. & Grzybowski, B. Self-assembly at all scales. Science. 295, 2418–2421 (2002).

2. Zhang, S. Fabrication of novel biomaterials through molecular self-assembly. Nat. Biotechnol. 21, 1171–1178 (2003).

3. King, N. P. & Lai, Y. T. Practical approaches to designing novel protein assemblies. Curr. Opin. Struct. Biol. 23, 632–638 (2013).

4. Seeman, N. C. DNA in a material world. Nature 421, 427–431 (2003).

5. Antonietti, M. & Förster, S. Vesicles and Liposomes: A Self-Assembly Principle Beyond Lipids. Adv. Mater. 15, 1323–1333 (2003).

6. Caruthers, M. H. Gene Synthesis Machines: DNA Chemistry and Its uses. Science. 230, 281–285 (1985).

7. Seeman, N. C. & Lukeman, P. S. Nucleic acid nanostructures: Bottom-up control of geometry on the nanoscale. Reports Prog. Phys. 68, 237–270 (2005).

8. Seeman, N. C. Nucleic acid junctions and lattices. J. Theor. Biol. 99, 237–247 (1982).

9. Holliday, R. A mechanism for gene conversion in fungi. Genet. Res. (Camb). 89, 285–307 (2008).

10. Ma, R.-I., R., N. R. K., D.Sheardy, R., L.Petrillo, M. & Nadrian C.Seeman. Three-arm nucleic acid junctions are flexible. Nucleic Acids Res. 14, 103–104 (1986).

11. Wang, X. & Seeman, N. C. Assembly and characterization of 8-arm and 12-arm DNA branched junctions. J. Am. Chem. Soc. 129, 8169–8176 (2007).

12. Wang, Y., Mueller, J. E., Kemper, B. & Seeman, N. C. Assembly and Characterization of Five-Arm and Six-Arm DNA Branched Junctions. Biochemistry 30, 5667–5674 (1991).

13. Seeman, N. C. An Overview of Structural DNA Nanotechnology. Mol. Biotechnol. 37, 246–257 (2007).

14. Saccà, B. & Niemeyer, C. M. DNA origami: The art of folding DNA. Angew. Chemie - Int. Ed. 51, 58–66 (2012).

15. Tsu-Ju, F. & Seeman, N. C. DNA Double-Crossover Molecules. Biochemistry 32, 3211–3220 (1993).

16. Ke, Y., Castro, C. & Choi, J. H. Structural DNA Nanotechnology: Artificial Nanostructures for Biomedical Research. Annu. Rev. Biomed. Eng. 20, 375–401 (2018).

17. Winfree, E., Liu, F., Wenzler, L. A. & Seeman, N. C. Design and self-assembly of two-dimensional DNA crystals. Nature 394, 539–544 (1998).

18. He, Y., Chen, Y., Liu, H., Ribbe, A. E. & Mao, C. Self-Assembly of Hexagonal DNA Two-Dimensional (2D) Arrays. J. Am. Chem. Soc. 127, 12202–12203 (2005).

19. He, Y., Tian, Y., Ribbe, A. E. & Mao, C. Highly connected two-dimensional crystals of DNA six-point-stars. J. Am. Chem. Soc. 128, 15978–15979 (2006).

20. Mathieu, F. et al. Six-helix bundles designed from DNA. Nano Lett. 5, 661–665 (2005).

21. Zhang, J., Liu, Y., Ke, Y. & Yan, H. Periodic Square-Like Gold Nanoparticle Arrays Templated by Self-Assembled 2D DNA Nanogrids on a Surface. Nano Lett. 6, 248–251 (2006).

22. Park, S. H. et al. Programmable DNA Self-Assemblies for Nanoscale Organization of Ligands and Proteins Sung. Nano Lett. 5, 729–733 (2005).

23. He, Y., Tian, Y., Ribbe, A. E. & Mao, C. Antibody nanoarrays with a pitch of ~20 nanometers. J. Am. Chem. Soc. 128, 12664–12665 (2006).

24. Sharma, J. et al. DNA-tile-directed self-assembly of quantum dots into two-dimensional nanopatterns. Angew. Chemie - Int. Ed. 47, 5157–5159 (2008).

25. Rothemund, P. W. K. Folding DNA to create nanoscale shapes and patterns. Nature 440, 297–302 (2006).

26. Yang, Y. R., Liu, Y. & Yan, H. DNA Nanostructures as Programmable Biomolecular Scaffolds. Bioconjug. Chem. 26, 1381–1395 (2015).

27. Douglas, S. M., Chou, J. J. & Shih, W. M. DNA-nanotube-induced alignment of membrane proteins for NMR structure determination. Proc. Natl. Acad. Sci. U. S. A. 104, 6644–6648 (2007).

28. Dietz, H., Douglas, S. M. & Shih, W. M. Folding DNA into twisted and curved nanoscale shapes. Science. 325, 725–730 (2009).

29. Andersen, E. S. et al. Self-assembly of a nanoscale DNA box with a controllable lid. Nature 459, 73–76 (2009).

30. Woo, S. & Rothemund, P. W. K. Self-assembly of two-dimensional DNA origami lattices using cation-controlled surface diffusion. Nat. Commun. 5, 4889 (2014).

31. Liu, W., Zhong, H., Wang, R. & Seeman, N. C. Crystalline two-dimensional DNA-origami arrays. Angew. Chemie - Int. Ed. 50, 264–267 (2011).

32. Zhao, Z., Liu, Y. & Yan, H. Organizing DNA origami tiles into larger structures using preformed scaffold frames. Nano Lett. 11, 2997–3002 (2011).

33. Langecker, M. et al. Synthetic lipid membrane channels formed by designed DNA nanostructures. Science. 338, 932–936 (2012).

34. Göpfrich, K. et al. Large-Conductance Transmembrane Porin Made from DNA Origami. ACS Nano 10, 8207–8214 (2016).

35. Jin, Z. et al. Metallized DNA nanolithography for encoding and transferring spatial information for graphene patterning. Nat. Commun. 4, 1663–1669 (2013).

36. Plutowski, U., Jester, S. S., Lenhert, S., Kappes, M. M. & Richert, C. DNA-based self-sorting of nanoparticles on gold surfaces. Adv. Mater. 19, 1951–1956 (2007).

37. Spatz, J. P. et al. A combined top-down/bottom-up approach to the microscopic localization of metallic nanodots. Adv. Mater. 14, 1827–1832 (2002).

38. Kershner, R. J. et al. Placement and orientation of individual DNA shapes on lithographically patterned surfaces. Nat. Nanotechnol. 4, 557–561 (2009).

39. Demers, L. M., Park, S.-J., Taton, T. A., Li, Z. & Mirkin, C. A. Orthogonal Assembly of Nanoparticle Building Blocks on Dip-Pen Nanolithographically Generated Templates of DNA. Angew. Chemie Int. Ed. 40, 3071–3073 (2001).

40. Robinson, B. H. & Seeman, N. C. The design of a biochip: A self-assembling molecular-scale memory device. Protein Eng. Des. Sel. 1, 295–300 (1987).

41. Gramotnev, D. K. & Bozhevolnyi, S. I. Plasmonics beyond the diffraction limit. Nat. Photonics 4, 83–91 (2010).

42. Gür, F. N. et al. DNA-Assembled Plasmonic Waveguides for Nanoscale Light Propagation to a Fluorescent Nanodiamond. Nano Lett. 18, 7323–7329 (2018).

43. Gür, F. N., Schwarz, F. W., Ye, J., Diez, S. & Schmidt, T. L. Toward Self-Assembled Plasmonic Devices: High-Yield Arrangement of Gold Nanoparticles on DNA Origami Templates. ACS Nano 10, 5374–5382 (2016).

44. Klein, W. P. et al. Multiscaffold DNA origami nanoparticle waveguides. Nano Lett. 13, 3850–3856 (2013).

45. Vogele, K. et al. Self-Assembled Active Plasmonic Waveguide with a Peptide-Based Thermomechanical Switch. ACS Nano 10, 11377–11384 (2016).

46. Liu, W., Halverson, J., Tian, Y., Tkachenko, A. V. & Gang, O. Self-organized architectures from assorted DNA-framed nanoparticles. Nat. Chem. 8, 867–873 (2016).

47. Wang, P. et al. DNA Origami Guided Self-Assembly of Plasmonic Polymers with Robust Long-Range Plasmonic Resonance. Nano Lett. 20, 8926–8932 (2020).

48. Lan, X. et al. Au nanorod helical superstructures with designed chirality. J. Am. Chem. Soc. 137, 457–462 (2015).

49. Urban, M. J. et al. Plasmonic toroidal metamolecules assembled by DNA origami. J. Am. Chem. Soc. 138, 5495–5498 (2016).

50. Pal, S. et al. DNA directed self-assembly of anisotropic plasmonic nanostructures. J. Am. Chem. Soc. 133, 17606–17609 (2011).

51. Ye, J., Helmi, S., Teske, J. & Seidel, R. Fabrication of Metal Nanostructures with Programmable Length and Patterns Using a Modular DNA Platform. Nano Lett. 19, 2707–2714 (2019).

52. Yang, Y., Endo, M., Hidaka, K. & Sugiyama, H. Photo-controllable DNA origami nanostructures assembling into predesigned multiorientational patterns. J. Am. Chem. Soc. 134, 20645–20653 (2012).

53. Turek, V. A. et al. Thermo-Responsive Actuation of a DNA Origami Flexor. Adv. Funct. Mater. 28, 1–7 (2018).

VITA

Shuo Yang was born in Yantai City, Shandong Province, China. He received his bachelor's degree in Polymer Materials and Engineering from Donghua University (Shanghai, China) in June 2015. He started his Ph.D. in Chemistry at Missouri S&T and joined Dr. Risheng Wang's group in Fall 2016, where he worked on the development of intelligent stimuli-responsive biomaterials and nanodevices. During his graduate studies, Shuo authored and co-authored seven peer-reviewed journal publications and gave four presentations in international and local conferences. He was awarded an Outstanding Graduate Teaching Assistant Award in 2020. He received the Doctor of Philosophy in Chemistry from Missouri S&T in July 2021.